LOCALIZED DAMAGE PROCESS IN METAL STRUCTURES UNDER HIGH VELOCITY DEFORMATION

FINAL TECHNICAL REPORT

by

Prof. Stefan Vodenicharov, Sc.Dr.

Prof. Angel Baltov, Sc.Dr.

Sen.Res. Ganka Zlateva, Ph.D.

Sen.Res. Zanka Kamenova, Ph.D.

Res.Fell. Ivailo Katzarov, Ph.D

Res.Fell. Stoyan Kolev

Res.Fell. Serioja Valkanov

Res.Fell. Vania Diakova

December 1999

United States Army

EUROPEAN RESEARCH OFFICE OF THE U.S.ARMY

London, England

Contract Number: 68171-98-M-5831

R+D no : 8258- MS-01

INSTITUTE OF METAL SCIENCE,

BULGARIAN ACADEMY OF SCIENCES

20000616 062

1. AGENCY USE ONLY	2. REPORT DATE December 1999	3. REPORT TYPE AND DATES COVERED Final report, December 1999	

4. TITLE AND SUBTITLE LOCALISED DAMAGE PROCESS IN METAL STRUCTURES UNDER HIGH-VELOCITY DEFORMATION	5. FUNDING NUMBERS C N 68171-98-M-5831

6. AUTHOR(S)

Prof. Stefan Vodenicharov, D.Sc.

7. PERFORMING ORGANIZATION NAME AND ADRESS Institute for Metals Science Bulgarian Academy of Sciences	8. PERFORMING ORGANIZATION REPORT NUMBER
9. SPONSORING/MONITORING AGENCY NAME AND ADRESS US Government through European Research Office of the US Army	10. SPONSORING/MONITORING AGENCY REPORT NUMBER

11. SUPPLEMENTARY NOTES

12a. DISTRIBUTION/AVAILABILITY STATEMENT	12b. DISTRIBUTION CODE

13. ABSTRACT

The ASB initiation and growht in high strength steel are investigated. An integrated energy theoretical approach is suggested for modeling ASB development and identifying post critical structure state in the bands. Criteria are formulated for both micro cracks and macro cracks initiation along the band length. On that basis a numerical simulation model is developed for axially symmetric body.

The process of ASB initiation and growth is descritized in time and in space co-ordinate steps. For defining process parameters a variant of the finite difference method, called Method of finite systems, is applied. In this method for every discrete moment of time and for every point of the body space mesh an iterative procedure is realized in which the calculations are made in blocks of the basic groups of equations for the process. The post critical state is calculated with an a priori assuming the type of distribution of the plastic strain and temperature across the ASB thickness. Thus considerable difficulties are overcome in the defining the mechanical-mathematical models for the different ASB structures.

The ASB initiation and growth are studied experimentally on high strength martensite steel. The strength properties of the initial material in dynamic conditions are identified by using the Hopkinson bar. An approximation of the yield condition is proposed taking into account the plastic and dynamic hardening and the thermal softening.

A series of experiments by Hopkinson bar of various sizes of impulse loading are carried out to investigate the process of plastic and temperature localization. The development of localization bands is studied by optical, scanning and transmission electron microscopy. The micro structural changes caused by localized plastic strain are traced and the required temperature increase for their occurrence accounted for. Zones along the band length are identified where the changed structure types appear. The crack propagation in dependence of the structure type of the respective zone are discussed.

On the basis of the performed experimental, theoretical and numerical investigations a method is suggested for studying and describing ASB in high strength steels. The comparison between the theoretical, numerical and experimental results shows good agreement. The method allows to identify the model functions and parameters.

14. SUBJECT ITEMS adiabtic shear band, dynamic loading, microstructure, loss of stability, computer simulation	15. NUMBER OF PAGES		
	16. PRICE CODE		
17. SECURITY CLASSIFICATION OF REPORT	18. SECURITY CLASSIFICATION OF THIS PAGE	19. SECURITY CLASSIFICATION OF ABSTRACT	20. LIMITATION OF ABSTRACT UL

ABSTRACT

The ASB initiation and growht in high strength steel are investigated. An integrated energy theoretical approach is suggested for modeling ASB development and identifying post critical structure state in the bands. Criteria are formulated for both micro cracks and macro cracks initiation along the band length. On that basis a numerical simulation model is developed for axially symmetric body.

The process of ASB initiation and growth is descritized in time and in space co-ordinate steps. For defining process parameters a variant of the finite difference method, called Method of finite systems, is applied. In this method for every discrete moment of time and for every point of the body space mesh an iterative procedure is realized in which the calculations are made in blocks of the basic groups of equations for the process. The post critical state is calculated with an a priori assuming the type of distribution of the plastic strain and temperature across the ASB thickness. Thus considerable difficulties are overcome in the defining the mechanical-mathematical models for the different ASB structures.

The ASB initiation and growth are studied experimentally on high strength martensite steel. The strength properties of the initial material in dynamic conditions are identified by using the Hopkinson bar. An approximation of the yield condition is proposed taking into account the plastic and dynamic hardening and the thermal softening.

A series of experiments by Hopkinson bar of various sizes of impulse loading are carried out to investigate the process of plastic and temperature localization. The development of localization bands is studied by optical, scanning and transmission electron microscopy. The micro structural changes caused by localized plastic strain are traced and the required temperature increase for their occurrence accounted for. Zones along the band length are identified where the changed structure types appear. The crack propagation in dependence of the structure type of the respective zone are discussed.

On the basis of the performed experimental, theoretical and numerical investigations a method is suggested for studying and describing ASB in high strength steels. The comparison between the theoretical, numerical and experimental results shows good agreement. The method allows to identify the model functions and parameters.

LIST OF KEY-WORDS

Adiabatic shear band
Yield condition
Plastic flow theory
Internal structural energy
Critical energetic levels
Hopkinson bar
Electron microscopy
Numerical process simulation
Finite difference method
High strength armour martensite steel
Microstructure
Localized deformation
Damage
Macro crack initiation

LOCALIZED DAMAGE PROCESS IN METAL STRUCTURES UNDER HIGH VELOCITY DEFORMATION

CONTENTS

1. INTRODUCTION. BASIC ASSUMPTION

1.1. Plastic strain localization as local loss of stability of plastic deformation process

The plastic strain localization is a phenomenon that has been observed already at the end of last and the beginning of the present century (Luder's bands etc.). As a phenomenon this is a loss of stability of plastic deformation process in a material particle, line or surface of plastically deformed body. To establish such instability it is required to accept experimentally verificable criterion. The internal energy level is stabilized again after the loss of stability and small one-dimensional zones, bands or stripes of small thickness are formed. The determination of the post-critical state and the stabilization zone thickness is of essential importance for material science. The structural changes which run in these zones lead to new thermal and mechanical properties of the material. These zones are dangerous for accumulation of failures in the material as well as for initiation of cracks due to the developed plastic deformation, i.e. they are areas of failure initiation. In every design or assessment of technological deformation processes of structures it is required to define the condition at which in certain areas occurs macro-failure (initiation and propagation of macro-cracks resulting the fragmentation of the body). This makes the problems of plastic strain localization particularly important. The initiation of localization zones strongly changes the field of stresses and strains in the body as the zones cause significant non-homogeneity in the plastic strian and temperature distributions. The temperature is also concentrated in these zones because of the dissipation of plastic deformation energy that offers an internal heat source. The changes of plastic strain and temperature are also localized in the zones of stable energy post-critical state. The characteristics of the plastic concentration in local areas depend on the type of the localization, determined by:

a) the structure level where we observe:
  - mezo level (crystal grains);
  - macro level (deformed continuum)

b) the external mechanical loading:
  - quasi static
  - dynamic impact
  - dynamic fluctuation (cyclic process)

c) the thermal conditions:
  - adiabatic
  - thermo-mechanically coupling

d) the type of plastic strain localization:
  - shear (e.g. shear bands)
  - tension (e.g. necking in one-dimension tension)
  - plastic looseness dilatation (dilatation bands)

e) the type of stress state in the plastically deformed zone of the body:
  - one dimensional (one dimensional zone of localization)
  - two dimensional (band of localization)
  - three dimensional (strip of localization)

After the plastic strain localizaion a change of the stress state occurs. For instance, in one dimensional tension and neck formation in cylindrical specimen the stress state in the zone of the neck becomes axially symmetric.

The determination of the initiation of the loss of stability of the plastic deformation process and of the zones of post-critical state arises considerable calculation difficulties because of

the essential non-homogeneity of plastic strain distribution. This imposes the search of reasonable compromises in the used models and criteria so that the results can be applied in the engineering practice.

1.2. Some model approaches for determination of plastic localization initiation

Depending on the type of plastic localization, in compliance with the classification in §1.1, different model approaches are applied for developing a criterion for the initiation of plastic localization. The criteria are based on the fundamental concept that the localization is due to the local loss of stability of the plastic deformation process.

We shall present some characteristic examples.

a) Neck formation in one dimensional tension

The conventional approach to determine the beginning of neck formation (localization in tension) is based on the assumption that loss of stability in one dimensional tension occurs when the relation between stress σ and strain ε reaches its maximum (conditional measures). For quasi-static experiments the dependence $\sigma = f(\varepsilon)$ reaches maximum at $\varepsilon = \varepsilon_B$, when neck is formed:

(1) $\dfrac{df}{d\varepsilon} = 0$, and $d^2 f < 0$

The curve $f(\varepsilon)$ can have maximum also if there is softening due to temperature or material damage.

This criterion is equivalent to the criterion for reaching critical plastic strain $\varepsilon^p = \varepsilon_B^p$ (See Fig. 1.1). ε_B^p corresponds to the critical strain $\varepsilon_B^p = \varepsilon_B^e + \varepsilon_B^p$, where ε_B^e is the elastic component.

In some cases the experiments show that neck is formed at $\varepsilon = \varepsilon_B^l > \varepsilon_B$. Explanation of that can be looked for in the materials' sensitivity to temperature. A dissipation of plastic energy occurs in certain material particle during plastic deformation with rate $\dot{W}^P = \sigma \dot{\varepsilon}^P$. A large part of the dissipated energy (about 90%) transforms in heat. So heat is generated in unit mass with rate $r_T = J K_p \dot{W}^P$ where $K_p \approx 0.9$ (Taylor), J is the heat equivalent coefficient of the mechanical work. This increases the temperature of the material particle and it causes it's plastic softening. The new relation $\sigma - \varepsilon$ takes the form $\sigma = \varphi(\varepsilon, \theta)$. where $\theta = T - T_o$, T_o - is the initial temperature and T - the actual. The condition for maximum as a criterion of localization takes the next form:

(2) $\dfrac{\partial \varphi}{\partial \varepsilon} = 0$, $\dfrac{\partial \varphi}{\partial \theta} = 0$,   for $\varepsilon = \varepsilon_B^l > \varepsilon_B$, $\theta = \theta_B$ for $d^2 \varphi < 0$.

Fig. 1.2 presents an illustration of this case.

If the process is dynamic one and the material is sensitive to the strain rate and temperature the localization criterion of type (1) shall have the form:

If

(3) $\sigma = \psi(\varepsilon, \dot{\varepsilon}, \theta)$

then

(4) $\dfrac{\partial \psi}{\partial \varepsilon} = 0$, $\dfrac{\partial \varepsilon}{\partial \dot{\varepsilon}} = 0$, $\dfrac{\partial \psi}{\partial \theta} = 0$,   for $\varepsilon = \varepsilon_B^{''}$, $\dot{\varepsilon} = \dot{\varepsilon}_B$,

2

$$\theta = \theta_B \text{ at } d^2\psi < 0$$

It is interesting to note that the neck is formed in the middle of the tensile specimen in spite of the assumption that the stresses and strains are constant along the whole length. This circumstance can be explained by the non-homogeneous distribution of the temperature along the length of the specimen. The homogeneous plastic strain distribution results in homogeneous rate of temperature supply $r_T = const$ (See Fig. 1.4) but the temperature has a maximum in the middle because of the heat exchange with the machine jaws. The higher temperature in the middle will result that the criterion (2) will be satisfyied in this specimen point.

b) Formation of the plastic localization zones in rigid-plastic bodies

We consider rigid-plastic material sensitive to strain rate and temperature. This is expressed in the dependence of the pure shear yield limit τ_P on the plastic sheeear strain $\gamma_p = \gamma$, strain rate intensity β_o and temperature θ, i.e. $\tau_p = \tau_p(\gamma, \beta_o, \theta)$. In the case of non-homogeneous stress and strain distribution in rigid-plastic body in the conditions of plane strain, localization shall also occur by loss of stability of the plastic deformation process. The loss of stability is assumed as bifurcation of the process in certain point on (Ox_1x_2) for the moment $t = t_C$. There will be two parameters of the process changes $\dot{f}^{(1)}$ and $\dot{f}^{(2)}$ for which

$\Delta \dot{f} = \dot{f}^{(1)} - \dot{f}^{(2)} \neq 0$. That is expressed by the conditions $\Delta \dot{\gamma} \neq 0$, $\Delta \dot{\beta} \neq 0$, $\Delta \dot{\theta} \neq 0$. For the bifurcations initiation the necessary condition of non-zero bifurcations is [35]:

$$(5) \quad \tau_\gamma + \frac{2\widetilde{K}_p}{\rho C_T} \tau_p \tau_\theta + K_\gamma \tau_\theta = 0$$

where

$$(6) \quad \tau_\gamma = \frac{\partial \tau_p}{\partial \gamma}; \qquad \tau_\theta = \frac{\partial \tau_p}{\partial \theta}; \qquad \tau_\beta = \frac{\partial \tau_p}{\partial \beta_o}$$

for $\widetilde{K}_p = K_p J$; ρ - material density; C_T - specific heat capacity. It is assumed that there is

proportionality between the bifurcations $\Delta \dot{\beta}_o = K_\gamma \Delta \dot{\gamma}$.

This approach was applied for shear plastic localization in:
- anisotropically hardening rigid-plastic bodies taking into account the plastic and dynamic hardening and the thermal softening [36];
- rigid-plastic bodies with damage initiation and growth [37];
- rigid-plastic porous bodies taking into account damage initiation and growth [38];

c) Formation of shear plastic localization bands in plane elastic-plastic bodies

We consider plane elements S in (Ox_1x_2) subjected to homogeneous stresses and strains, i.e. $\{\sigma_{\alpha,\beta}\}$ and $\{V_{\alpha,\beta}\}$ are constant in S, $(\alpha, \beta = 1,2)$. $\{\sigma_{\alpha,\beta}\}$ is Cauchy stress tensor and V_α the velocity of the body points in (Ox_1x_2). By comma it is designated the differentiation by x_β. The material is elasto-plastic at large deformations with constitutive relation:

(7) $\quad \overset{\nabla}{\sigma}_{\alpha\beta} = L_{\alpha\beta\gamma\delta} D_{\gamma\delta}$, $\qquad D_{\gamma\delta} = \frac{1}{2}(V_{\gamma\delta} + V_{\gamma\delta})$

where $L_{\alpha\beta\gamma\delta}$ is the elasto-plastic tensor; $D_{\gamma\delta}$ - is the rate tensor of high deformations; $\{\overset{\nabla}{\sigma}_{\alpha\beta}\}$ - Yauman stress time derivative in the plane $(Ox_1 x_2)$.

At local loss of plastic stability of the body bifurcation of the rate gradients occurs, i.e.

$\Delta V_{\alpha,\beta} = V_{\alpha,\beta} - V_{\alpha,\beta} = g_\alpha n_\beta \neq 0$ where n_β is the single unit to the line where shear strain localization is realized. The condition of non-zero bifurcation $g_\alpha \neq 0$ is reduced to a condition of zero solution for the system of equations /[46], [53]/:

(8) $\quad (n_\alpha L_{\alpha\beta\gamma\delta} \, n_\delta + D_{\beta\gamma}) g_\gamma = n_\alpha \Delta L_{\alpha\beta\gamma\delta} \, D_{\gamma\delta}$

for

(9) $\quad A_{\beta\gamma} = -n_\beta \, (n_\alpha \sigma_{\alpha\gamma}) + (n_\alpha \sigma_{\alpha\delta} n_\delta) \delta_{\beta\gamma} - \sigma_{\beta\gamma}$

Thus the condition for the initiation of the shear plastic strain localizaion becomes:

(10) $\quad det\{n_\alpha L_{\alpha\beta\gamma\delta} n_S + A_{\beta\gamma}\} = 0$

By the same approach a number of conditions is defined for initiation of localization in elasto-plastic materials with accounting for:
- plastic dilatation [59]
- thermal effects [47]
- damage [67], [29], [7]
- induced anisotropy [48], [25], [28]
- sensitivity to the strain rate and temperature [23], [26], [49], etc.

d) Perturbation criteria for initation of localization lines in plane bodies

Another approach for determination of the initiation of the plastic shear strain localization in rigid-plastic or elasto-plastic plane bodies taking into account the sensitivity to the strain rate and temperature, are the so called perturbation criteria (See e.g. [50], [17], [30], etc.). These criteria are based again on the concept that localization is a result of local loss of stability of the plastic deformation process. Bifurcation of the process parameters is expressed as perturbation of these values. For homogeneous strain γ^o, stress τ^o and temperature θ^o distribtions perturbations γ',τ',θ' are preset according the following formulae:

(11) $\quad \gamma' = \gamma * .exp\{\alpha.t + ik\xi\}$;

$\qquad \tau' = \tau * .exp\{\alpha.t + ik\xi\}$;

$\qquad \theta' = \theta * .exp\{\alpha.t + ik\xi\}$,

where $\gamma*, \varepsilon*, \theta*, \alpha$ and k are constants and ξ is the coordinate in the direction of the localization line.

The localization criterion in this case is reduced to conditions of non-zero perturbations.

e) Criteria for ASB initiation in dynamic loaded plastic deformable bodies

For the aims of the present investigation we shall analyze the used criteria for ASB initiation in two-dimensional and three-dimensional bodies. The bodies are subjected to external dynamic impulse loading. Processes of shock wave propagation, acceleration waves, etc., develop in. The criteria of ASB initiation are physically based again on the concept of local loss of stability of the plastic deformation. We shall consider the most often used criteria.

4

- Criteria for occurrence of stationary surface of acceleration jumps /See [23], etc./. The criterion refers to elasto-plastic materials which are not strain rate sensitive. The local loss of stability of the considered dynamic process results in appearance of surface of acceleration jumps $[\overset{\circ}{V}_i] \neq 0$ and temperature rate $[\overset{\circ}{\theta}_i] \neq 0$ etc., with zero propagation speed. The condition for this is expressed in the following way:

(12) $\quad det\{A_{ij}^*\} = 0$

where $\{A_{ij}^*\}$ is the especially introduced acoustic tensor.

- Criterion for bifurcation of the values of process parameters /See [26], etc./. For elasto-plastic strain rate sensitive materials the viscous effects hinder ABS nucleation as a stationary wave surface. The condition in this case is based on the occurrence of local bifurcation of the dynamic process parameters changes. The constitutive equations in this case are:

(13) $\quad \overset{\circ}{\sigma}^{ij} = L^{ijkl} D_{kl}$

where $\{\overset{\circ}{\sigma}^{ij}\}$ is the constitutive time derivative of Cauchy stress tensor; L^{ijkl} is the constitutive elasto-plastic tensor. It depends on the process factors: strain rate intensity β_o, temperature θ and possibly the density of micro-defects ζ. The condition of non-zero bifurcations $\Delta\overset{\circ}{\sigma}^{ij} \neq 0$; $\Delta D_{kl} \neq 0$; $\Delta\overset{\circ}{\theta} \neq 0$ etc., is reduced to

(14) $\quad det\{L^{2jk2}\} = 0$

if Ox_2 is directed along the normal to the surface on which ABS is initiated.

These criteria are developed with accounting for: plastic anisotropy [25]; thermal softening [23]; substructure of the crystals in which ABS is initiated /See [27], [60], [71], [74], etc./.

- Perturbation criteria for ASB initiation /See [30], [70], [78], etc./. To these criteria approaches could be referred the criteria in which ASB initiate in the point with preliminary defect /[51], [79], etc./.

f) Energy criteria of plastic localization

There is a trend towards search of energy criteria for initiation of plastic localization based on energy criteria for local loss of the plastic deformation stability. The reason for this is to formulate criteria of more general applicability to the great variety of plastic localization types /See § 1.1/

Frequently used criteria are those where zero change of certain energy parameter is formulated as condition for loss of plastic stability. We shall mention Druker's approach [61] where the plastic deformation energy changes its sign from stable into unstable state, i.e.

(15) $\quad \overset{\cdot}{\sigma}_{ij} \varepsilon_{ij}^p = 0$

This criterion is well motivated thermodynamically [18]. However, it results some difficulties for determination of the stressed state change in the post critical state [6].

A more general energy approach for formulation of a criterion for loss of plastic deformation stability is developed in publications [3], [4], [5], [6], [89], etc. This criterion could be applied also for local loss of stability of the plastic deformation process and for inititation of the localization zones [6].

It is reduced to the following:

(16) $\quad \delta\overset{\cdot}{E} = 0$

where E is especially defined energy potential.

The inconvenience of these criteria is that they give only the unstable change of the achieved energy level in certain point of plastic deforming body with no assessment of the structure of the material that will correspond to this level.

g) Further comments

The criteria presented above give the necessary conditions for plastic localization. The sufficient conditions for that should be obtained by mathematical methods [30] or microstructure analysis [69].

1.3. Some approaches for assessment of post critical state in the localization bands

The localization process as discussed in § 1.1. starts with loss of stability of plastic deformation in points, lines or surfaces. Bifurcation of the deformation process parameter rate arise and stable post critical condition is achieved. At this stabilization one dimensional zones, two dimensional bands or three dimensional stripes are formed where the plastic deformation, temperature and the structure changes will be strongly localized. The material in these zones possess different physical and mechanical properties [35].

The strong localization of the plastic strain can cause:
- effects of dipolarity /See [22], [33], [75], [69], etc./
- effects of influence of the plastic strain gradient (non-local theories of plasticity) /[11], [80], [82], etc./
- effects of essential change in the material structure /See § 4/

We shall give examples of non-local plasticity models:

a) The yield condition depends on the derivatives of the hardening parameter $\chi_p = \int\limits_{to}^{t} s_{ij}\dot{\varepsilon}_{ij}^{p}\, dt$,

as:

(17) $\tau_o = \tau_p^{*}(\chi_P) - g\nabla^2\chi_p$

where τ_o is the intensity of the tangential stresses; g - material characteristic.

b) The yield condition depends on the plastic deformation gradient:

(18) $\tau_o = \tau_P(\gamma_o^{P}, (\gamma_o^{P}), k, \theta, \beta_o)$

Another approach is to formulate initiation-boundary problem of coupled thermo-plasticity. In case of ASB the adiabatic conditions are also formulated. As a result of the distribution of plastic strain and temperature across the band thickness are obtained. For non-homogeneous stress and strain fields the band thickness will change along its length, as well as the maximum values of the plastic deformation and temperature /See [4], [75], etc. /

In some cases lines or localization surfaces are used and they are treated as places of acceleration jumps, rate temperature jumps, etc. Problems are formulated for determination of the size of these jumps /See [35], [71], [72], etc./

In numerical simulations of the plastic deformation process the localization zones are defined approximately. These zones are considered immersed in the plastic deforming body /See [84], [85], etc./

The obtained distributions of plastic strain and temperature across the thickness of the zone has a bell shape distribution with exponential or other localization functions. The distributions essencially depends on the zone thickness /See [82], [84], etc./

6

1.4. Some methods for numerical simulation of the plastic localization process

In numerical simulation of the plastic localization process should be simulated, localization criteria introduced, post critical state in the zones obtained and criteria for micro-cracks initiation checked. This imposes essential numerical and model problems consisting in:

- solving the problems of plastic strain distribution in the body with points, lines or surfaces of strong discontinuity or non-homogeneity /See [35], [81], [51], [79], [74], etc./
- overcoming the solution dependence on the mesh density in FE descritization [84], [83].
- accepting adequate models for the material in the band at condition of highly impeded experimenting to find its properties [35], [21], [69].
- determination of the localization zones thickness [31].

Most frequently descritization of the process is made according to time and to space with steps of sizes which ensure stability and convergence of the numerical procedure. Space descritization is usually carried out:

- by the FEM /See [51], [74], [75], [78], etc./
- by the method of particles /See [72], [34], etc./
- by the FDM /See [68], etc./

A variant of the finite difference method called method of finite systems is of special interest. The calculation is realized by the iterative procedure for every time step and every point of the space mesh in the body. The convergence of the procedure is ensured by suitable relationship between the time and space steps. The calculations are divided into blocks containing the constitutive equations, the equations of motion and the geometrical relations in velosities. We shall illustrate the method by simple example of one dimensional dynamic problem with non-linear relation between the stresses $\sigma(x,t)$ and deformations $\varepsilon(x,t)$.

The system of equations that is to be solved has the next form:

$$(19) \quad \sigma(x,t) = f[\varepsilon(x,t)]$$

$$\rho \frac{\partial V(x,t)}{\partial t} = \frac{\partial \sigma(x,t)}{\partial x} + \rho f$$

$$\frac{\partial \varepsilon(x,t)}{\partial t} = \frac{\partial V(x,t)}{\partial x}$$

for the corresponding initial and boundary conditions of the considered dynamic problem. The calculation by the finite diferences method is organized for every discrete moment and every discrete point of the one dimensional body by iterative procedure (Fig. 1.7). The convergence condition of the procedure is:

$$(20) \quad \Delta x \le \overline{C_l}.\Delta t, \quad \overline{C_l} = a_l C_l$$

where $C_l = \sqrt{\dfrac{E_t}{\rho}}$, $E_t = \dfrac{d\sigma}{d\varepsilon}$; a_l is a parameter which depends on the assumed dofferemce operators $D_x = (...)$ and $D_t(...)$. The meaning of the condition (20) is that the descritization error should propagate slower than the longitudinal wave propagation speed C_l. The advantage of the finite systems method is that it overcomes numerical comparatively easily strong non-linearities in systems of equations describing the process and the block of the constitutive equations is easily replaced in the calculation program when we have to solve the problem for different materials. The case of the localization bands is of this type as the material out of the bands and the material in the bands are modeled by different constitutive equations.

1.5. Further comments

The present investigation treats also some other essential problems such as:
- Experimental investigations of the ASB initiation and growth /See § 3/
- Experimental investigations on the change of the material in ASB /See § 4/
- Criteria of micro and macro cracks initiation along the ASB length /See § 2.5/.

2. THEORETHICAL BASES FOR DESCRIPTION OF ASB INITIATION AND DEVELOPMENT IN HIGH STRENGTH STEELS

2.1. Formulation of the problem. Program of investigations

Purpose of the present development is to study and describe experimentally, theoretically and numerically the ASB initiation and growth in impulse loaded plane or axially symmetric deforming bodies made of special high strength steels.

That is achieved by realizing the following investigation program:

(1) Carrying out standard tests including also dynamic experiments by means of experimental set "Hopkinson bar" to determine the mechanical and strength properties of a typical high strength steel;

(2) Experimental determination of the conditions for ASB initiation and growth in cylindrical specimens of the studied steel subjected to impulse loading by the incident bar of the "Hopkinson bar" set. The bar end has a cone shaped tip;

(3) Experimental study of the structure changes occurring in the material along the length and width of the adiabatic band for various energy level of loading;

(4) Development of a theoretical model based on energy approach and containing:
- criterion of ASB nucleation;
- model description of post critical condition in the band;
- model of stress and strain state of the cylindrical body in which ASB have developed;
- criterion of micro cracks initiation and model of its development in the band material;
- criterion of shear macro cracks initiation along band length.

(5) Development of simulation numerical model for the process of ASB nucleation and growth in cylindrical bodies of high strength steel. The simulation numerical model is based on the theoretical model of the process and time descritization of the process as well as digitization of the area occupied by the body with the application of the finite systems model;

(6) Development and application of methods for verification of the theoretical and numerical models as well as for identification of the model functions and parameters of the steel studied;

In the following text they will successively present the results of the realization of this program.

2.2. Criterion of ASB nucleation

The cylindrical body considered made of high strength steel is subjected to dynamic loading experiments. The material is sensitive to the strain rate and temperature /See § 3/. Up to ASB formation the body is elastic-plastic with development of plastic zones in the stress concentrations at the cylinder-loading cone contact /Fig. 1.1/. The dynamic process is with relatively not so not big deformations which allows to approximately assume geometric linear theory. The material is initially isotropic and at the present stage of investigations we shall not take into account induced anisotropy [61].

9

The process measures are: Cauchy stress tensor $\{\sigma_{ij}\}$, $(i,j=1,2,3)$ (in rectangular coordinate system), the strain rate tensor $\{\dot{\varepsilon}_{ij}\}$ and the temperature difference θ. We assume the well known conventional variant of the plastic flow theory [61].

The strain rate consists of elastic $\dot{\varepsilon}_{ij}^e$, plastic $\dot{\varepsilon}_{ij}^p$ and thermal $\dot{\varepsilon}_{ij}^t$ parts i.e.

(21) $\dot{\varepsilon}_{ij} = \dot{\varepsilon}_{ij}^e + \dot{\varepsilon}_{ij}^p + \dot{\varepsilon}_{ij}^t$, $(i,j=1,2,3)$

where:

(22) $\dot{\varepsilon}_{ij}^e = H_{ijkl}\sigma_{kl}$ (Hook's law)

$\dot{\varepsilon}_{ij}^p = A_{ijkl}\overset{\circ}{s}_{kl}$, $\qquad \dot{\varepsilon}_{kk}^p = 0$, $\qquad \dot{s}_{ij} = \dot{\sigma}_{ij} - \frac{1}{3}\delta_{ij}\dot{\sigma}_{kl}$ (Plastic deformation law)

$H_{ijkl} = \Lambda\sigma_{ij}\delta_{kl} + \frac{1}{2}M(\delta_{ik}\delta_{jl} + \delta_{jk}\delta_{il})$ $\Lambda = const.$, $M = const.$, $\delta_{ij} = \{^{1,i\neq j}_{0,i\neq j}\}$,

$A_{ijkl} = h_p \dfrac{\partial F}{\partial\sigma_{ij}} \cdot \dfrac{\partial F}{\partial\sigma_{kl}} \neq 0$ for $\dfrac{\partial F}{\partial\sigma_{kl}}\dot{\sigma}_{kl} > 0$ (loading)

at

(23) $F(s_{ij},\beta_o,\theta) = 0$ or $F(s_{ij},\beta_o,\theta,\zeta) = 0$

(yield condition)   (yield condition with micro defect development)

$\beta_o = \sqrt{\frac{3}{2}\dot{\varepsilon}_{ij}\dot{\varepsilon}_{ij}}$ is the strain rate intensity; $\{\dot{s}_{ij}\}$ is the stress speed deviator; h_p is the parameter of plasticity which depends on the process factors: strain rate β_o, temperature θ and eventually density of defects in unit volume ζ_o; the condition of plasticity can be assumed to be of Mises type, i.e.

(24) $F = \tau_o - \tau_p = 0$, $\qquad \tau_p = \tau_p(\varepsilon_o^p,\beta_o,\theta)$ or $\tau_p = \tau_p(\varepsilon_o^p,\beta_o,\theta,\xi)$

where ε_o^p is the measure for plastic strain intensity $\varepsilon_o^p = \int\limits_{t_o}^{t}\beta_o dt$ (t_o - initial moment of the process); τ_p is shear yield limit; $\tau_o = \sqrt{\frac{1}{2}s_{ij}s_{ij}}$ is the intensity of tangential stresses. Material time differentiation is designated by a dot; by comma and subsequent index - space differentiation and the summarion convention for the repeated indices is accepted.

For thermal strain rate:

(25) $\dot{\varepsilon}_{ij}^t = \alpha_t\delta_{ij}\dot{\theta}$

where α_t is the thermal expansion coefficient.

For measure of the internal structure energy we accept the accumulated plastic work, i.e.

$W^p = \int\limits_{t_o}^{t}s_{ij}\dot{\varepsilon}_{ij}^p dt$

We assume that there are no external heat sources and that heat is generated by the plastic energy dissipation with rate $r_T = JK_p\dot{W}^p$, where J is the thermal equivalent of mechanical work, $K_p \approx 0.9$ is the well known Taylor coefficient [62].

The temperature equation shall take the next form

(26) $\rho C_T\dot{\theta} = K_T\theta,_{ii} + 3JK_p\dot{W}^p$

for C_T in the specific heat capacity; ρ - material density, K_T - Fourier heat conductivity coefficient. The initial and boundary conditions are assumed according to the problem treated by us /See § 5/.

We assume that any stable internal structure condition in the non-elastic area of deformation is characterized by energy levels W_J^P, $(J = I, II...)$ where (J) is the structure type of the material. Any unstable internal structure state is characterized by energy levels W_{ck}^P, $(k = 1, 2...)$. Fig 5a presents an illustrative diagram of possible relation $W^P - \varepsilon_o^P$ $(W^P - \gamma_o^P = \frac{2}{\sqrt{3}}\varepsilon_o^P$, respectively) at constant intensity of the strain rate $\beta_o = const$. Fig. 1.5b shows the energy interpretation for two structure states, type I and type II, for the relation $\tau_o - \gamma_o^P$. The diagrams have maximum due to the temperature softening which (above certain level) can combine with softening due to the damage /See 2.5/. We consider the case of ASB initiation where localization of plastic shear strain occurs.

The criterion for ASB initiation of the basic structure (type I material) could be formulated as:

(27) $\quad W^P = W_{c_I}^P(\beta_o, \theta)$

After ASB formation and post critical stabilization of the internal energy state a new structure of II type develops there. If the external loading increases the internal energy in ASB until the achievement of a new critical level $W_{c_2}^P$ then transition to the new stable state W_{II}^P occurs, etc. These energy limits are determined by the methods discussed in § 2.5.

2.3. Analysis of the internal structural state of the ASB

We consider crystalline grain metals at mezo level. Each grain is a monocrystal immersed in the intergranular area. We can estimate the structural changes on mezo level by the grains and their orientation. At present we are not considering nucleation and growth of mezo defects in the intergranular area. We study the case of planar or axially symmetric stress and strain state according to the experimental studies made in item 3.

We consider in the plane Ox_1x_2 a representative element with m_z number of grains. Let the grains are of one type of material. Every projection of the grain (α) $(\alpha = 1,2,...m)$ in $O\xi_1\xi_2$ (local co-ordinate system where $O_L\xi_1$ is parallel to Ox_1 and $O_L\xi_2$ to Ox_2 (See Fig. 1.5)) we approximate to ellipse with axes $a_z(\alpha)$ and $b_z(\alpha)$. Let the main axis of the ellipse corresponding to $a_z(\alpha)$ is with $\vartheta_z(\alpha)$ slope towards $O_L\xi_1$ (Ox_1 respectively). We consider the following three characteristics of the grain:

- mean diameter $d_z(\alpha) = \frac{1}{2}[a_z(\alpha) + b_z(\alpha)]$
- grain elongation $\chi_z(\alpha) = a_z(\alpha) : b_z(\alpha)$
- grain orientation $\vartheta_z(\alpha)$

We introduce their statistical averages for the set of m_z - grains, i.e.

(28) $\quad \overline{d}_z = \langle d_z(\alpha) \rangle, \qquad \overline{\chi}_z = \langle \chi_z(\alpha) \rangle, \quad \overline{\vartheta}_z = \langle \vartheta_z(\alpha) \rangle$

We accept them as macro structural grain characteristics. We interpret these values from thermodynamic point of view as internal state parameters [61]. Let the macro parameters $\bar{p}_z$, $\bar{q}_z$ and $\bar{s}_z$ are thermodynamically conjugated with them, i.e.

$$(29) \quad \bar{p}_z = -\rho \frac{\partial Z'_p}{\partial \bar{d}_z}$$

$$\bar{q}_z = -\rho \frac{\partial Z'_p}{\partial \bar{\chi}_z}$$

$$\bar{s}_z = -\rho \frac{\partial Z'_p}{\partial \bar{\vartheta}_z}$$

Z is the specific free energy. We consider it divided into elastic part Z_e and plastic part Z_p. The plastic part itself we assume to be the sum of the grains energy part Z'_p and the intergranular energy part Z''_p, i.e.

$$(30) \quad Z = Z(\sigma_{ij}, \varepsilon_{ij}^p, \beta_o, \theta)$$

at

$$(31) \quad Z = Z_e + Z_p, \quad Z_p = Z'_p + Z''_p$$

for

$$(32) \quad Z'_p = Z'_p(\bar{d}_z, \bar{\chi}_z, \bar{\vartheta}_z \beta_o, \theta)$$

Let the relationship between the two parts is $K'_z = Z'_p / Z_p$, $K''_z = Z''_p / Z_p$, $K'_z + K''_z = 1$.

The values of these relationships with approximation could be assumed as percent content of grains and intergranular areas in the representative element according to the simplified model for two-component composites. In relation to the homogenization theory, the simplified composite model is a comparatively strong approximation.

The macro plastic deformation itself $\{\varepsilon_{ij}^p\}$ is a good, macro characteristics of the metal structural state. If the macro plastic power is $\dot{W}^P = s_{ij}\dot{\varepsilon}_{ij}^p$, then the part of it for the grains we assume as $\dot{W}_z^P = K'_z\dot{W}^P$. We express $\dot{W}_z^P$ in the following way:

$$(33) \quad \dot{W}_z^P = K'_z\dot{W}^P = \bar{p}_z\dot{\bar{d}}_z + \bar{q}_z\dot{\bar{\chi}}_z + \bar{s}_z\dot{\bar{\vartheta}}_z) = K'_z s_{ij}\dot{\varepsilon}_{ij}^p$$

For the internal parameters of grain state we assume evolution equations of the type:

$$(34) \quad \dot{\bar{d}}_z = P_{ij}\dot{\varepsilon}_{ij}^p, \quad \dot{\bar{\chi}}_z = Q_{ij}\dot{\varepsilon}_{ij}^p, \quad \dot{\bar{\vartheta}}_z = \Omega_{ij}\dot{\varepsilon}_{ij}^p$$

Then:

$$(35) \quad s_{ij} = \frac{\bar{p}_z}{K'_z}.P_{ij} + \frac{\bar{q}_z}{K'_z}.Q_{ij} + \frac{\bar{s}_z}{K'_z}.\Omega_{ij}$$

It is seen that P_{ij}, Q_{ij}, Ω_{ij} act as inner stresses arising from the structural changes while the parameters $(\bar{p}_z, \bar{q}_z, \bar{s}_z)$ are connected with the weight coefficients of these stresses $(\frac{\bar{p}_z}{K'_z}, \frac{\bar{q}_z}{K'_z}, \frac{\bar{s}_z}{K'_z})$.

The evolution equations and weight coefficients require special experimental investigations. For the structures in the localization band such experiments can be, for instance, those presented in § 3 and § 4.

It is interesting to relate the averaged geometric parameters $\overline{\chi}_z$ and $\overline{\theta}_z$ with the main macro plastic strains - Ox_1x_2: ε_I^P and ε_{II}^P. Let $\chi_p = \dfrac{\varepsilon_I^P}{\varepsilon_{II}^P}$ and ϑ_p is the angle between the main direction Ox_1 and Ox_1. It is concenient to present in polar diagram vectors of value $\overline{\chi}_z$ (χ_p respectively) under slope $\overline{\vartheta}_p$ (ϑ_p respectively) (See Fig. 1.6). Thus it can be estimated to what extent the plastic deformation has caused corresponding elongation and orientation of the grains. This is important for the assessment of the induced anisotropy after plastic deformation due to grain orientation and elongation. Co-linearity or close to co-linearity of the two vectors is possible for some structures and strongly developed plastic deformation. The present investigation does not treat induced anisotropy. In the simulation numerical model the estimation of the structure and its changes is performed by the plastic strain and the plastic strain rate. Information about the structural changes in ASB is obtained by the method in § 2.6. /See § 4/.

2.4. Post critical stable structure state in the localization bands

If the criterion (27) is satisfied the system loses its stability. Changes start until reaching new stable internal structural state. Internal structural energy levels W_J^P, $J = II, III, \ldots$ correspond to that states (See § 2.2). The structure changes develop in the localization zone where concentration of the intrastructural energy occurs. In the localization zone the plastic strain changes considerably and the material there may becomes sensitive to the plastic strain gradients. The material in the zone should be described by the so called non-local theories of plasticity where the yield condition depends on the plastic strain gradients (See § 1.2). As a result of simulating the process, with present there localization zones of non-local plastic properties, we may determine of the transverse and longitudinal distribution of the plastic strain and temperature in the localization zone. The transverse distribution is of bell shape character. These problem are difficult to be solved because the localization zones change during the process and the non-local plastic properties of the material are difficult for experimental determination. Therefore we suggest a simplified approach that possesses satisfactory accuracy because the thickness of the localization zones is very small compared to the dimensions of the body.

We consider the cases of plane or axially symmetric plastic deformation. The approach consists in the following. A priori we assume a partucular bell shape transverse distribution of plastic strain and temperature $\gamma^P(\eta, s, t)$ and $\theta(\eta, s, t)$ for a fixed moment t and for every point s from the middle line of the band ($\eta \in [0, \dfrac{\delta(s,t)}{2}]$). $\delta(s,t)$ is the band thickness and the distribution is symmetric towards the middle line $(\eta = 0)$.

We shall present some possible cases of this transverse distributions:

a) sine law

$$(36) \quad \gamma^P(\eta, s, t) = max\gamma^P(s,t)[1 + cos(\frac{2\eta\pi}{\delta(s,t)})]$$

and also

13

$$\theta(\eta,s,t) = max\theta(s,t)[1+cos(\frac{2\eta\pi}{\delta(s,t)})]$$

where $\eta \in [0,\frac{\delta(s,t)}{2}]$, $s \in [0,s_f(t)]$, $t \in [t_o,t_1]$, $s(0)=0$ for fixed s and t.

The final co-ordinate s_f will depend on time as we consider ASB growth in the time interval $[t_o,t_1]$. We assume that the thickness changes along the band length according to linear law, i.e.

(37) $\delta(s,t) = a(t).s$, $\qquad s \in [0,s_f(t)]$

the coefficient a being experimentally determined /See 4/.

b) exponential law

(38) $\qquad \gamma^P(\eta,s,t) = max\gamma^P(s,t).exp(-\frac{2\eta^2}{\delta^2(s,t)})$

and $\qquad \theta(\eta,s,t) = max\theta(s,t).exp(-\frac{2\eta^2}{\delta^2(s,t)})$

for $\eta \in [0,\frac{\delta(s,t)}{2}]$, $s \in [0,s_f(t)]$, $t \in [t_o,t_1]$, $s(0)=0$ and fixed s and t.

c) power law

(39) $\qquad \gamma^P(\eta,s,t) = max\gamma^P(s,t)(1-\frac{4\eta^2}{\delta^2(s,t)})$

$\qquad \theta(\eta,s,t) = max\theta(s,t)(1-\frac{4\eta^2}{\delta^2(s,t)})$

for $\eta \in [0,\frac{\delta(s,t)}{2}]$, $s \in [0,s_f(t)]$, $t \in [t_o,t_1]$, $s(0)=0$ and fixed s and t.

The determination of the parameters of these laws is essential problem. The thickness can be approximately found by the formula (37) or experimentally (See 3 and 4).

The other values characterizing the band (eqs. (30), (38) or (39)) are the maximum values of plastic shear strain $max\gamma^P(s,t)$ and temperature $max\theta(s,t)$ for every point S from the middle curve of the band in the plane Ox_1x_2 and for any moment t of the process $/t \in [t_o,t_1]$, $s(0)=0/$. For their determination and for numerical simulation of the process of plastic deformation of the body with ASB presence we divide the process into time steps $\Delta t(K) = t(K+1) - t(K)$, $K = 1,2,...L$. For each time interval $\Delta t(K)$ we describe the band through selection of points from the middle curve of the band $s(J,K)$, $J = 1,2,...M$ with steps $\Delta S(J,K) = S(JH,K) - S(J,K)$. We assume for the part of the band of $\Delta S(J,K)$ length that the stresses $\tau(J,K)$, the increase of the plastic shear strain $\Delta\gamma^P(J,K)$ and the band thickness $\delta(J,K)$ are constant in this length.

For the time interval $\Delta t(K)$ we determine the balance of the energies for the body:

(40) $\qquad \Delta U(K) = \Delta W(K) + \Delta Q(K)$

where $\Delta U(K)$ is the increase of the external energy, $\Delta W(K)$ is the change of the internal deformation work, and $\Delta Q(K)$ is the heat change in the body.

We assume that we know $\Delta U(K)$ and there are no external sources of heat. Heat generates only as a result of dissipation of internal plastic energy, i.e. $\Delta Q(I) = \tilde{K}_p \Delta W^P(K)$,

$\tilde{K}_p = K_p J$. The internal deformation work consists of elastic part $\Delta W^e(K)$ and plastic part $\Delta W^P(K)$. Then:

(41) $\Delta U(K) = \Delta W^P(K)(1 + \tilde{K}_p) + \Delta W^e(K)$

where the increase of the works per unit thickness of the body are:

(42) $\Delta W^e(K) = 1\int_S \sigma_{ij}(x_1,x_2;K)\Delta\varepsilon_{ij}^e(x_1,x_2;K)dS$ $(i,j = 1,2,3; K = 1,2,...L)$

$\Delta W^P(K) = \Delta W_M^P(K) + \Delta W_L^P(K)$

$\Delta W_M^P(K) = \int_{S_p} s_{ij}(x_1,x_2;K)\Delta\varepsilon_{ij}^P(x_1,x_2;K)dS$

Then

(43) $\Delta W_L^P(K) = \dfrac{1}{1 + \tilde{K}_p}\{\Delta U(K) - W^e(K)\} - \Delta W_M^P(K)$

where S is the area of the body in the plane Ox_1x_2 and S_p is the corresponding area of the plastic zone; $\Delta W_p(I)$ is the increase of the plastic deformation work in the plastic zones and $\Delta W_L^P(I)$ - in the band. The latter increase we express in the following way:

(44) $\Delta W_L^P(K) = \sum_{J=1}^{M} \bar{\tau}(J,K).\Delta\bar{\gamma}^P(J,K).\delta(J,K).\Delta S(J,K)$

where $\bar{\tau}(J,K)$ is the average stress in the band zone of length $\Delta S(J,K)$ and $\Delta\bar{\gamma}^P(J,K)$ is the respective increase of the average plastic shear strain. This average shear strain is related to the maximum shear strain in compliance with the accepted distributions (30), (38) or (39). For example, for the (30) distribution law it is obtained:

(45) $\bar{\gamma}^P = 2 max\gamma^P(1 + \dfrac{s}{2\pi\delta} sin\dfrac{2\pi\delta}{s})$

and in the increases (approximately)

(46) $\Delta\bar{\gamma}^P(J,K) = 2\Delta[max\gamma^P(J,K)].(1 + \dfrac{s}{2\pi\delta} sin\dfrac{2\pi\delta(J,K)}{s})$

assuming that for the time interval $\Delta t(K), \delta(J,K)$ does not change.
By analogy:

(47) $\Delta[max\theta(J,K)] = \dfrac{\Delta\bar{\theta}(J,K)}{2[1 + \dfrac{s}{2\delta(J,K)\pi}.sin\dfrac{2\pi\delta(J,K)}{s}]}$

The adiabatic nature of the band connects $\Delta\bar{\gamma}^P$ with $\Delta\bar{\theta}$ ($\Delta(max\gamma^P)$ with $\Delta(max\theta)$, respectively) as follows:

(48) $\rho C_T \Delta\bar{\theta}(J,K) = \tilde{K}_p.\bar{\tau}(J,K)\Delta\bar{\gamma}^P(J,K)$

The stresses $\bar{\tau}(J,K)$ are obtained numerically after simulation of the process (See 5).
The simulation of the process allows to determine the change of the band length $\Delta s_f(K)$ according to the condition (27). The summation of $\Delta W_L^P(J,K)$ up to the moment $t(K)$ we verify if the another critical energy levels W_{2C}^P, W_{3C}^P are achieved. In this case they have transition from II state of the structure into III state, etc. Thus, along the band, the zones of different structures and thermal-mechanical properties are obtained for any t(K) moment. The

15

comparison with the corresponding experiments can be used to determine the type of structure and its thermal-mechanical properties (See § 2.6).

2.5. Development of micro defects in the ASB material. Criteria for damage and macro crack initiation

There are many investigations revealing that with the development of the plastic deformation micro defects will appear in the material mezo structure. It is well known that the two processes: plastic deformation and the damage are connected /[86], [87], etc./. The plastic strain in ASB high values and in the damage may develop /See [37], [42], [44], etc./. In our investigations this was observed as well /See 4/. In accordance with the assumed energy approach the criterion of micro defects initiation will have the form:

(49) $\quad W^P = W^P_{DK}(\beta_o, \theta), \quad (K = 2,3,...)$

For every structure type (K) of the material in ASB there will be energy limit W^P_{DK} above which micro defects will initiate. This limit will depend on the process factors (β_o, θ). Above that limit the damage energy will be added to the internal structure energy, i.e.

(50) $\quad \dot{W}^P = s_{ij}\dot{\varepsilon}^P_{ij} + \eta_D \dot{\varsigma} \quad$ for $W^P > W^P_{DK}$

where η_D is thermodynamically conjugated with ς parameter:

(51) $\quad \eta_D = -\rho \dfrac{\partial Z}{\partial \varsigma}$

where $Z = Z(\sigma_{ij}, \varepsilon^P_{ij}, \beta_o, \theta, \varsigma)$ is in this case the specific free energy depending on the process factors $(\beta_o, \theta, \varsigma)$.

We accept the evolution equation of the internal state parameter in accordance with the statistical concept. A number of investigations show that the evolution of micro defects is in good agreement with Boltzman statistic law [88]. Therefore, we assume the equation in the form:

(52) $\quad \varsigma = Y_D . exp\{ \dfrac{C_D}{K_B J} \langle (W^P - W^P_{DK}) \rangle \}$ for $W^P \geq W^P_{DK}$

where Y_D and C_D are material characteristics; K_B is Boltzman constant. The rate of defect changes shall depend on exceeding the internal structure energy of certain energy limit W^P_{DK} and has an exponential character in compliance with Boltzman statistic law.

With the damage development the macro shear crack will appear at certain internal energy level. The criterion of the macro crack initiation will have the form:

(53) $\quad W^P = W^P_{FK}(\beta_o, \theta, \varsigma)$

The limit W^P_{FK} will depend on the process factors. This is discussed in 2.6.

The connection of the plastic deformation process and damage provoke the dependence of the yield condition on the parameter ς, i.e.:

(54) $\quad F(\sigma_{ij}, \varepsilon^P_{ij}, \beta_o, \theta, \varsigma) = 0$

If the case of Mises type [61] yield condition (54) takes the form:

(55) $\quad F = \tau_o - \tau_p = 0, \qquad \tau_p = \tau_p(\gamma^P_o, \beta_o, \theta, \varsigma)$

γ^P_o and β_o cause hardening of material, while θ and ς - softening.

2.6. Method for verification of the proposed model and identification of model functions and parameters

For the verification of the model and identification of the model functions and parameters we propose the following method realized in stages:

I STAGE. Carrying out experiments for identifying the static and dynamic properties of the high strength steel considered;

II STAGE. Carrying out experiments by cylindrical bodies subjected to dynamic impulse by the incident bar of the "Hopkinson bar" set. The experiments are performed by series of impulses with different intensity. For wich impulse the initiation and growth of ASB in the cylindrical specimens is registered for each impulse. The initiation of shear macro crack along ASB length is also registered.

III STAGE. Carrying out micro structural investigations of the material outside and inside the ASB for the different impulse levels. The type of structure (material) in ASB and its transition. Determination of the damage initiation and growth in the different structure types on ASB as well as in the transition to initiation of shear macro cracks are realized.

IV STAGE. On the basis of the worked out simulation numerical model the measures of stres, strain and thermal states and their changes during the time of the dynamic deformation process are calculated for the different impulses. Numerical procedure based on the method of finite systems is applied.

V STAGE. By the simulation model based on the theoretical model the following is calculated:

- ASB initiation;
- post critical stage and ASB growth (thickness and length) for the different impulses by special approximation of the distribution of plastic strain and temperature along the adiabatic band thickness.

They verify by comparison with the experimental results for the different impulses:

- the criterion of ASB initiation;
- the model presentation of post critical state in ASB.

VI STAGE. Along the ASB, through the simulation model, the internal structure energy, deformation rate and temperature are calculated for the different cases of impulse dynamic impacts. Comparison is made with the experiments at structure level and the internal energies of transition from one into another type of structure are obtained as well as the conditions in which this transition occurs (the values of the process factors - strain rate, temperature and degree of defects). In this way the internal energy levels of transition related to process factors can be determined. The average stresses, plastic deformation and temperature for the points of the middle ASB curve can be found numerically. This permits to obtain information about the relation between these measures for the different new structures formed in post critical condition states of the ASB.

VII STAGE. Numerically, by the simulation model based on the theoretical assumptions and by comparison with the experiments the internal energy levels of micro defects initiation can be defined in the different types of new structure and their development. Thus the critical energy levels for damage initiation and the parameters of evolution of these defects identified.

VIII STAGE. Numerically and by comparison with the experiments the internal energy levels of shear macro cracks initiation in ASB can be obtained for the different type of new structures.

17

The method suggested combines experimental, model and numerical studies to obtain information which by other means is very difficult to achieve. The method is applied to typical high strength steel and the results are discussed in § 6.

3. EXPERIMENTAL INVESTIGATIONS AT MACRO LEVEL

3.1. Experiments to determine high strength steel properties

Static and dynamic testing are carried out for the determination of the mechanical, strength and thermal properties of the used high strength steel with composition and heat treatment presented in § 4.

The dynamic experiments were performed on experimental set "Hopkinson bar" (Fig. 3.1).

The set consists of Hopkinson bar and measuring apparatuses.
1. Hopkinson bar including:
   - pneumatic gun for acceleration of the striker
   - incident намоварващ bar suspended on elastic pads
   - receiving предаващ bar suspended on rubber pads
   - rear pad to limit the motion of the receiving bar
   - strain gauges reading axial deformation
   - incident bar with cone tip suspended on elastic pads of dimensions given in Fig. 3.2.
2. Measuring installation consisting of:
   - two fast amplifiers
   - two-channel fast Automatic Digital Convertor (sample rate sous) with memory and monitor
   - interface plate
   - Computer with monitor to collect the experimental data

Block diagram of the connections is shown in Fig. 3.3.

For the steel considered in quenched state the following is found:
   - initial static yield limit ($\sigma_p^o = 1530$ MPa);
   - static plastic hardening;
   - dynamic hardening for different deformation rates;
   - thermal softening;

After approximation of the experimental data the following major dependence is established:

$$(56) \quad F = \tau_o - \tau_p = 0, \qquad \tau_p = [(A + B\gamma_o^n)(1 + C.ln(\frac{\beta_o}{D}))](1 + \tilde{\theta})$$

where $\tilde{\theta} = \dfrac{\theta}{T_f - T_o}$, T_f is melting temperature; A, B, C, D, n and m are material constants.

For the studied by us steel they have the following values: $A = 1552 MPa$, $B = 309 MPa$, $C = 0.015$, $n = 1.03$, $D = 0.013$, $m = 1.03$.

3.2. Experiments for ASB nucleation and development in cylindrical specimens

The following experiments were carried out to determine ASB nucleation and development. In the "Hopkinson bar" set incident bar with modified tip in accordance with the principle shown in Fig. 3.4 was used. The experiments were performed in the following sequence:

19

1. The test body and operational surfaces of the incident and receiving bars are coated by fine lubricant to decrease friction
2. The test body is centered and pressed between the cone tip of the incident bar and the receiving bar.
3. By means of vacuum the striker is charged in the barrel of the pneumatic gun
4. The tank of the gun is filled with compressed air up to defined operational pressure. By variation of the operational pressure of the pneumatic gun the velocity of the striker is regulated and from there the amplitude of stress (deformation) of the dropping impulse, energy respectively, that is applied to the test body.
5. The apparatuses are prepared for single record.
6. By opening the gun valve the pressure from the tank enters the barrel and accelerates the striker.
7. Striking the front flat head of the modified incident bar the striker produces in it an elastic stress wave (deformation) of certain energy.
8. Through the cone tip of the incident bar the energy is transferred to the test body being+divided in three basic parts:
   - energy for deformation of the test body;
   - reflected energy that goes back to the incident bar;
   - transmitted energy that passes over to the receiving bar through the test body.
9. The characteristics of the impact (Fig. 3.5), reflected (Fig. 3.6) and transmitted (Fig. 3.7) deformation impulses are recorded in the two channel Automatic numerical processor.
10. By program, by means of interface plate, the data from the Automatic numerical processor are transferred to the computer to be saved and further processed.

Two series of experiments were carried out with stepwise increase of energy (amplitude of deformation stress)) of the dropping impulse.
The first series of experiments is performed with variation of the gun operational pressure from 0.5 to 4 atmospheres and step of half an atmosphere. The loaded test bodies are subjected to macro and micro structural analyses to establish the presence of the phenomenon adiabatic sliding lines. The range of the second series of test is determined - 2 to 3 atmospheres. In that range of investigating the phenomenon adiabatic sliding lines tests of test bodies are carried out at pressure step of 0.2 atmospheres. The energies of all experiments are calculated and macro and micro structural analyses of the tested bodies are made.

The results of the tests are presented in Table 3.1 where:
   U_i - energy of the impact impulse
   U_r - energy of the reflected impulse
   U_t - energy of the transmitted impulse

The results of the micro structural studies of the produced ASB are presented and analyzed in § 4. The simulation numerical method describing their nucleation and development is presented in § 5.

Table 3.1

No	Specimen	Wi [J]	Wr[J]	Wt[J]
1	25-26	27.3	3.8	11.6
2	29-30	40.2	3.8	14.2
3	27-28	53.1	4.0	16.9
4	31-32	66.9	6.7	19.9
5	5-6	67.8	6.2	8.4
6	19-20	80.6	8.9	21.0
7	21-22	82.8	6.5	21.9
8	1-2	85.8	6.9	21.3
9	23-24	96.9	7.2	25.5
10	3-4	114.3	7.8	18.7
11	3-4	114.3	7.9	19.5
12	41-42	118.9	7.1	31.8
13	45-46	135.4	10.8	31.4
14	43-44	140.3	12.3	19.0

4. CHANGES OF MICROSTRUCTURE CAUSED BY DEFORMATION LOCALIZATION IN ASB

The chemical composition of the investigated steel is shown on Table 1.

Table 4.1

% C	% Mn	% Mo	% Ni	% Cr	% Si
0,19	1,38	0,17	0,16	0,08	1,35

Delivery material was annealed rolled sheet with hardness on rolling plane HB=12-15. Cylindrical test pieces of 20 mm diameter, 10 mm length with axis parallel to the rolling plane were heat treated as follows: 10 minutes tempering at 970°C and quenching in water, 3 hours tempering at 270°C and cooling in water. The hardness of heat treated specimens was HRc=45.

Split Hopkinson bar with conic top of incident bar, cone diameter 4 mm, cone angle 60 deg., was used for the dynamic loading. Absorbed in the specimen energy W_a calculated as $U_a=U_i-U_r-U_t$ was used for tesing conditions and specimens designation. ASB formation and propagation were studied by light (LM) and scanning electron microscopy (SEM) on axial cross-sections of tested specimens after etching in 5%HNO_3 or $HCl:HNO_3=3:1$ solution. The microstructure of different zones along ASB was analyzed by transmission electron microscopy (TEM) on thin foils prepared parallel to the plane of SEM samples. Thin foils were produced by electrolytic jet-polishing in 10%$HClO_4$-90%CH_3COOH solution.

Results and Discussion

A. Macrostructure

Set of macrographs of specimens dynamic loaded with increasing energy is presented on Figs.1-9. Only traces of deformation localization were observed in specimens tested at energy under 12 J (Fig. 4.1). The tests of higher energy produced ASBs of semi-conic shape starting from the edges of the impact crater (Figs.3-9). The base diameter and base angle of ASB cone were approximately equal to the dimensions of the incident bar top. ASB appeared as continuous semi-conic line only in the specimen tested at 109 J (Fig. 4.9). In the other specimens ASBs were approximately straight lines whit tendency for bending towards specimen axis at the highest energy levels (Fig. 4.8). ASB lengths increased with energy (Table 2) and ASB widths decreased linearly with the distance from crater surface (Figs.10-15).

Table 4.2

No	Specimen	Ua [J]	ASB length [μm]	Crack length [μm]
1	25-26	12	-	
2	29-30	22.2	100	
3	31-32	40.3	328	
4	19-20	50.7	800	725
5	21-22	54.4	975	
6	23-24	64.2	1450	1368
7	41-42	80.0	1760	
8	45-46	93.2	2812	
9	43-44	109.0	3250 full cone	

Cracks developed in some of the specimens, but no clear relation between testing conditions and crack length could be established (Table 2). Cracking usually initiated at the edge of crater bottom but in some of the specimens cracks were detected at random distance from ASB start.

B. Microstucture

The microstructure of heat treated material was tempered lath martensite with length of martensite laths under 10 mm and width under 1 mm (Fig. 4.16). Grain boundaries of parent austenitic grains (diameter about 20-30 mm) were well defined. Fine carbide needles about 500 nm long and 10 nm thick were arranged in laths interior at 60 deg. to lath length.

The larger part of ASB length (more than 90%) appeared white in LM when etched in 5%HNO$_3$ solution (Figs.17-23). Cracks initiating from crater edge developed along the ASB middle line in some of the specimens (Figs.19,21). Islands of relatively large grained metal (grain diameter over 1 μm) were left between crack walls.

SEM observations revealed various microstructure zones along the length of ASB. Homogenous relief of fine etching pits was found outside cracks and in the initial part of ASBs without cracks (Fig. 4.24). The more severe etching by HCl:HNO$_3$=3:1 solution revealed in this part fine cells or grains (diameter under 500nm) (Fig. 4.25). The boundary between ASB structure and matrix was rather diffuse and the adjacent martensite laths were not affected by the deformation.

Further along the ASB the structure of fine etch-pits and cells gradually transformed into packages of parallel laths oriented along the band direction (Fig. 4.26). The boundary between ASB and the matrix in this region was more sharp and the adjacent matrix martensite laths showed some tendency for orientation along ASB direction.

At the very ASB end the longitudinal orientation of laths was substituted by fan-like orientation (Fig. 4.27). The band of localization broadened and gradually dissipated into the non-affected structure. This segment (less than 10% of ASB length) appeared dark in LM, which is characteristic for the behavior of deformation shear bands.

Several types of transformed microstructure were discovered by TEM observations: martensite laths with altered internal structure, dislocation cells, bands of ultrafine grains. All transformations were accompanied by carbides dissolution and all transformed structures showed accelerated rate of electrolytic thinning. It is worth to note that only body centered cubic crystal lattice (BCC) and no traces of face centered cubic crystal lattice (FCC) was registered by means of electron diffraction in all zones with transformed structures.

Altered internal structure of martensite was observed in bands 1-2 μm wide. They contained longitudinally oriented laths similar to those of martensite but of larger width (up to several μm) (Fig. 4.28). Significant changes of carbide phase and dislocation structure were observed in laths volume. Carbide needles which were present in the initial tempered martensitehad suffered different stages of dissolution in the modified laths (Fig. 4.16). The dissolution was complete in the central part and partial near the periphery where only traces of half-solved particles could be seen (Fig. 4.29). No modification was found in the structure of modified laths-adjacent matrix boundaries.

The high density dislocation structure which is a base characteristic of martensite was absent in modified laths. Only small number of dislocations were observed in separate islands in laths volume (Fig. 4.30). They were arranged in dislocation cells with diameter under 0,5 μm and wall width about 100 nm, slightly elongated along lath direction. Features of recrystallization contrast were observed in some places on TEM images of cells (Fig. 4.30a).

23

As a rule no diffraction spots could be obtained from regions of laths without defects but the regions containing dislocation cells showed BCC crystal lattice.

The next type of modified structure was observed always in the form of band of metal attached to the wall of narrow cracks. The band presented on Fig. 4.31 was less than 1 μm wide and was divided by transverse low-angle boundaries into grains up to 500 nm long. The diffraction patterns from ultrafine grains corresponded to BCC structure which was in accordance with the observed dislocations arrangement in tangles.

Crack trajectory in the initial part of ASB contained segments parallel to ASB direction divided by kick-offs along impact axis direction (Fig. 4.19, 4.21, 4.32a). The frequency of kick-offs decreased with the distance from crater and further the crack propagated as a continuous line. This line run always at the outer side of ASB cone along the boundary between ASB and adjacent matrix (Fig. 4.32b). The middle-line crack propagation was characteristic for ASB zones with enlarged grains, and the one-side propagation - for zones with parallel arrangement of laths or directionally grown fine grains. Crack walls in the second case had characteristic jagged shape with average length of separate steps 0,5 μm (Fig. 4.32c) which corresponded to the diameter of cells and ultrafine grains.

Discussion

The development of metallurgical processes leading to formation of structure in the different zones of ASB could be better explained in reverse sequence - starting from the end of ASB. On the base of microstructural observations the following characteristic zones along ASB length could be determined:

- Zone A: Fan-like orientation of martensite laths
- Zone B: Parallel arrangement of martensite laths
- Zone C: Parallel laths of modified martensite
- Zone D: Chains of directionally grown ultrafine ferrite grains
- Zone E: Recrystallized ferrite grains.

In Zone A the deformation causes only reorientation of tempered martensite laths without any change of their characteristics. The localization is not very active and this results in the larger width of deformation zone. Zone B is characterized by localization of deformation in a band with strictly parallel arrangement of martensite laths. Deformation conditions are still too mild to provoke phase transformations and the laths of tempered martensite preserve all characteristics of initial state. These facts together with the dark appearance permit to classify ASBs in Zones A and B like deformation shear bands.

The white contrast of the whole remaining part of ASB results on phase transformations, i.e. it is of transformation type. Transformation includes carbides dissolution in all zones of this part and this is probably the main reason for the white contrast of ASB.

The dissolution of carbides in Zone C is accompanied by annihilation of defects in laths interior without change of laths shape, parallel orientation or boundaries character. On the base of the temperature necessary for carbides dissolution the temperature increase in this zone should be estimated as 700°C or more.

The islands of dislocation cells in laths interior in Zone C result most probably on the incomplete annihilation of initial dislocation structure. The cells can serve as nuclei for the next stage of recrystallization of fine ferrite grains. The transformation of tetragonal martensite crystal lattice to BCC δ-ferrite demands temperature rise up to 1400°C. It is hard to explain the absence of austenite transformation in this zone, but similar results have been reported by other investigators also [90, 91].

The directional growth of columnar crystals observed in Zone D can result only on rapid crystallization of remelted metal which demands temperature rise in Zone D up to 1500°C.

Unfortunately we could not study by TEM the structure of larger grains bordered by crack walls in Zone E but on our opinion they are produced by secondary recrystallization of primary ultrafine grains. The realization of this recrystallization mechanism is due to the larger duration of high temperature cycle in Zone E.

The number of observed zones depends on the conditions of dynamic test. At energy 22.2 J we registered only structure types A and B (Fig. 4.17). The full sequence of transformation was observed in the specimen loaded at 64.2 J (Fig. 4.21).

Our observations show that fracture always occurs in the transformed parts of ASB. In Zone D where the grains are produced by directional growth the cracks propagate along the outer ASB side only. This is due to the different strain condition at the two ASB boundaries, but it can result on some difference in their structure and properties also (for example non-homogenous carbon distribution). Cracking is most active in Zone E where the weakest structure element are obviously the boundaries of largest grains located along ASB middle-line.

5. SIMULATION NUMERICAL MODEL OF THE PROCESS OF ASB INITIATION AND GROWTH IN HIGH STRENGTH STEEL

We develop simulation numerical model for the ASB initiation and growth in cylindrical bodies subjected to impulse loading. The bodies are made of high strength steel (See Table 4.1). The simulation model is based on the theoretical model in § 2. Descritaziation of the process in time steps and space co-ordinates is accepted. The various impulse effects are presented in Table 4.2.

The simulation model contains the following components:

1. Calculation of the stressed and deformed condition and their variation in time till ASB initiation. The cylindrical bodies are loaded by impulse in accordance with the scheme in & 3 (See Table 4.2). The major system of equations describing processes and based on the model in item 2 has the form:

a) Equations of motion

$$(57) \quad \frac{\partial \sigma_r}{\partial r} + \frac{\partial \tau_{rz}}{\partial z} + \frac{\sigma_r - \sigma_\theta}{r} = \rho \frac{\partial v_r}{\partial t}$$

$$\frac{\partial \sigma_z}{\partial z} + \frac{\partial \tau_{rz}}{\partial r} + \frac{\tau_{rz}}{r} = \rho \frac{\partial v_z}{\partial t}$$

where $\sigma_r(r,z,t)$, $\sigma_\theta(r,z,t)$, $\sigma_z(r,z,t)$, $\tau_{rz}(r,z,t)$ are components of Cauchy stress tensor; $v_r(r,z,t)$ and $v_z(r,z,t)$ are the speeds of the points of the body. The axial symmetry of the problem is taken into account. $r \in [0,R]$ where R is the radius of the test body (R=10 mm), $z \in [0,H]$ where H is the height of the test body (H=10 mm) /See Fig. 5.10/, $t \in [t_0,t_1]$ t_0 - start, t_1 - end of impulse duration (t_1-t_0=25μs).

b) Geometrical relations in velocities:

$$(58) \quad \dot{\varepsilon}_r = \frac{\partial v_r}{\partial r}, \; \dot{\varepsilon}_\theta = \frac{v_r}{r}, \; \dot{\varepsilon}_z = \frac{\partial v_z}{\partial z}, \; \dot{\gamma}_{rz} = \frac{1}{2}\left(\frac{\partial v_r}{\partial z} + \frac{\partial v_z}{\partial r}\right)$$

where $\dot{\varepsilon}_r(r,z,t)$, $\dot{\varepsilon}_\theta(r,z,t)$, $\dot{\varepsilon}_z(r,z,t)$, $\dot{\gamma}_{rz}(r,z,t)$ are components of the strain rate tensor.

c) The constitutive equations for elasto-plastic material in isothermal conditions (T_0=const)

$$(59) \quad \dot{\varepsilon}_r = \dot{\varepsilon}_r^e + \dot{\varepsilon}_r^p, \; \dot{\varepsilon}_\theta = \dot{\varepsilon}_\theta^e + \dot{\varepsilon}_\theta^p, \; \dot{\varepsilon}_z = \dot{\varepsilon}_z^e + \dot{\varepsilon}_z^p, \; \dot{\gamma}_{rz} = \dot{\gamma}_{rz}^e + \dot{\gamma}_{rz}^p$$

where

$$\varepsilon_r^e = \frac{1}{E}[\sigma_r - v(\sigma_z + \sigma_\theta)]$$

$$\varepsilon_\theta^e = \frac{1}{E}[\sigma_\theta - v(\sigma_z + \sigma_r)]$$

$$\varepsilon_z^e = \frac{1}{E}[\sigma_z - v(\sigma_r + \sigma_\theta)]$$

$$(59) \quad \gamma_{rz}^e = \frac{(1+v)}{E}\tau_{rz}$$

where E = const is Young elastic modulus (E=2,1.10^{11} N/m^2), v = const is Poison coefficient (v=0,3).
Also:

$$\dot{\varepsilon}_r^P = \lambda_p \left[\frac{2}{3}\sigma_r - \frac{1}{3}(\sigma_z + \sigma_\theta) \right]$$

$$\dot{\varepsilon}_\theta^P = \lambda_p \left[\frac{2}{3}\sigma_\theta - \frac{1}{3}(\sigma_z + \sigma_r) \right]$$

(60)

$$\dot{\varepsilon}_z^P = \lambda_p \left[\frac{2}{3}\sigma_z - \frac{1}{3}(\sigma_r + \sigma_\theta) \right]$$

$$\gamma_{rz}^P = \lambda_p \tau_{rz} , \quad \dot{\varepsilon}_r^P + \dot{\varepsilon}_\theta^P + \dot{\varepsilon}_z^P = 0$$

for

(61) $\lambda_p = \begin{cases} 0, & \tau_0 < \tau_p \ or \ \tau_0 = \tau_p \ and \ \ s_{\alpha\beta}\,\dot{\sigma}_{\alpha\beta} \le 0 \\ \tau_0 & for \ \ \tau_0 = \tau_p \ \ and \ \ s_{\alpha\beta}\,\dot{\sigma}_{\alpha\beta} = 0 \end{cases}$

for /See formula (56)/

$$F = \tau_0 - \tau_p$$

(62) $\tau_p = (A + B\gamma_0^n)(1 + C\ln(\beta_0/D))(1 - \tilde{\theta}^m)$

for A=1552 MPa, B=309 MPa, C=0,015; n=1,03,

(63)   D=0,013, m=1,03 /See & 3.1/

The initial state (t=t_0) is assumed to be unstressed and undeformed. The boundary conditions are formulated with preset pressing speed at z=H and zero speed at z=0. The lateral surfaces of the cylindrical bodies are free.

The formulated problem is solved by the Method of finite differences /See & 2/ with descritaziation by time step Δt (Δt=0.01 μs) and space co-ordinates Δr and Δz ($\Delta r = \Delta z = 0.2$ mm).

The differential operators we replace by difference ones in the following scheme:

$$D_t f(r,z,t) = \frac{f(I,J,K+1) - f(I,J,K)}{\Delta t}$$

(64) $D_r f(r,z,t) = \frac{1}{2\Delta r^2}\{f(I+1,J,K+1) - 2.f(I,J,K+1) + f(I-1,J,K+1)\}$

$$D_z f(r,z,t) = \frac{1}{2\Delta z^2}\{f(I,J+1,K+1) - 2.f(I,J,K+1) + f(I,J-1,K+1)\}$$

where I=1,2,...,N (discreteaziation for r); J=1,2,...M (discreteaziation for z); K=1,2,...,L (discreteaziation for t)

For every moment of the time (K+1) we know the process measures for moment (K) including also the initial conditions for K=1.

We use iterative, according to the block diagram of the Method of finite differences, the values of the process measures in the nodes (I, J) (Fig. 1.7). The calculations account for the boundary conditions. The values of the steps Δt, Δr and Δz are selected in such a way as to meet the condition of convergence /See § 1.4/.

2. At every step of the process we verify the condition of ASB formation /§ 2.2/

3. After ASB formation we apply the approach of § 2.4 by setting distribution of the plastic deformation and temperature in the band thickness according to formulae (39) for post critical condition of the material. We calculate the maximum and average values of stresses $\bar{\tau}$, angular plastic deformations $\bar{\gamma}^P$ and temperature $\bar{\theta}$ for every point from the ASB middle line and for the corresponding thickness δ.

4. Experimentally /See § 4/ the new structures of the material in ASB are identified and by the simulation model the values of the inner structure energy calculated along the band length. The values of this energy are numerically defined for the points of transition from one

structure in another, i.e. numerical information for the boundary values of the inner structure energy is obtained in compliance with the theoretical model in § 2.5.

5. The values for the inner structure energy for micro cracks initiation and also for the formation of shear macro cracks along the ASB length are determined by numerical-experimental method.

The method described above was applied for numerical simulation and calculation of the physical fields in the cylindrical area of 10 mm height and 10 mm radius. We assume that initially the body (steel cylinder) is at rest, not subjected to internal stresses and is uniformly heated to room temperature T_0. One of the cylinder ends is loaded under the action of external force doing a work for a time interval, known from the experimental data. The pressure is applied on area of the cylinder upper base having the shape of a circle of 2 mm radius. The following values to the material parameters are assigned in order to compute numerical results.

$$\rho = 7640 \text{ kg/m}^3; \qquad T_m = 1793 \text{ K} \qquad c = 477 \text{ J/kg}^0\text{C}$$

We consider two types of loading: in the first case the duration of the impulse is 25 μs and the work done by the external force is U=50.7 [J] corresponding to experiment No.4 (Table 4.2) and in the second one with the same duration of 25μs and U=64.2 [J] corresponding to experiment No.6. The calculated physical fields as functions of time and ASB length for the both cases are presented at fig. 5.1 – 5.24.

6. APPLICATION OF THE METHOD IN & 2.6. DISCUSSION OF THE RESULTS

The method described in & 2.6 was applied to armour martensite high strength steel. In order to verify the energy approach we compare the ASB parameters (lengths, widths, etc.) obtained experimentally for various impulses applied to the cylindrical specimens with those calculated by simulation approach.

Fig. 5.1, 5.2 and 5.3 present the evolution of the effective stress, effective plastic deformation and the temperature, after the beginning of localization, in points along the ASB length for loading force doing work of U=50.7 [J], and duration of action Δt=25 μs. As seen in Fig. 5.1 the effective stress decreases rapidly after achieving its maximum value. The stress drop is quite rapid near to the crater surface and decreases slowly with the distance. There are various concepts for determination of the moment of ASB initiation. In [65] it is postulated that ABS starts to develop when the effective stress drops to 90% of its maximum value. In [66] for beginning of ASB it is assumed the moment when the effective stress has dropped to 80% of its maximum value. Depending on the choice of a criterion for ASB nucleation the values of the effective plastic deformation and the temperature varied in the moment of its occurrence. The temperature rise at the initiation of the shear band is nearly 100^0C but the temperature reaches the melting temperature about 10 μs later. The effective deformation and temperature continue to grow by increasing speed in the post localization period till the end of the loading action in the respective point, after which gradually reach saturation. Depending on the accepted criterion for ASB beginning the values of the times can be determined of ASB nucleation in the different points. Fig. 5.4 depicts the history of the external plastic work done in points along the ASB length.

The distribution of the calculated effective plastic deformation, temperature and external work along ASB length are presented in Fig. 5.5, 5.6 and 5.7. Fig. 5.8 presents the change of ASB with the increase of its length. The width is calculated on the basis of the condition for adiabatic process in the ASB zone.

The evolution of the effective stress field in a cross-section of the considered cylindrical area is presented in Fig. 5.9. In analogy, Fig. 5.10, 5.11 show the history of the distribution of effective plastic deformation and temperature. In Fig. 5.12 the ASB development can be observed in space and time.

Analogous results are obtained also in the numerical simulation of dynamic loading of the considered cylinder by external pressure of duration Δt=25 μs and loading force doing external work U=64.2 [J].

Fig. 5.13, 5.14 and 5.15 present the evolution of the effective stress, effective plastic deformation and temperature in points along ASB length. The evolution of the performed external work in points along ASB length is presented in Fig. 5.16.

The distribution of the calculated effective plastic deformation, temperature and external work along the ASB length are shown in Fig. 5.17, 5.18 and 5.19. It can be seen in Fig. 5.20 the change of the ASB width with the increase of its length. The evolution of the effective stress field as well as that of the effective plastic deformation and temperature in a cross-section of the considered cylindrical area are presented in Fig. 5.21, 5.22 and 5.23, respectively. The ASB development in this case is demonstrated in Fig. 5.24.

The comparison of the experimental with numerical results shows satisfactory coincidence. The results of the numerical simulation (Fig. 5.12, 5.24) confirm the experimentally observed fact that the produced ASBs are cone shaped and start from the edges of the crater produced by incident bar tip. The comparison of the calculated width of ASB as a function of its length (Fig. 5.8, 5.20) with the experimental results (Fig. 4.11, 4.13) shows adequate coincidence. The calculated temperature along the length of ASB (fig. 5.6, 5.18) confirms the formation of structure zones C (type II) and D (type III) observed in & 4.

29

The application of the theoretical-experimental and numerical methods provides the possibility to determine a number of energy boundaries for the accumulated inner structure energy U^P.

In transition from ASB zone of matrix structure (type I) in structure zone C (type II) the following data were obtained:

- beginning - about 4.5 - 5 µs after ASB initiation
- temperature - 700^0C
- effective plastic deformation - 0.6 - 0.7
- effective plastic deformation rate - $4.5 \times 10^5 \, s^{-1}$
- density of plastic work - $2 \times 10^9 \, [J/m^3]$
- effective stress - 700-800 MPa

In transition from ASB zone C (structure type II) into structure D (type III):

- beginning - about 8 - 9 µs after ASB initiation
- temperature - 1400-1500^0C
- effective plastic deformation - 2.5
- effective plastic deformation rate - $3 \times 10^5 \, s^{-1}$
- density of plastic work - $6 \times 10^9 \, [J/m^3]$
- effective stress - 450-500 MPa

CONCLUSIONS

1. Integrated energy approach is presented for theoretical modeling of the process of ASB initiation, their post critical state, structure changes in the adiabatic band material, micro cracks and macrocracks initiation in the band.

2. The approach with a priory assumed shape of the plastic strain and temperature distribution across the ASB thickness is found suitable for overcoming the considerable difficulties in modeling of the new formed structures in the bands.

3. The proposed method for description of ASB initiation and growth combines well experimental, theoretical and numerical results. It has been experimentally verified for high strength steel.

4. There are obtained the new results about micro structural changes occurring in the plastic strain localization band. Successive structure zones are defined along the ASB length and conclusions drawn for the temperature increase required for the transformations in the zones.

5. It was found out by comparison with experimental results that by the numerical simulation method can be obtained for the critical levels of the internal structure energy and for the process parameters inside and outside the localization band.

6. The obtained experimental, theoretical and numerical results are a good basis for future investigations with further model development for taking into account additional effects like: induced anisotropy, microdefects development and macrocracks propagation along the band length.

REFERENCES

1. Charalambakis N. C, E. N. Honstis, Adiabatic shearing of one-dimentional thermoviscoelastic flows caused by bondary and internal forces, Eng. Anal., 1985, vol. 2, No 4, pp.205-210.

2. Bitans K., P.W.Whitton, Stress-strain curves for oxygen-free high conductivity copper at shear strain rates of up to $10^{3\,S-1}$, Inst. Mech. Eng., vol. 185, No 70/71, p. 1149-1158.

3. Arnold V.I., Bifurcation and singularities in Mathematics and Mechanics, XVII Int. Cong. Theor. Appl. Mech., Moscow, 1988, Opening Conference.

4. Son N.Q., Stability and bifurcation in dissipative media, Proceed. of IUTAM Congress, 1993, pp. 339-353.

5. Son N.Q., C. Stolz, G. Debruyne, Energy methods infracture mechanics: stability, bifurcation and second variations, Eur. J. Mech. A /Solids, 1990, vol. 9, pp. 157-173.

6. Petryk H., Instability of plastic deformation processes, Proceed. XIX th. IUTAM Congress, Kyoto, 1996, pp.1-20.

7. Desoyer T., S. Leroux, Etude de la localization pour une loi de comportement elastique - endommageable avec gradients de deplacement d'ordre superieur, 1994, C. R. Sci. Paris, t. 318, ser. II, pp. 277-282.

8. Lippmann H., Velocity field equations and strain localization in rigid - plastic materials, Int. J. Sol. Str., 1989, vol. 25, No 5, pp. 459-464.

9. Moss G. L., D. S. Pitchard, Adiabatic shear band velocities, J. de Physique, C-5, 1985, No 4, pp. 315-321.

10. Ortiz M., Y. Leroy, A. Needleman, Comp. Meth. Appl. Mech., 1987, vol. 61, pp. 189-214.

11. Aifantis E.C., J. Eng. Mater. Technol., 1984, vol. 106, pp.326-330.

12. Pomey J., Apercu sur la plasticite adiabatique, Annals of the C.I.R.P., 1966, vol.13, pp. 93-109.

13. Pecherski R. B., Macroscopic measures of the rate of deformation produced by micro-shear banding, Arch. Mech., 1997, vol. 49, No 2,pp. 385-401.

14. Guelin P., W.K. Nowacki, H.V. Nguyen, Localization of thermoplastic deformation in the case of simple shear, J. de Physique, France -7, 1997, C-3, d'aout 97.

15. Gary G., W.K. Nowacki, J. de Physique, C-8. vol.4, sept. 94.

16. Bai Y. L., J. Mech. Phys. Sol., 1982, vol.30, No 4, pp.195-210.

17. Fressengeas C., A. Molinari, Formation des bandes de cisaillemant: une analyse de stabilite relative, J. de Physique, C-51985, pp.283-288.

18. Nicolis G., I. Prigogine, Self-organization in nonegnilibrium systems, J. Wiley & Sons, N.Y., 1977.

19. Gradi D., L. Kipp, The growth of inhomogeneneons thermoplastic shear, J. de Physique, C-5, 1985 pp.291-298.

20. Ludygowski T., P. Perzyna, Localized fracture in inelastic polycristalline solids under dynamic loading processes, Int. J. Damage Mech., 1997, vol.6,pp.364-407.

21. Pecherski R. B., Macroscopic effects of micro-shear banding in plasticity of metals, Acta Mech., 1998, vol. 131, pp. 203-224.

22. Becker K.H., H Lippmann, C. Sailer, E. Teubl, Localization and dead metal zones in warm extrusion, Ad. Techn. of Placticity, 1988, vol. 1, pp.556-573.

23. Perzyna P., Instability phenomena and ASB localization in thermoplastic flow processes, Acta Mech., 1994, vol.106,pp.173-205.

24. Perzyna P., Analysis of the influence of various effects on criteria for ASB localization in single cristals, Acta Mech., 1998, vol. 129, pp 31-62.

25. Perzyna P., Analysis of the influence of anisotropic effects on ASB localization phenomena, IUTAM Symposium on Anisotropy, D.F. Parker and A.H. England (Eds), 1995, Kluwer Acad. Publ., pp. 201-210.

26. Perzyna P., ASB localization in rate dependent plastic solids, MECAMAT-91,1993, C. Teodosiu, F. Sidoroff (Eds), Balkema, Rotterdam, pp.247-254.

27. Perzyna P., K. Korbel, Analysis of the influence of the substructure of a cristal on ASB localization phenomena of plastic deformation, Mech. of Mat., 1996, vol. 24., pp. 141-158.

28. Duszek M., Perzyna P., Analysis of anisotropy and plastic spin effects on localization phenomena, Arch. Appl. Mech., 1998, vol. 68, pp. 352-374.

29. Perzyna P., ASB localization fracture of solids in dynamic loading processes, J. de Physique, C 8, 1994,pp. 441-446.

30. Seaman L., D.R. Curran, D.C. Erlich, T.Cooper, Q. Dullum, Shear band observation and derivations of requirements for shear band model, J. de Physique, C 5, 1985, pp. 273-282.

31. Dorneval R., J. P. Ausart, Cisaillement adiabatique; influence d'une predeformation, J. de Physique, C-5, 1985, pp. 299-306.

32. Sangoy L., J. Moureaud, Etude du cisallement adiabatique dans les aciers a blindage soumis a des tirs de perforation, J. de Physique, C-5, 1985, pp. 307-314.

33. Wright T. W., R.C. Batra, Further results of the initiation and growth of ASB at high strain rates, J. de Physique, C-5, 1985, pp. 323-330.

34. Curran D.R., L. Seaman, Compitational models for nucleation, growth and coalescence of ASB, J. de Physique, C-5, 1985, pp. 395-401.

35. Bontcheva N., A. Baltov, St. Todorov, M. Pesheva, J. of Theor. Appl. Mech., 1988, vol. 19, No 4, pp. 85-94.

36. Bontcheva N., A. Baltov, Influence of anisotropic hardening on plastic localization during metal forming processes, (NRS-Symposium, "Yielding, Damage and Failure of Anisotropic Solids, Vilar-de-Lans, 1990, pp. 199-206.

37. Bontcheva N., A. Baltov, Plastic localization in damage materials, Adv. in Cont. Mechanics (To Horst Lippmann) Ed. J. Najar, Springer-Verlag, Berlin, 1991, pp. 242-251.

38. Bontcheva N., A. Baltov, Initiation of plastic localization in powder based materials, Eur. J. of Mechanics A/Solids, 1998, vol. 17, pp. 807-818.

39. Kafka V. General mesomechanical concept of modeling inelastic deformation, continuum damage and localization, Acta Techn., 1998, vol. 43, pp. 51-75.

40. Kafka V., On mathematical modeling of the material structure changes in the plastic localization band, Proceed.IUTAM - Symposium, Bochum, "Micro and Macro aspects of Thermoplasticity", Kluwer Acad. Publ., 1999, pp. 231-240.

41. Presniakov A. A., Localized plastic deformation, Moskwa, 1983 (in russian).

42. Saje M., J. Pan, A. Neadleman, Void nucleation effects on shear localization in porous plastic solids, Int. J. Fracture, 1982, vol. 19, pp. 163-182.

43. Borre G., G. Maier, On linear versus nonlinear flow rules in strain localization analysis, Meccanica, 1989, vol. 24, pp. 36-41

44. Tvergaard V., Effect of yield surface curvature and void nucleation on plastic flow localization, J. Mech. Phys. Sol., 1987, vol. 35, No 1, pp. 43-60.

45. Doigoni D., D. Zaccaria, Loss of strong ellipticity in non-associative elasto-plasticity, J. Mech. Phys. Sol., 1991, pp. 11-43

46. Rice J. K., The localization of plastic deformation, Theor. Appl. Mech., Koiter (Ed.), 1976, Amsterdam.

47. Anand L., A. Spitzig, Initiation of localized shear bands in plane strain, J. Mech. Phys. Sol., 1980, vol. 28, pp. 113-128.

48. Hutchinson J. W., V. Tvergaard, Shear band formation in plane strain, Int. J. Sol. Struct., 1981, vol. 17, pp. 451-470.

49. Anand L., K. H. Kim, T. G. Shawki, Onset of shear band localization in viscoplastic solids, J. Mech. Phys. Sol., 1987, vol. 35, No 4 pp. 407-429

50. Bai Y. L., Thermo-plastic instability in simple shear, J. Mech. Phys. Sol., 1982, vol. 30, No 4, pp. 195-207.

51. Le Monds J., A. Needlemann, FE analysis of shear localization in rate and temperature dependent solids, Mech. of Mat., 1986, vol. 5, pp. 339-361.

52. Runesson K., P. Steinmann, R. Larsson, On localization in thermo-elastic solids subjected to adiabatic conditions, Eur. J. of Mech. A/Solids, 1999, No 4, pp. 557-580.

53. Rice J. R., Rudnicki J. W., A note of some features of the theory of localization of deformation, Int. J. Sol. Struct., 1980, vol. 16, pp. 597-605.

54. Marchand A., Duffy J., An experimental study of the formation process of ASB in a structural steel, J. Mech. Phys. Sol., 1988, vol. 36, pp. 251-283.

55. Brekelmans W. A., Nonlocal formulation of the evolution of damage in a one-dimentional configuration, Int. J. Sol. Str., 1993, vol. 30, No 11, pp. 1504-1512.

56. Rattazzi D. J., Analysis of ASB in a thick-walled steel tube by the FEM., Thesis, 1996, Blacksburg, Virginia.

57. Tirupataiah Y., V. M. Radhakrishanan, K. R. Raju, Adiabatic shear and associated cracks on balistic steel targets, J. de Physique, C-5, 1985, pp. 312-319.

58. Batra R. C., C. H. Kim., Effect of thermal conductivity on the initiation, growth and band width of ASB, Int. J. Eng. Sci., 1991, vol. 29, No 8, pp 949-960.

59. Cherniavski U.E., A. Cherniakov Localazed plastic deformation in hardening medium, Prikl. Mech., 1984, vol. 20, No12, pp. 85-89 /in russian/

60. Batra R. C., Effect of matarial parameters on the initiation and growth of ASB, Int. J. Sol. Struct., 1987, vol. 23, No 10, pp. 1435-1446.

61. Kolarov D., A. Baltov, N. Bontcheva, Mechanics of plastic media, Moskwa, 1977 /in russian/

62. Paren, W. S. and Tylor, G. I. The head developed during plastic extrusion of metal. Proc. R. Soc., 1925, A 207, pp. 422-426.

63. Johnson. G. R. and Cook W.H. A constitutive model and data for metals subjected to large straines, high strain rates and high temperatures. Proc. 7 Int. Symp. Ballistics, The Hague, The Netherlands, 1995, pp. 541-548.

64. Batra, R. C. and Ko K. J. An adaptive mesh refinement technique for the analysis of shear bands in plane strain compression of a thermoviscoplastic block. Comp. Mechs.1992, No 10, pp. 369-379.

65. Batra, R. C. and Zhang, X. On the propagation of shear band in a steel tube. J. Eng'g Materials & Tech., 1994, pp. 151-161.

66. Deltort, B. Experimental and numerical aspects of adiabatic shear in a 4340 steel. J. de Physique, Colloque C-8, 1988, pp. 447-452.

67. Dragon A., F. Corwery, T. Desoyer, D. Halm, Localazed failure analysis using damage models, Rep. ENSMA, Futuroscope, France, 1996.

68. Baltov A., Analysis of the finite deflection of visco-plastic plates using the Finite System Method, Proceed. IUTAM Symp., Rio-de Janeiro, Springer Verlag, Berlin, 1986, pp. 411-452.

69. Pecherski R., Discussion of sufficient condition for plastic flow localization, Eng. Fr. Mech., vol. 21, 1985 No 4, pp. 767-779.

70. Wright T.W., J.W. Walter, On stress collapse in ASB, J. Mech. Phys. Sol., vol. 35, 1987, No 6, pp. 701-720.

71. Dusrek - Perzyna M., P. Perzyna, ASB localization of inelastic single crystals in symmetric double-slip process, Arch. Appl. Mech., 1996, vol. 66, pp. 369-384.

72. Mogilevski M. A., I. O. Mynkin, Computer modelling of the shear nucleation and development under plane shook wave loading, Inst. Phys. Conf. Ser. No 70, 1984, pp. 119-125.

73. Mengmei X., The factors of the influence on balistic properties of targets of Al-Allays, J. de Physique, C-5, 1985, vol. 46, pp.357-362.

74. Duszek - Perzyna M., K. Korbel. P. Perzyna, ASB localization in single cristals under dynamic loading processes, Arch. Mech., 1997, vol. 49, No 6, pp. 1069-1090.

75. Batra R. C., The initiation and growth of ASB in simple and dipolar materials, Int. J. of Plasticity, 1987, vol. 3, pp. 75-89.

76. Batra R. C., Z. G. Zhu, Dynamic shear band development in a thermally softening bimetalic body containing two voids, Acta Mech., 1991, vol. 86, pp. 31-52.

77. Zbib M. M., E. C. Aifantis, On the localization and postlocalization behaviour of plastic deformation, Res Mech., 1988, vol. 23, pp. 261-277.

78. Clifton R. J., J. Duffy, K. A. Hartley, T. G. Shawki, On critical conditions for shear band formation at high strain rate, Scripta Met., 1984, vol. 18, pp. 443-448.

79. Kim K. H., L. Anand, A note of adiabatic flow localization in viscoplastic solids in Computational Methods for Predicting Material Processing Defects, Ed. M. Predeleanu, Elsevier Publ., Amsterdam, 1987, pp. 181-250.

80. Eringen A. C., Theories of nonlocal plasticity, Int. J. Eng. Sci., vol. 21, 1983, pp. 741-751.

81. Belytschko T., J. Fish, B. E. Engelmann, A Finite element with embedded localization zones, Compt. Meth. Appl. Mech. Eng. 1988, vol. 70, pp. 59-89.

82. R. de Borst, H. B. Munlhans, Gradient- dependent plasticity, Int. J. Num. Meth. Eng., 1992, vol. 35, pp. 521-539.

83. Dvorkin E. N., A. M. Guitino, G. Gioia, FE with displacement interpolated embedded localization lines insensitive to mech size and distortions, Comp. Meth. Appl. Mech. Eng., 1990, vol. 90, pp. 829-844.

84. A. Needlemann, Material rate dependence and mesh sensitivity in localization problems, Comp. Meth. Appl. Mech. Eng., 1987, vol. 67, pp. 68-85.

85. Vodenitcharov St., Doc. Thesis, Institute of Metal Science and Technology, Bulgarian Academy of Sciences, Sofia, 1987.

86. Baltov A., St. Vodenitcharov, Tz. Kamenova, T. Stojchev, Influence of the induced damage anisotropy in Adv. in Fracture Res. And Str. Integriby, Ed. V. V. Panasyuk, Pergamon Press, London, 1996, pp. 589-596.

87. Baltov A. St. Vodenitcharov T. Stojchev, Tz. Kamenova, Influence of the Induced Damage Anisotropy of the Anisotropic Fracture of Metals, J. Mat. Sci. and Techn., 1993, vol. 1, No 1, pp. 33-47.

88. Zachariev G., A. Baltov, Deformation and Fracture of Materials as an Evolutionary Processes on Statistical Basis, J. Theor. and Appl. Mech., 1999, vol. 29, No 4, pp. 60-71.

89. Hill R., Adv. Appl. Mech., 1978, vol. 18, pp. 1-12.

90. Witman C.L., M.A. Meyers, H. Pak Met.Trans., A., v.21A, 1990, 707-716.

91. Kyung-Mox Cho, S. Lee, S.R. Nutt, J.Duffy. Acta Met. Mat., v.41, 1993, 923-932.

APPENDIX
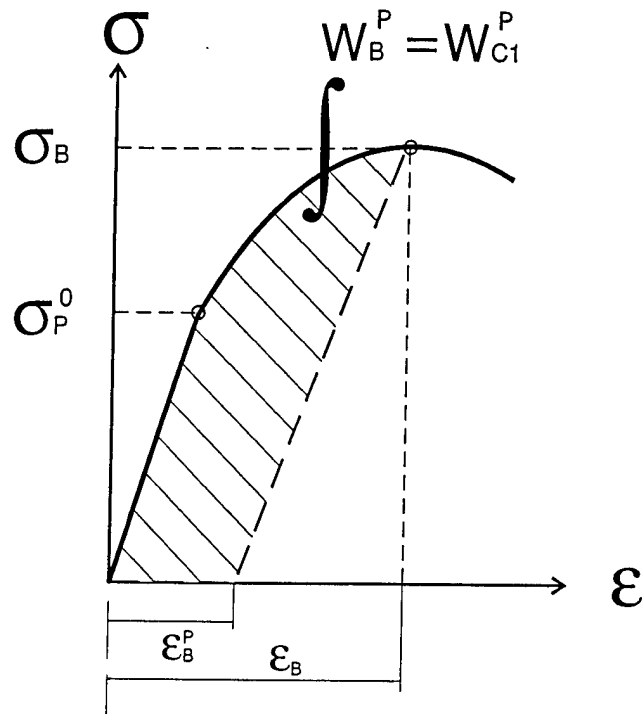
Fig.1.1. Critical condition of neck formation in one dimensional tension
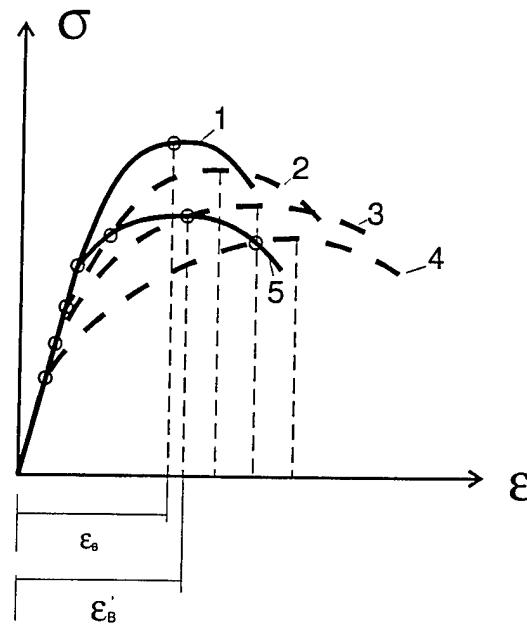
Fig.1.2. Shift of the critical strain > for materials sensitive to temperature.
Curves:
1 - at $20^{\circ}C$
2 - at $1 > 20^{\circ}C$
3 - at $2 > 1$
4 - at $3 > 2$
5 - at variable (due to internal heat source, caused by plastic strain energy dissipation)

$r_T = \overline{K}_p \dot{W}_{p} = \text{const.}$

a.

b.
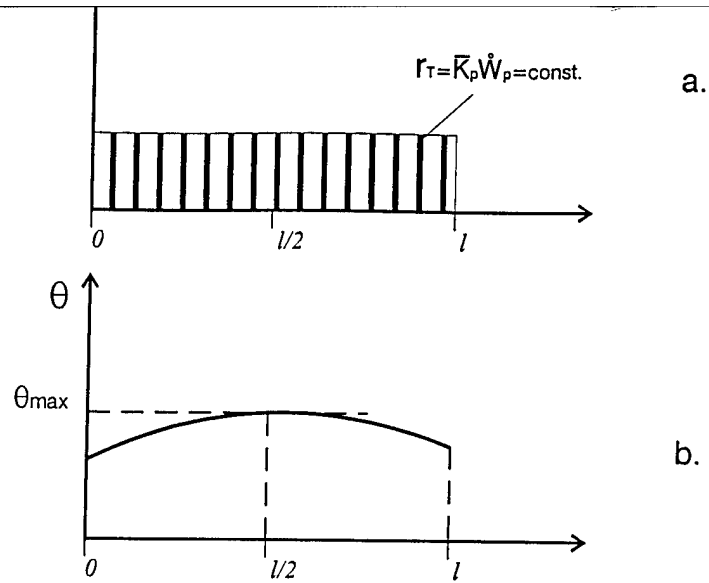
Fig.1.3. One dimensional tension test. Thermal effects
a) constant rate of heat delivery due to constant plastic
strain energy dissipation along the test piece
b) non-homogenous heat distribution along the test pieece
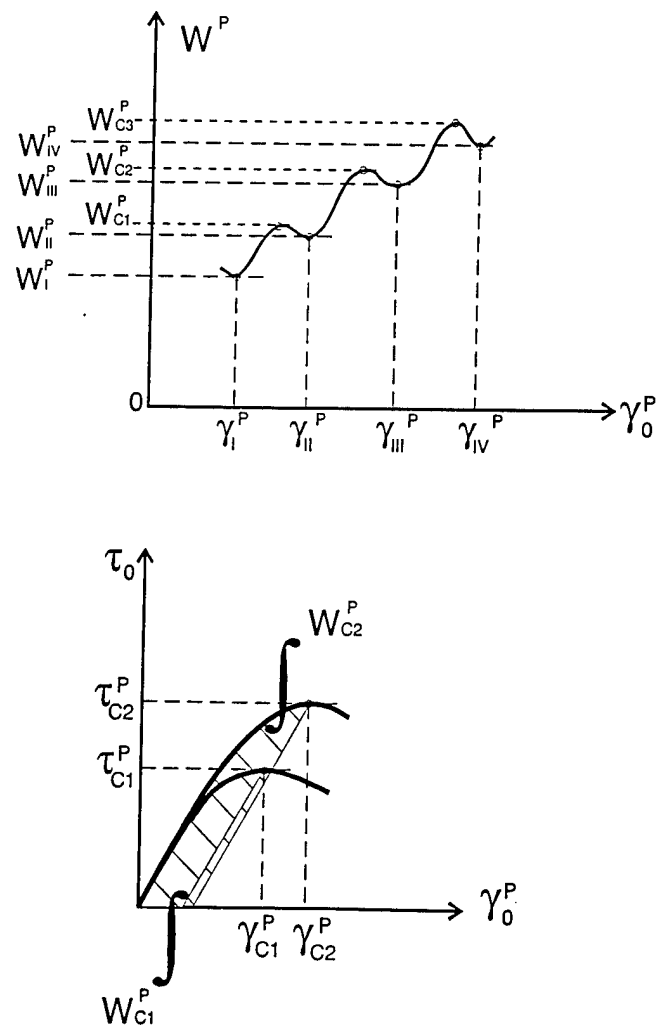
Fig.1.4. Critical and post-critical stable internal energy levels of the structure

a)

b)
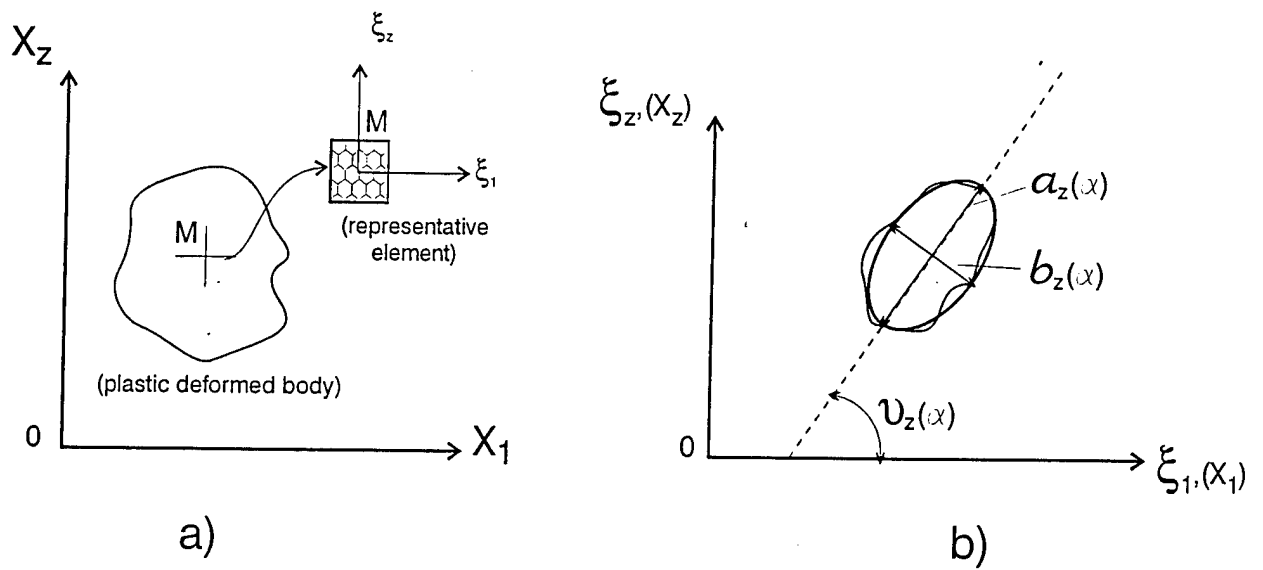
Fig.1.5.
a) Representative element of the mezo structure of the material
of plastically deformed body
b) Grain geometry approximation by ellipse in the plane case
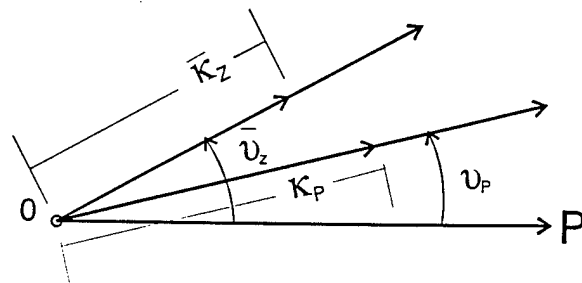
Fig.1.6. Polar diagram for the mean length-to-width ration
and the orientation of grains in the representative element

$$\sigma = f(\varepsilon)$$
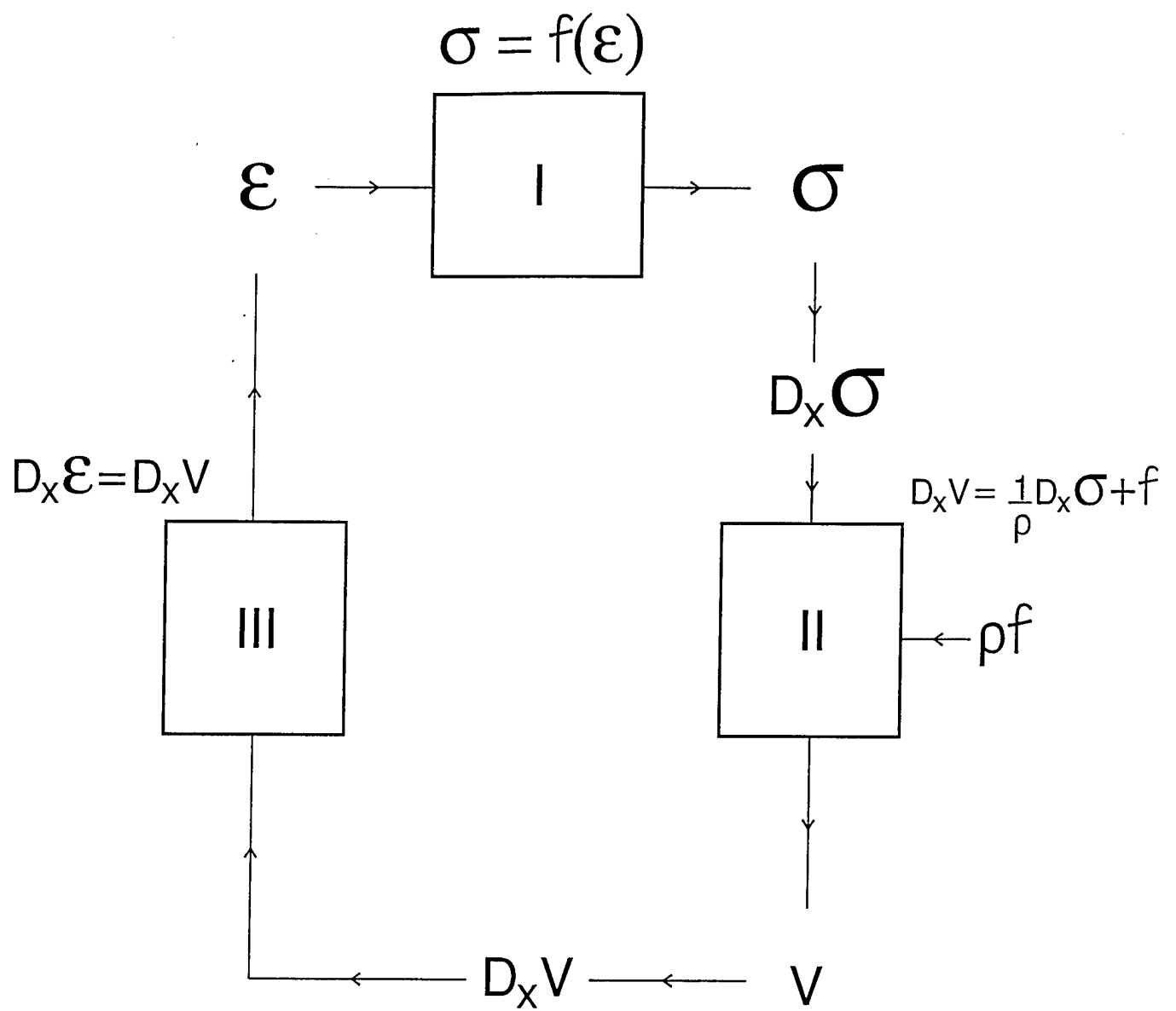
Fig.1.7 Scheme of the iterative procedure
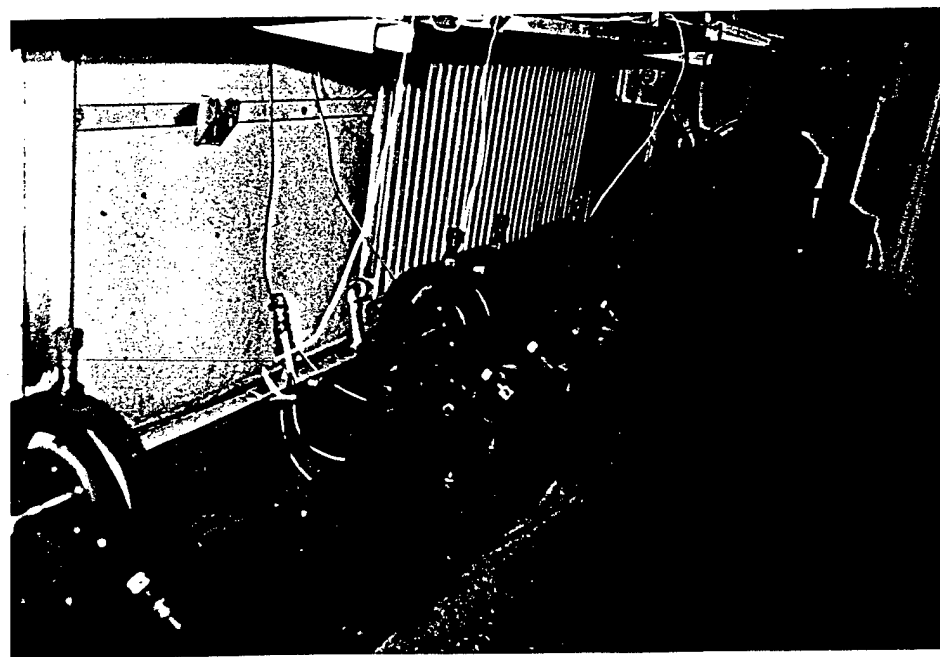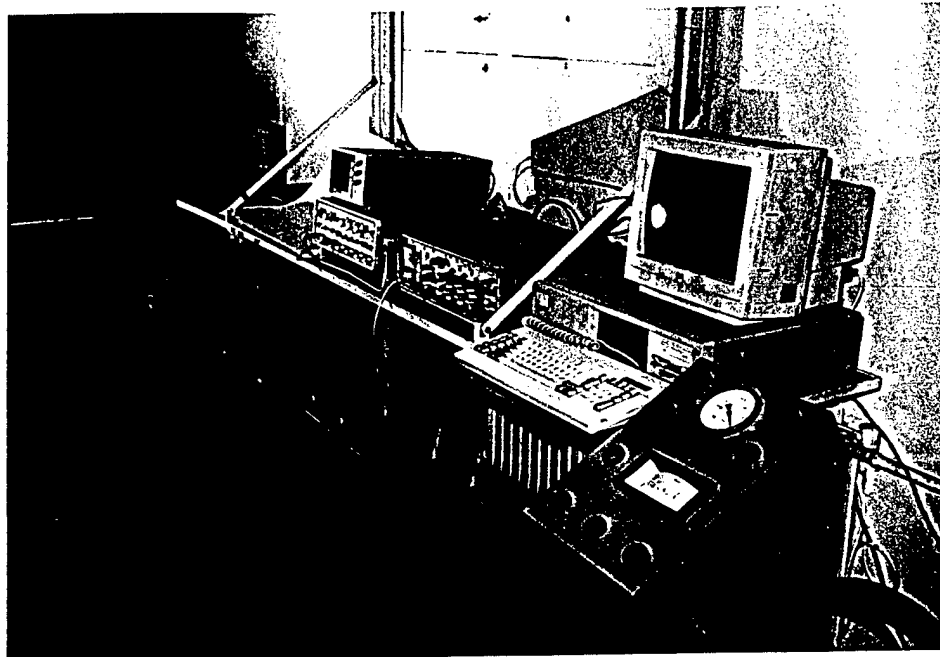
Fig. 3.1
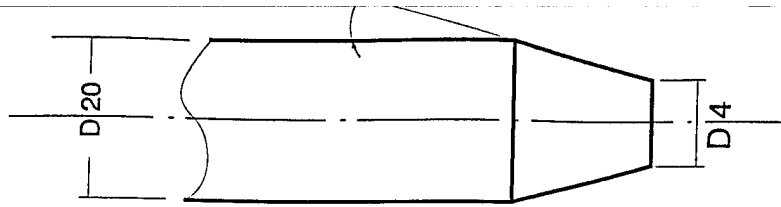
Fig. 3.2
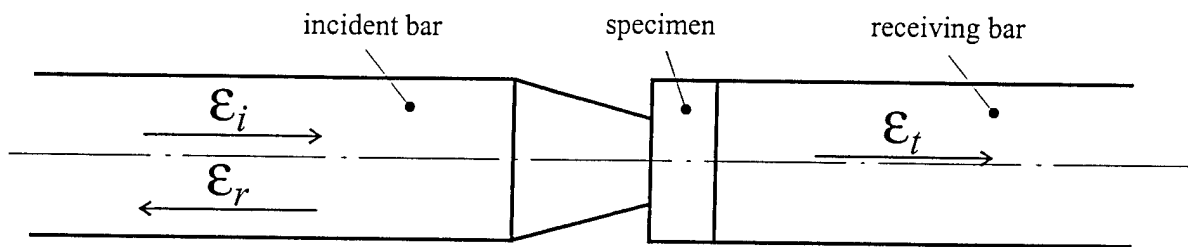
Fig. 3.3
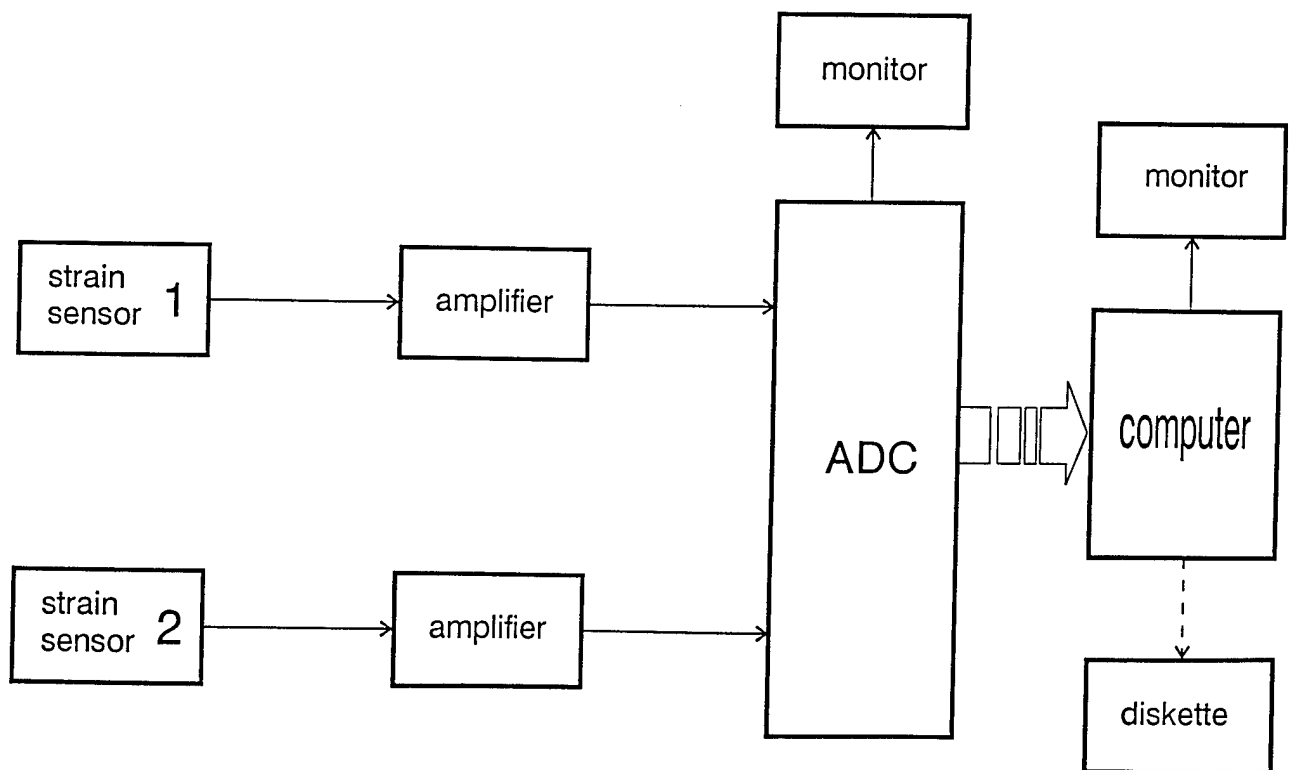
Fig. 3.4
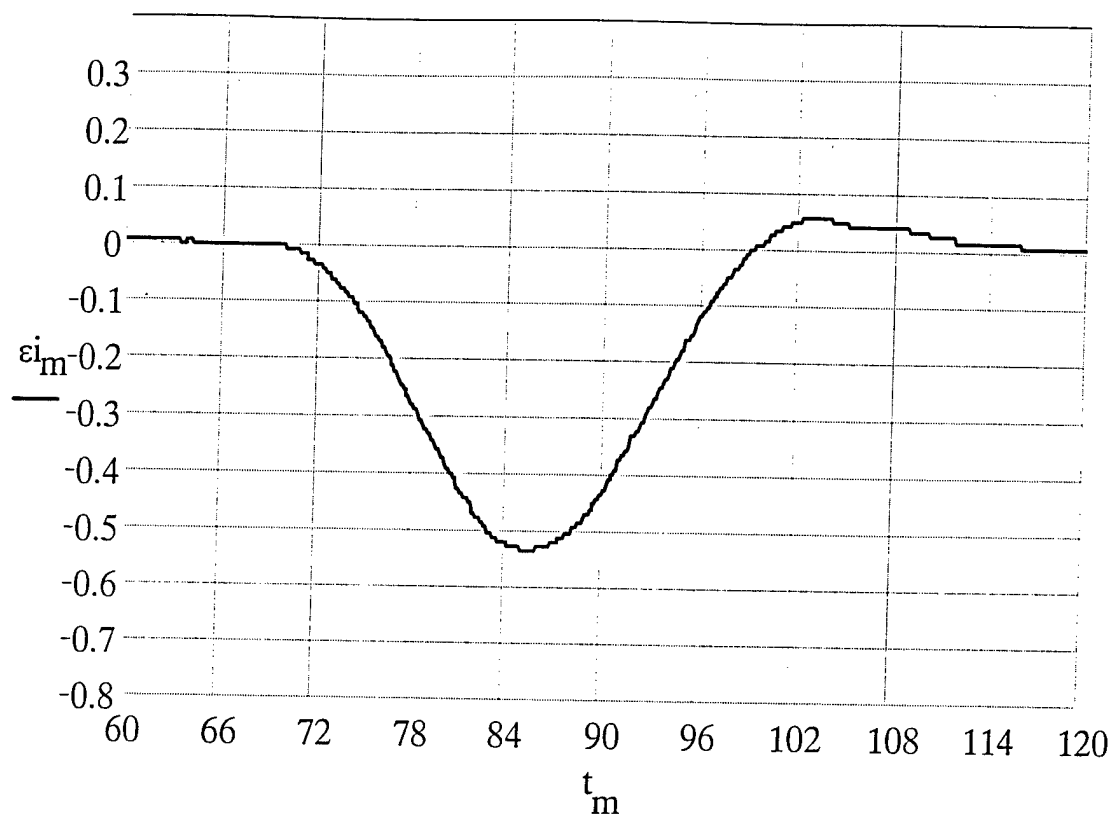
Fig. 3.5

Fig. 3.6
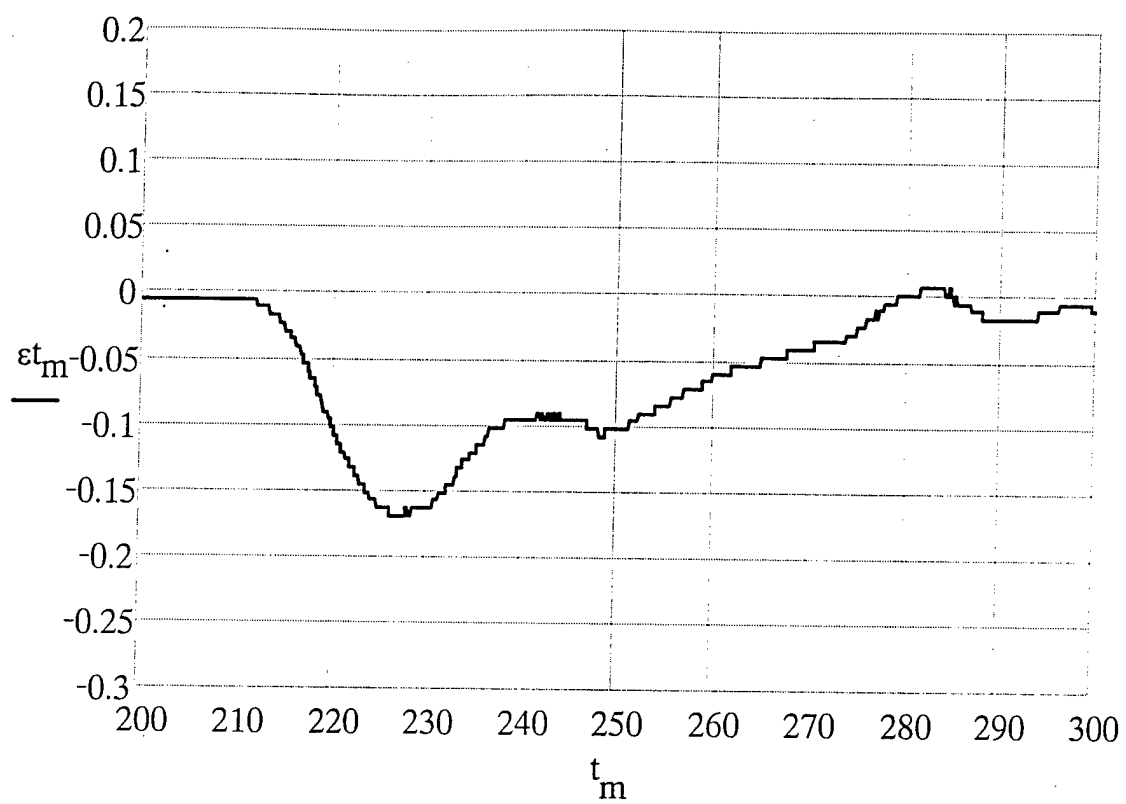
Fig. 3.7
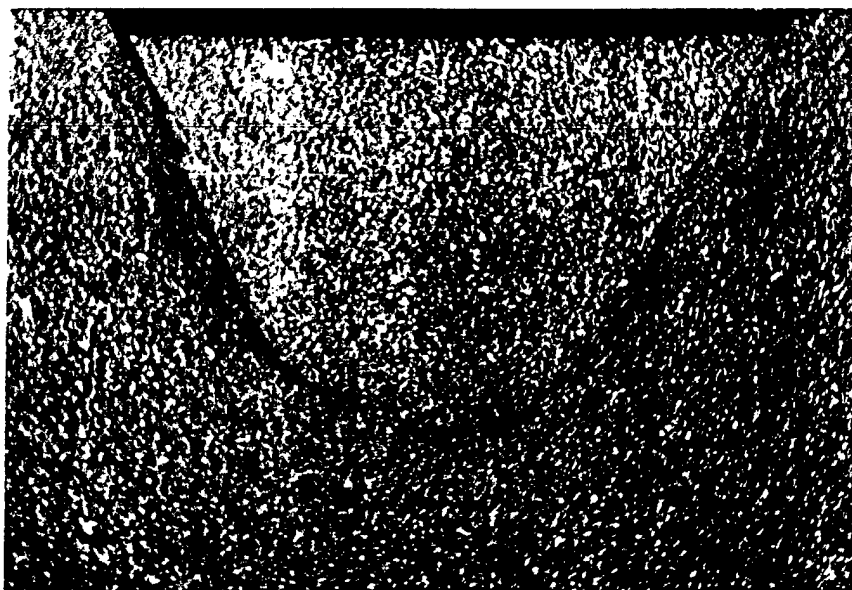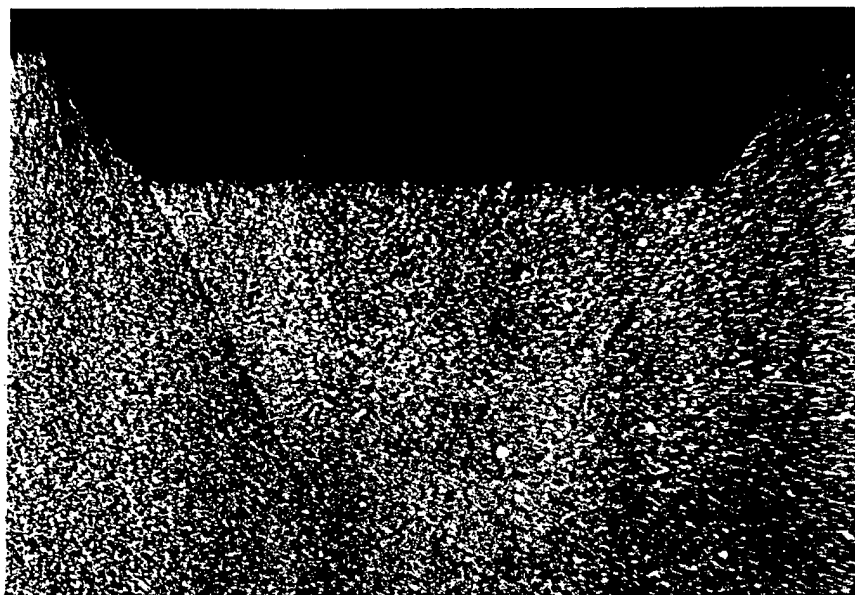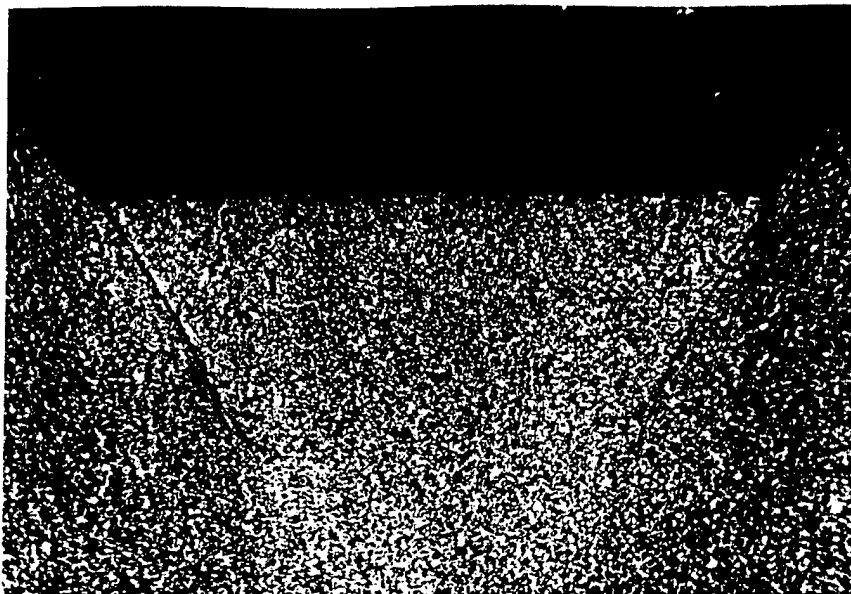
Fig.4.7. Macrostructure of specimen, loaded with energy 80,0 J. LM, x20
Fig.4.8. Macrostructure of specimen, loaded with energy 93,1 J. LM, x20
Fig.4.9. Macrostructure of specimen, loaded with energy 109,0 J. LM, x20
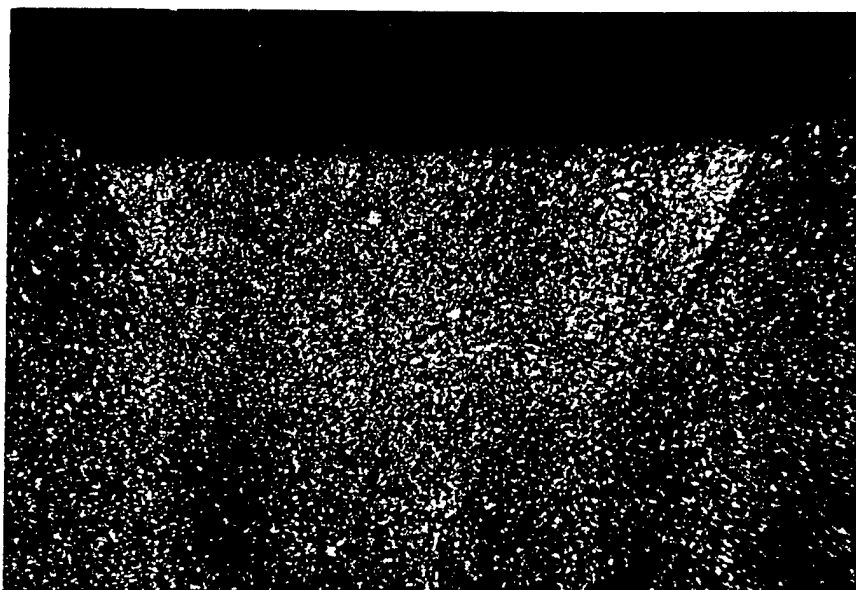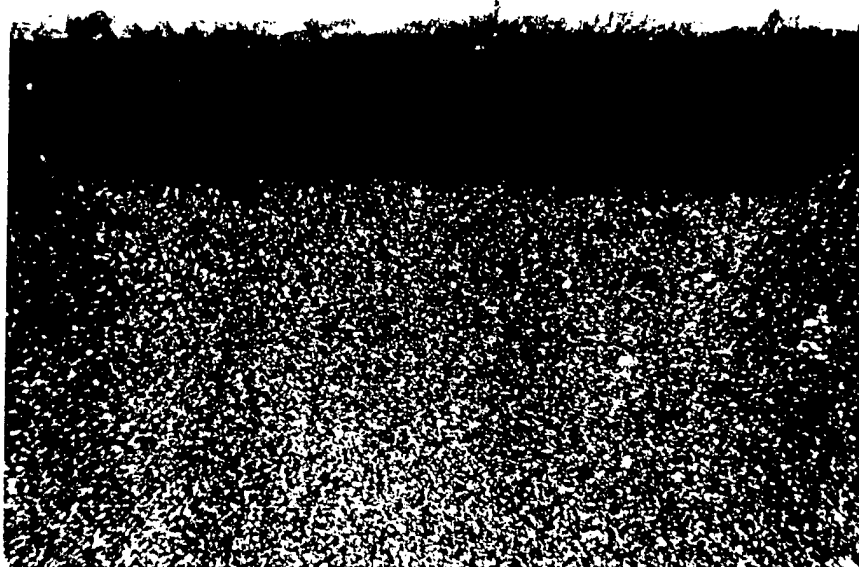
Fig.4.4. Macrostructure of specimen, loaded with energy 50,7 J. LM, x20
Fig.4.5. Macrostructure of specimen, loaded with energy 54,4 J. LM, x20
Fig.4.6. Macrostructure of specimen, loaded with energy 64,2 J. LM, x20
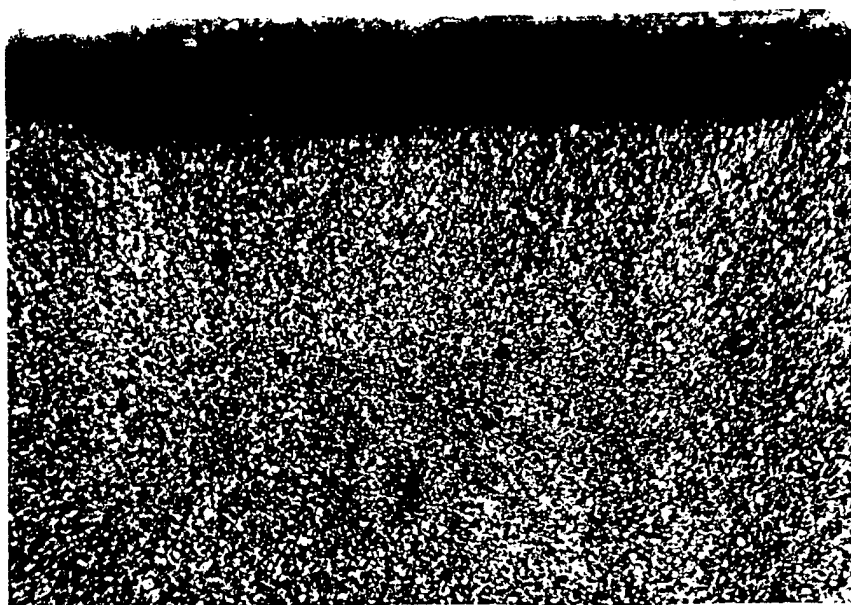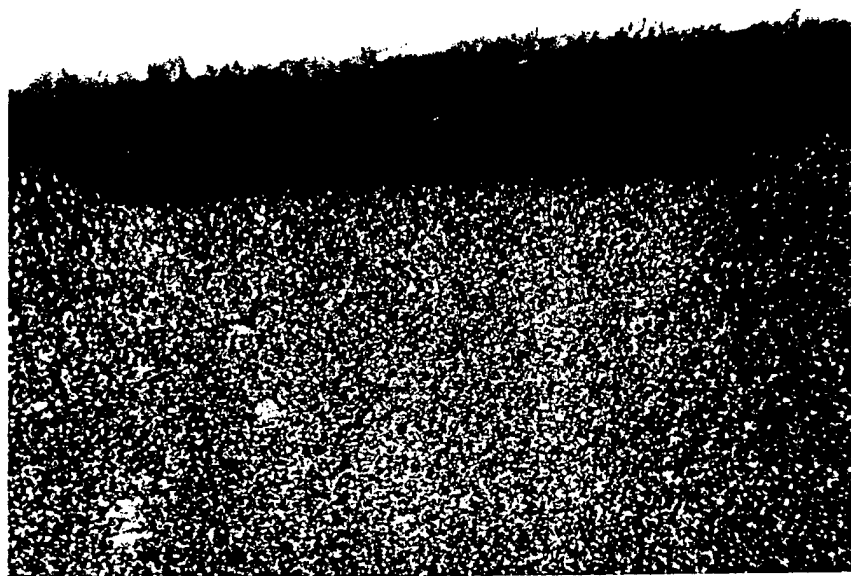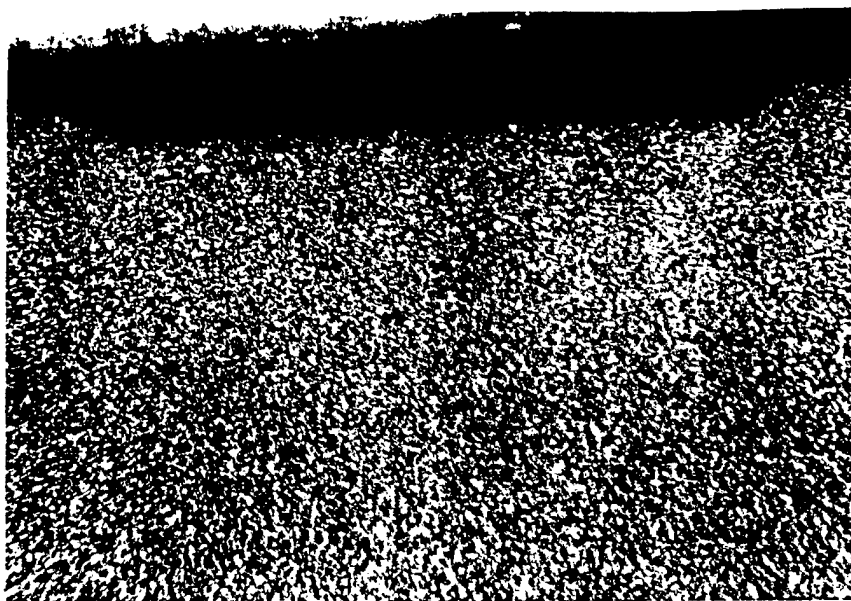
Fig.4.1. Macrostructure of specimen, loaded with energy 12,0 J. LM, x20
Fig.4.2. Macrostructure of specimen, loaded with energy 22,2 J. LM, x20
Fig.4.3. Macrostructure of specimen, loaded with energy 40,2 J. LM, x20
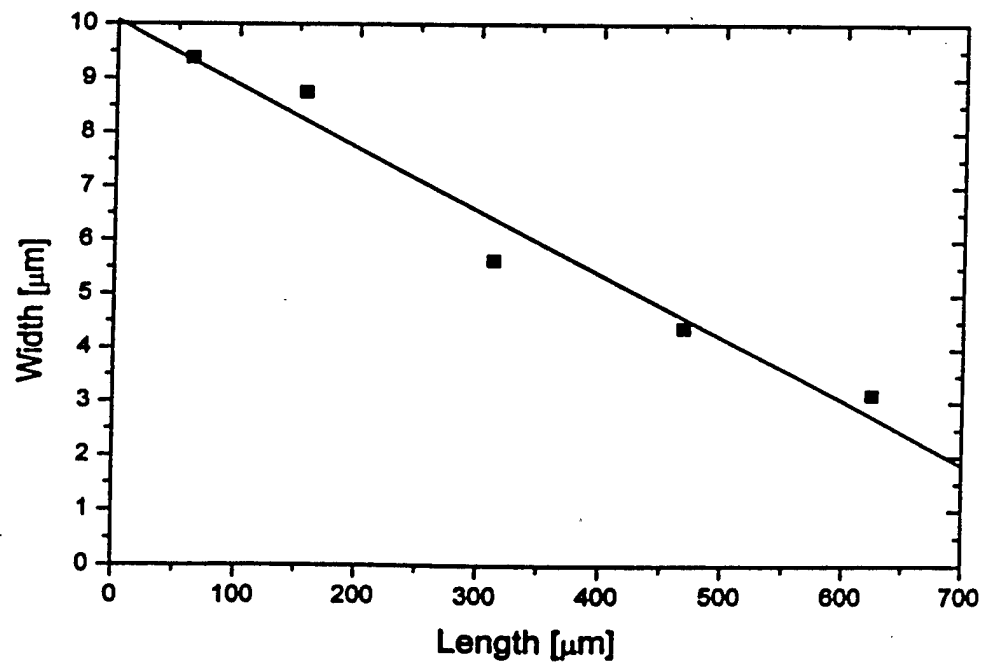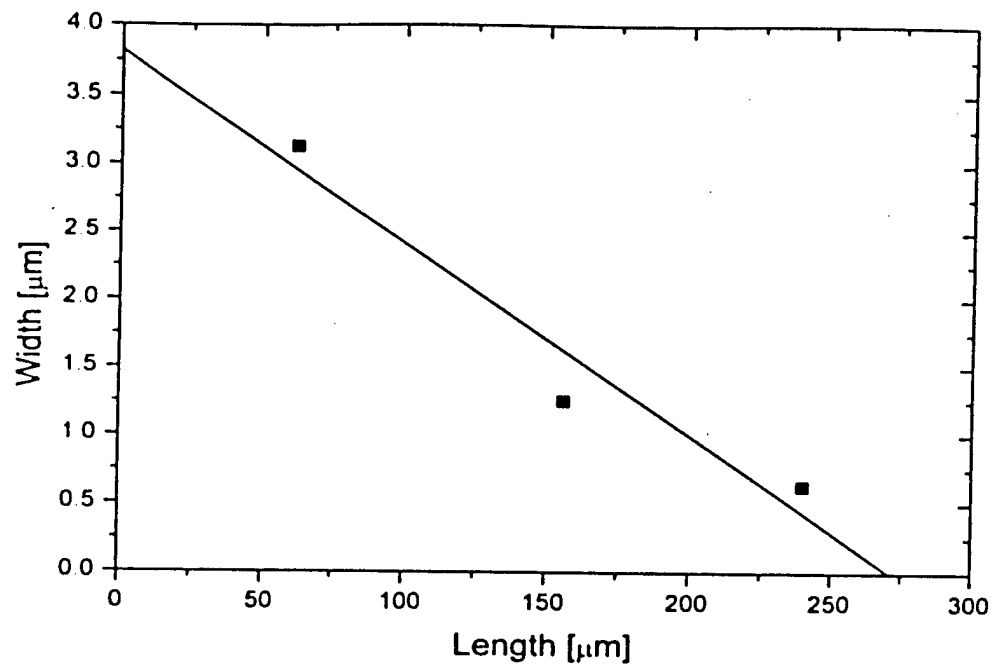
Fig.4.10. Length-width dependence of ASB in specimen, loaded with energy
40,2 J. LM, x180

Fig.4.11. Length-width dependence of ASB in specimen, loaded with energy 50,7 J.
LM, x180
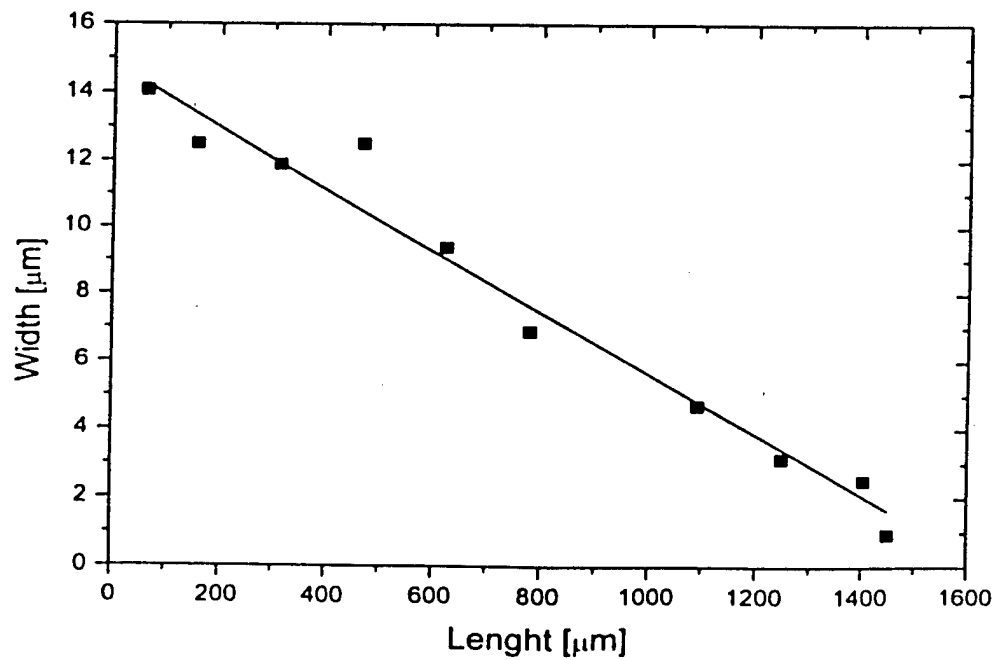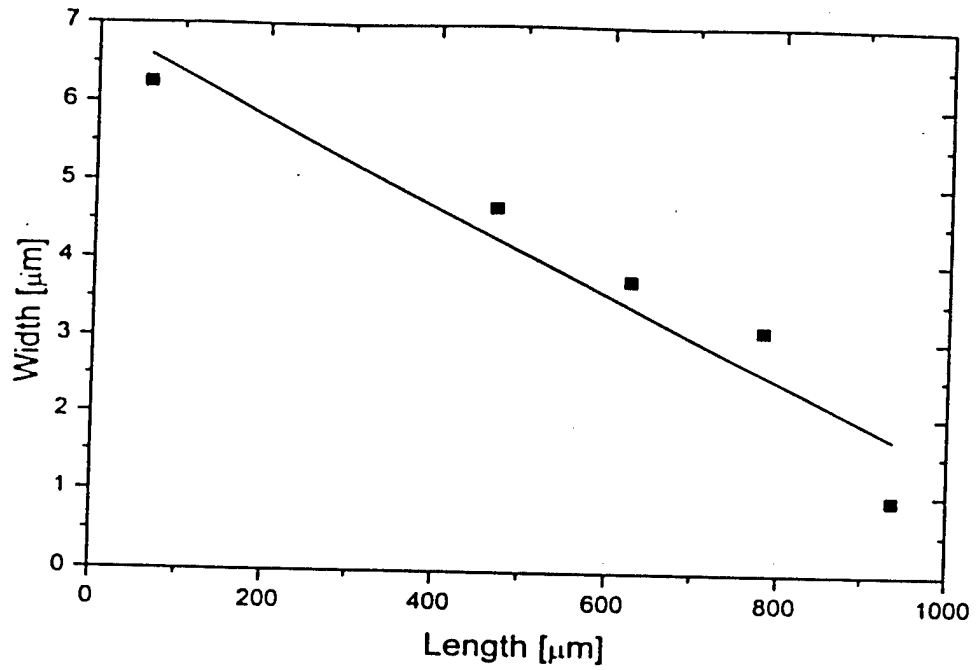
Fig.4.12. Length-width dependence of ASB in specimen, loaded with energy 54,4 J. LM, x180

Fig.4.13. Length-width dependence of ASB in specimen, loaded with energy 64,2 J. LM, x180
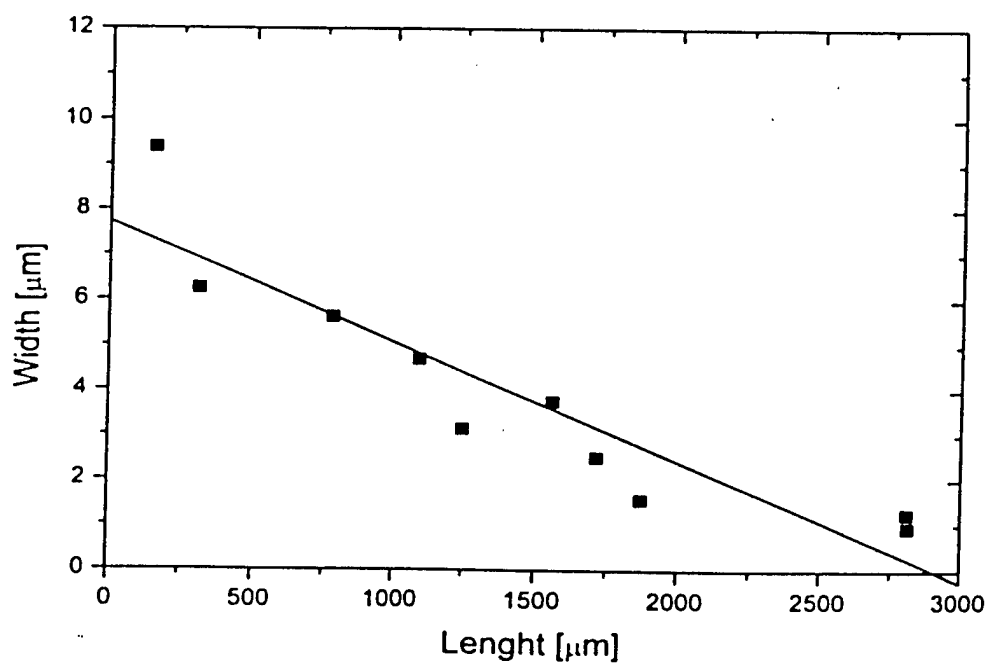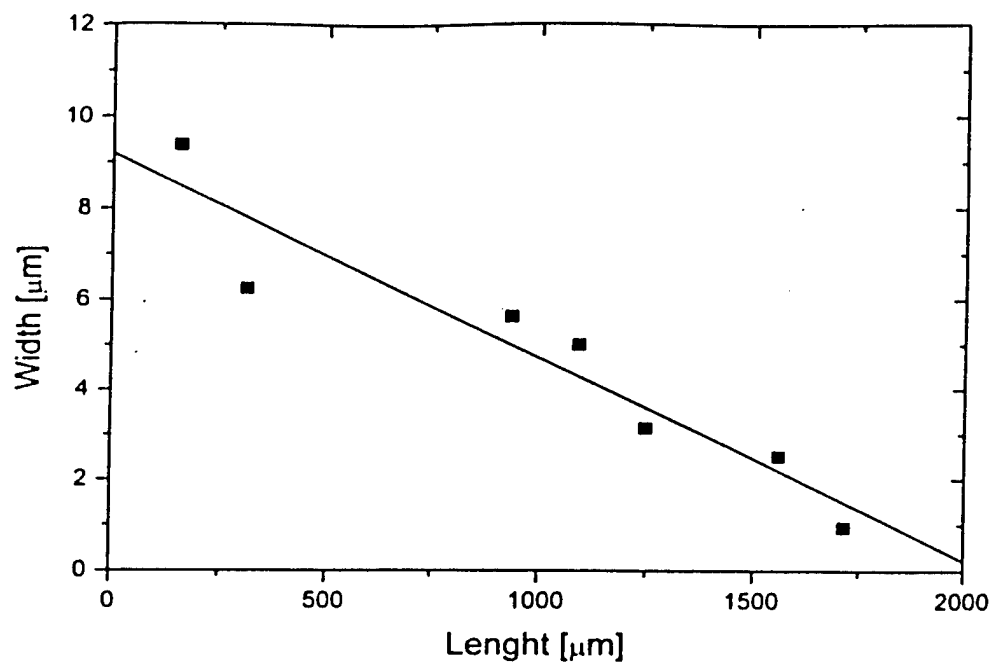
Fig.4.14. Length-width dependence of ASB in specimen, loaded with energy 80,0 J. LM, x180

Fig.4.15. Length-width dependence of ASB in specimen, loaded with energy 93,1 J. LM, x180
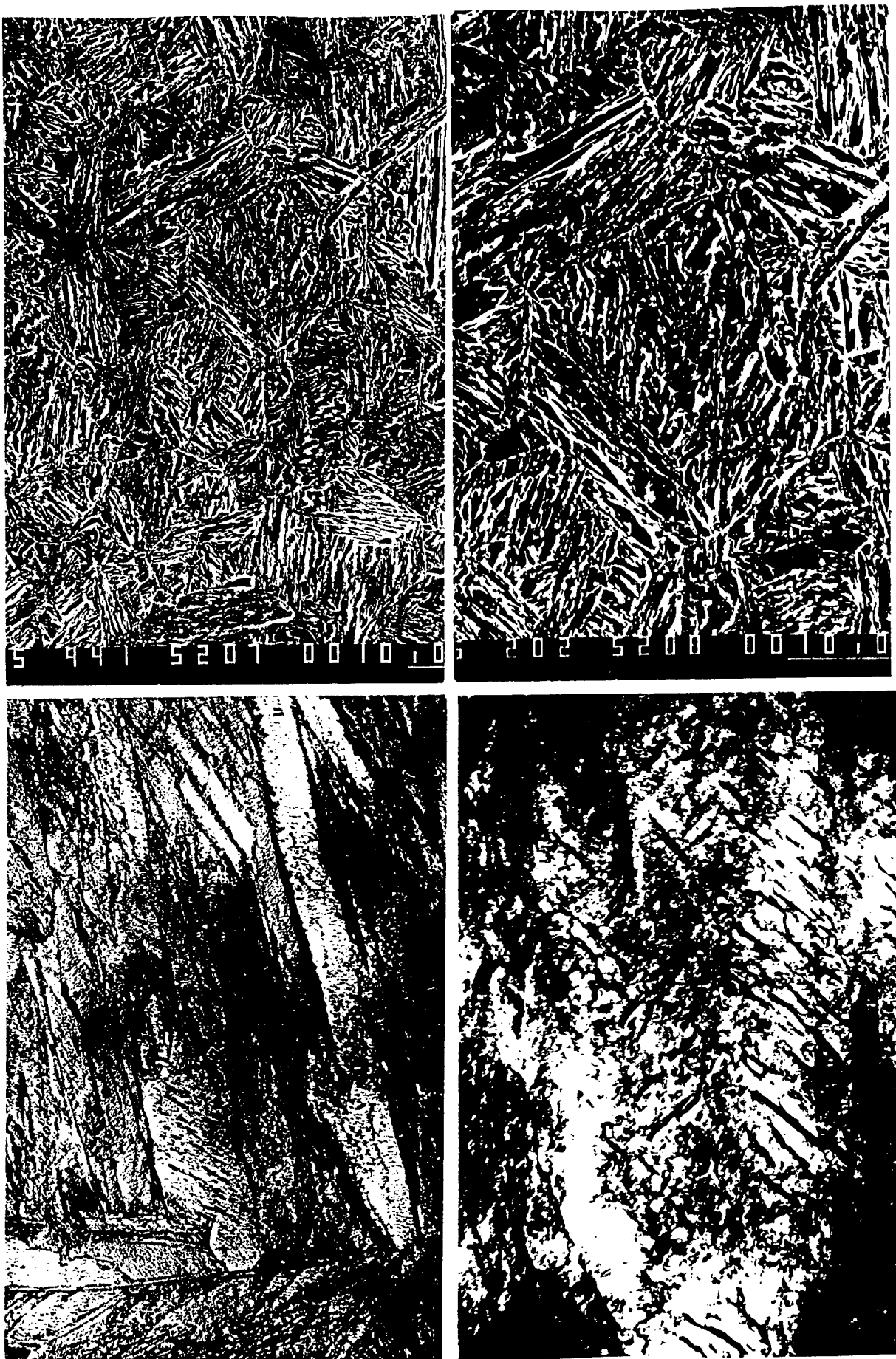
Fig.4.16. Microstructure of initial state of the investigated steel
a) SEM, x940; b) SEM, x 2000; c) TEM, x 20000; d) TEM, x 40000

Fig.4.17. Microstructure of specimen, loaded with energy 22,2 J. LM, x180
Fig.4.18. Microstructure of specimen, loaded with energy 40,2 J. LM, x180
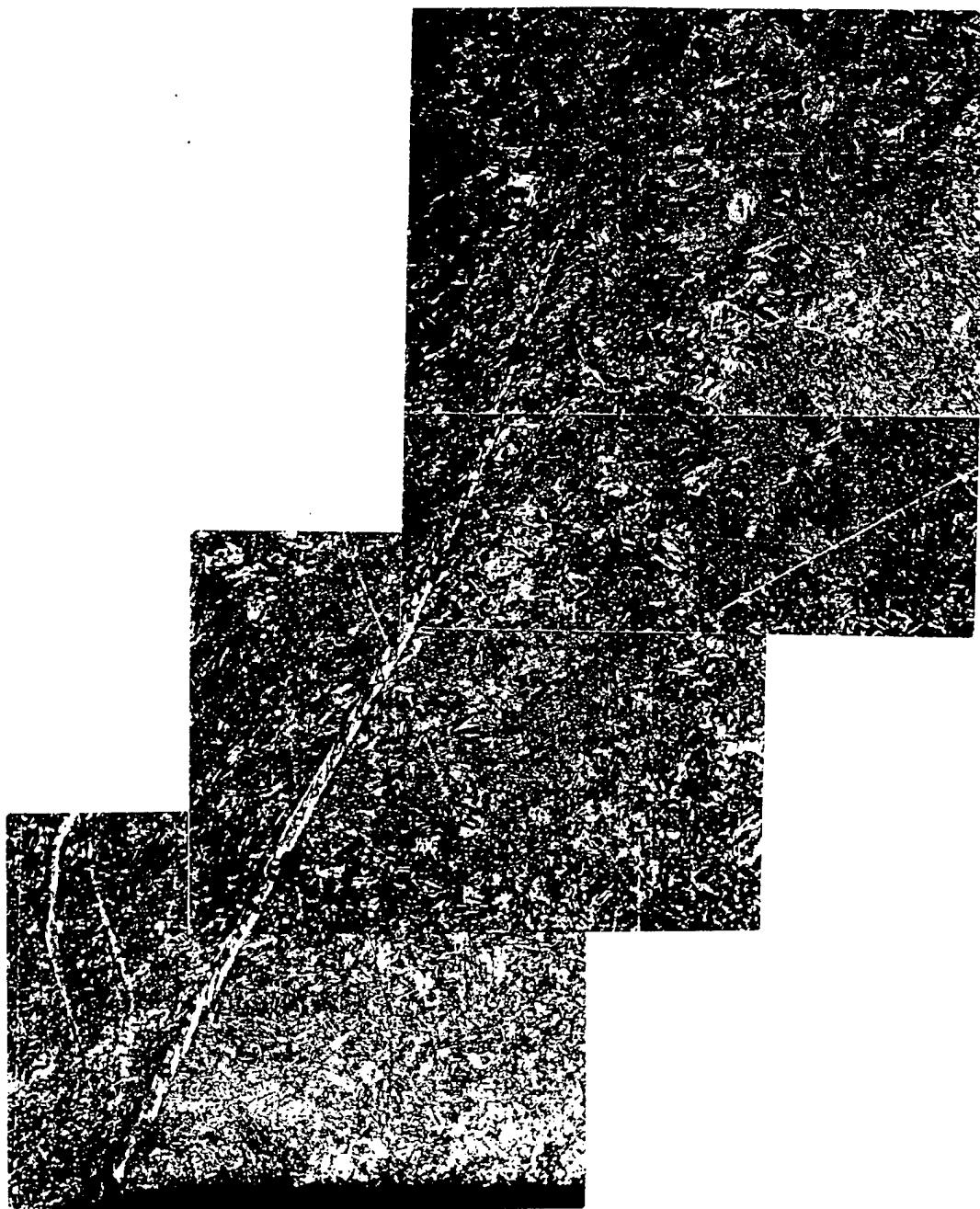
Fig.4.19. Microstructure of specimen, loaded with energy 50,7 J. LM, x180
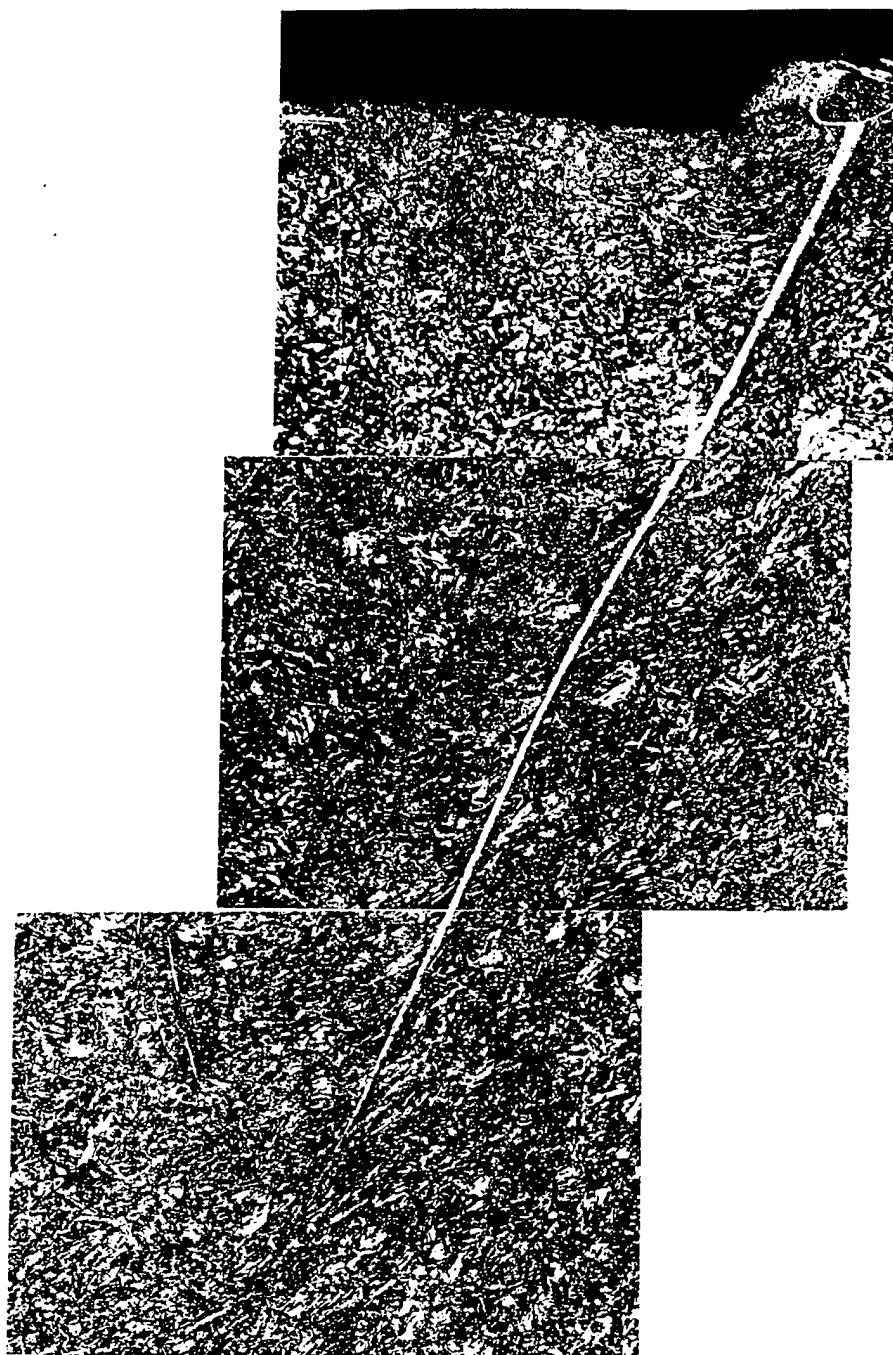
Fig.4.20. Microstructure of specimen, loaded with energy 54,4 J. LM, x180
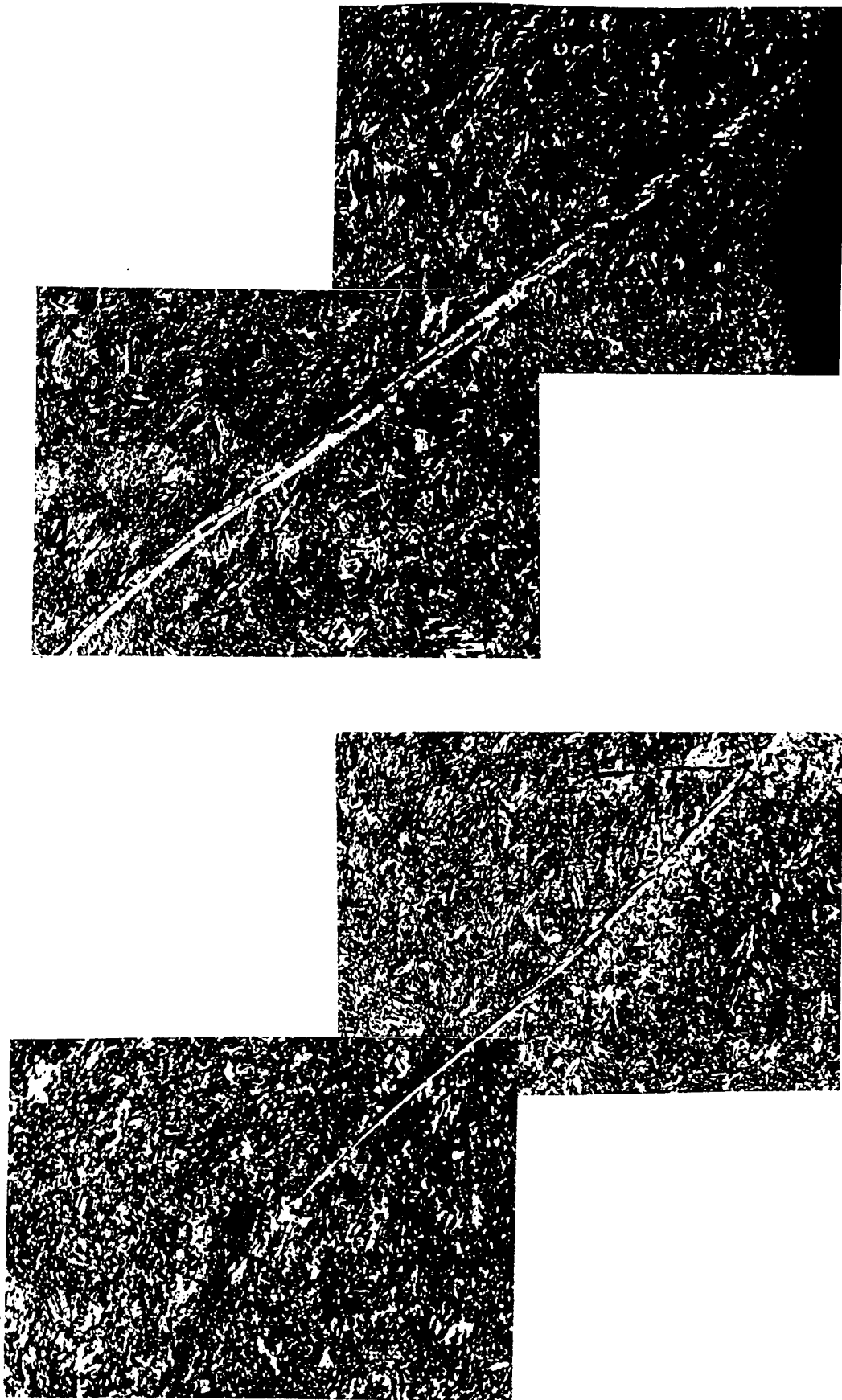
Fig.4.21. Microstructure of specimen, loaded with energy 64,2 J. LM, x180
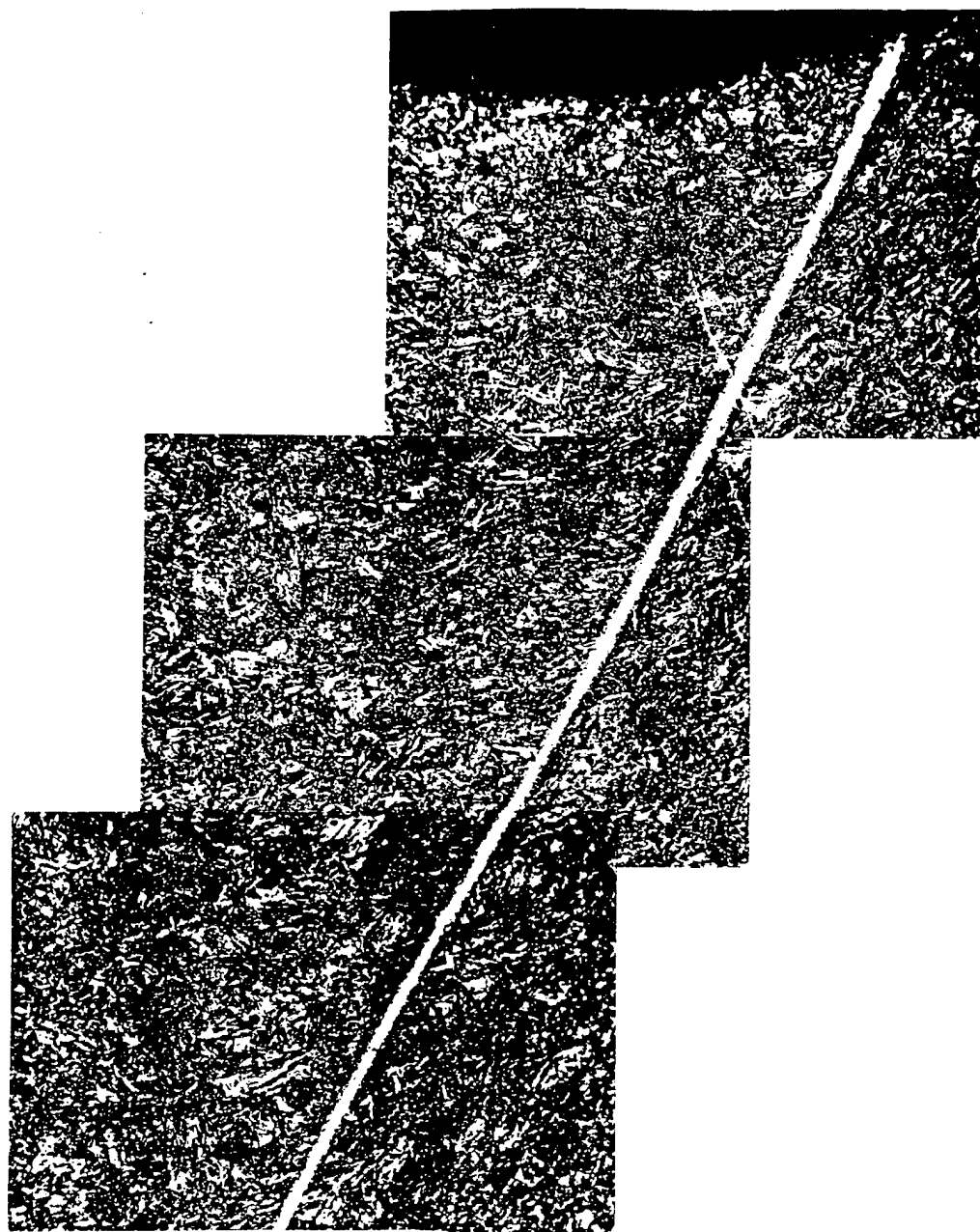
Fig.4.22. Microstructure of specimen, loaded with energy 80,0 J. LM, x180
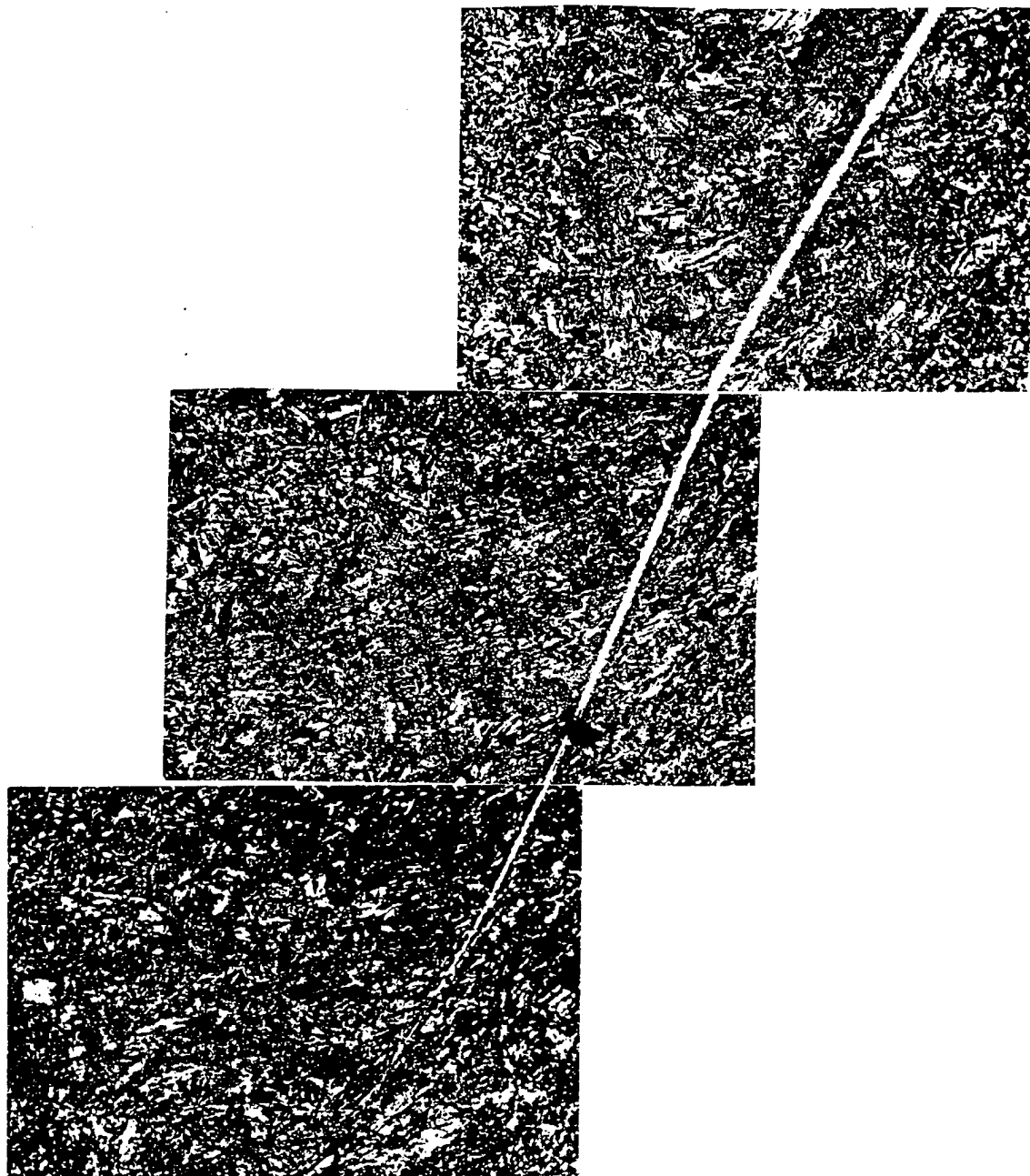
Fig.4.22. Microstructure of specimen, loaded with energy 80,0 J. LM, x180
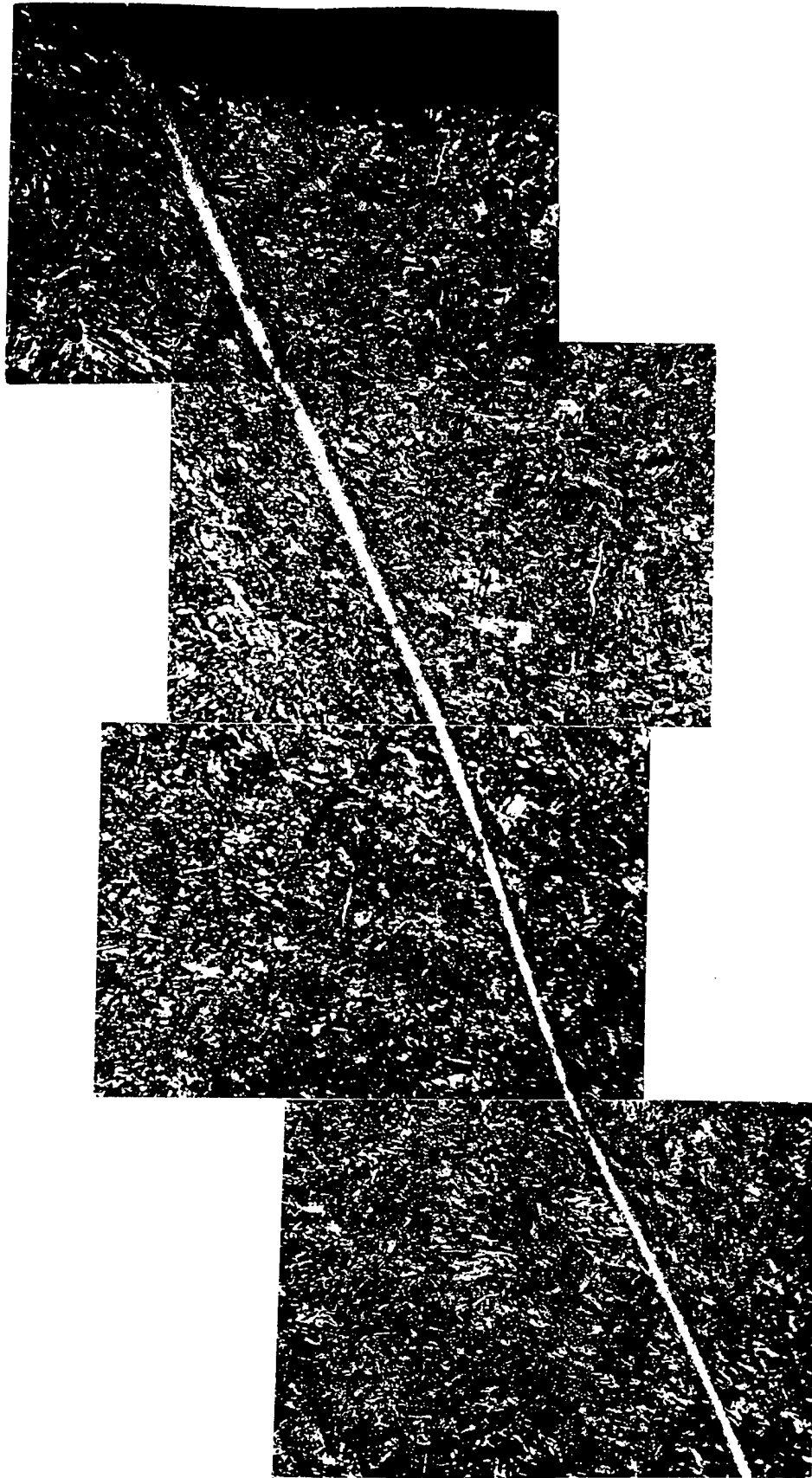
Fig.4.23. Microstructure of specimen, loaded with energy 93,1 J. LM, x180
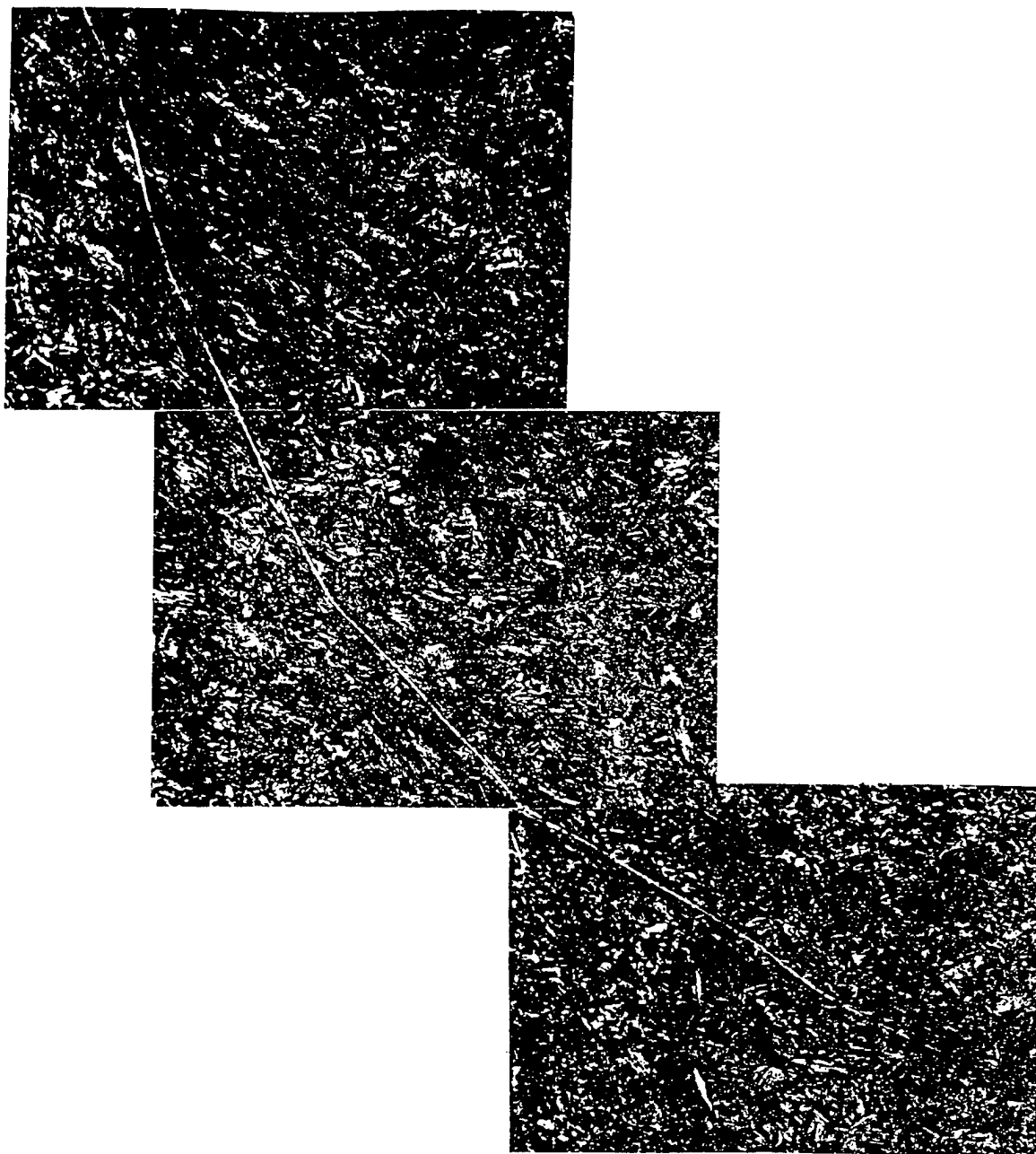
Fig.4.23. Microstructure of specimen, loaded with energy 93,1 J. LM, x180
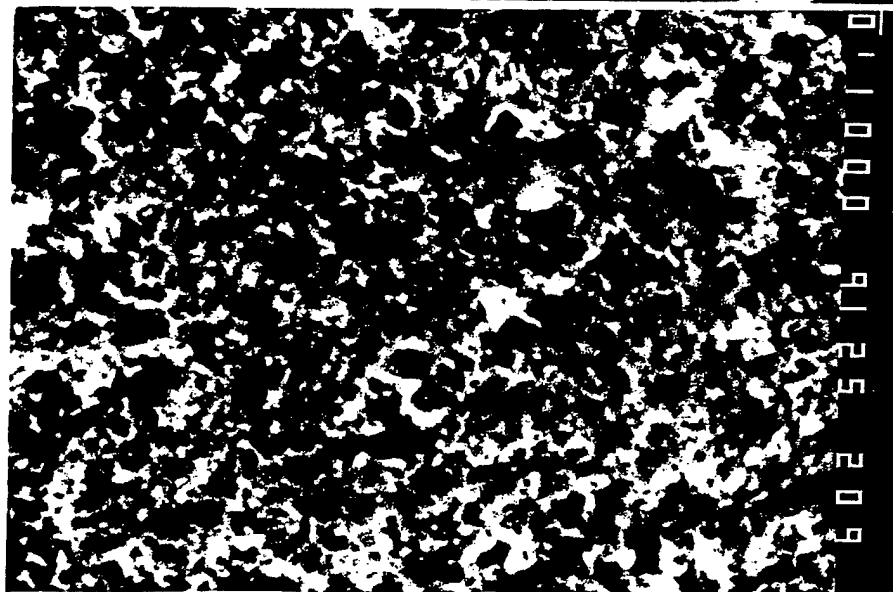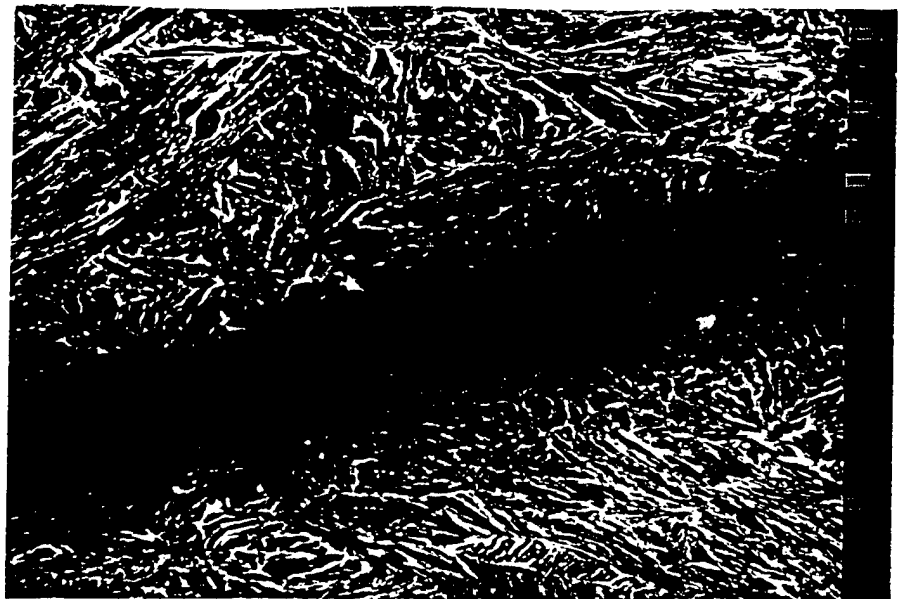
Fig.4.24. Etch-pits relief in the initial part of ASB in specimen, loaded with energy
54,4 J. Etching in 5% HNO₃. SEM:
a) x2000, b) x6000, c) x6000
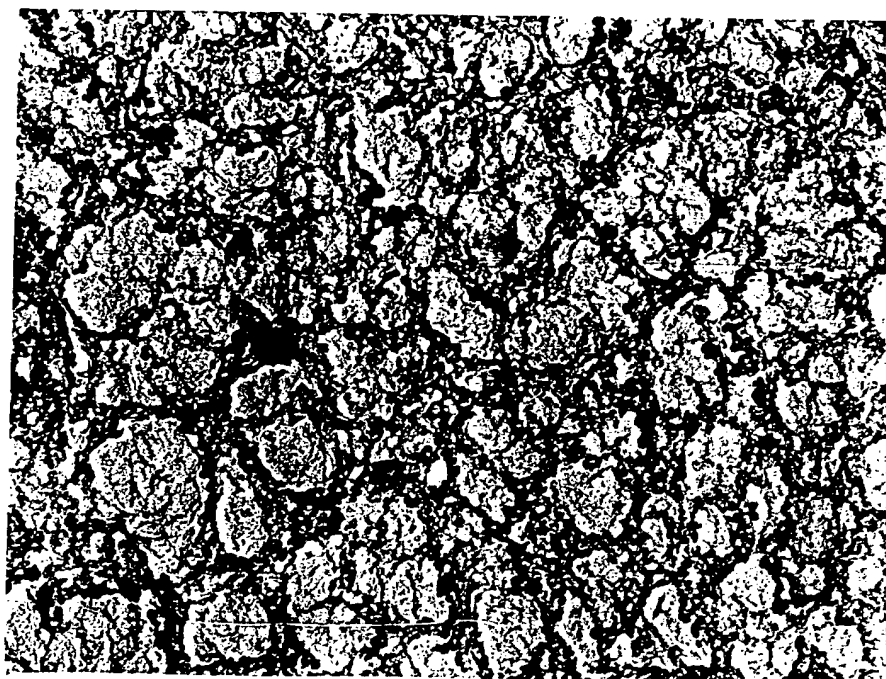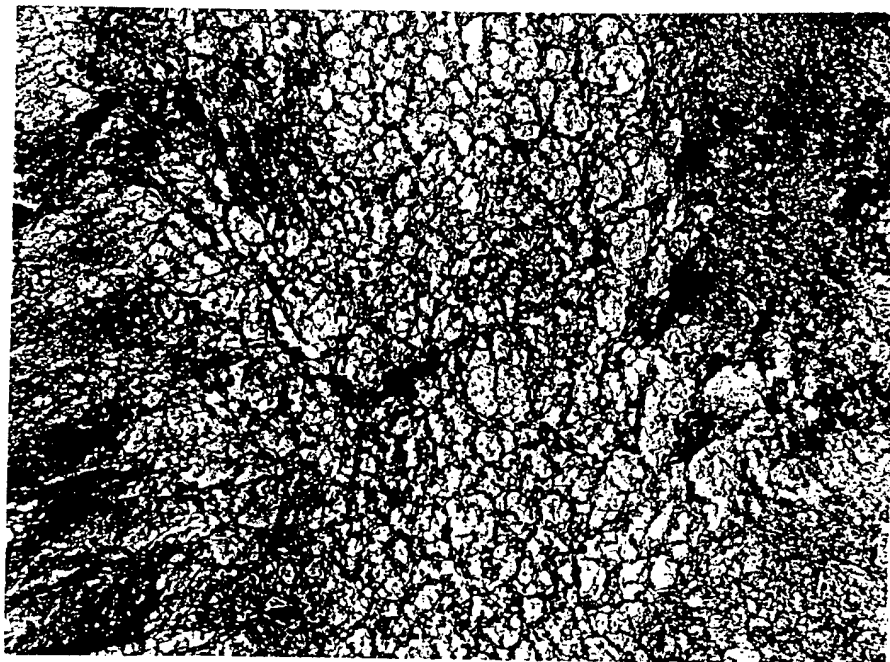
a) Fig.4.25. Cells in the initial part of ASB in specimen, loaded with energy 54,4 J.
b) Etching in HCL:HNO₃=1:3 solution. TEM replica: a) x6000, b) x20000
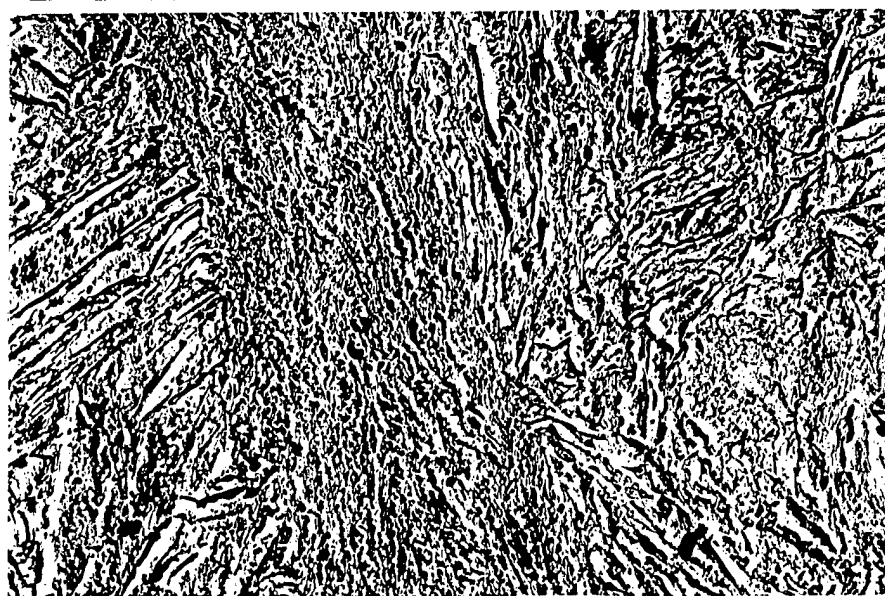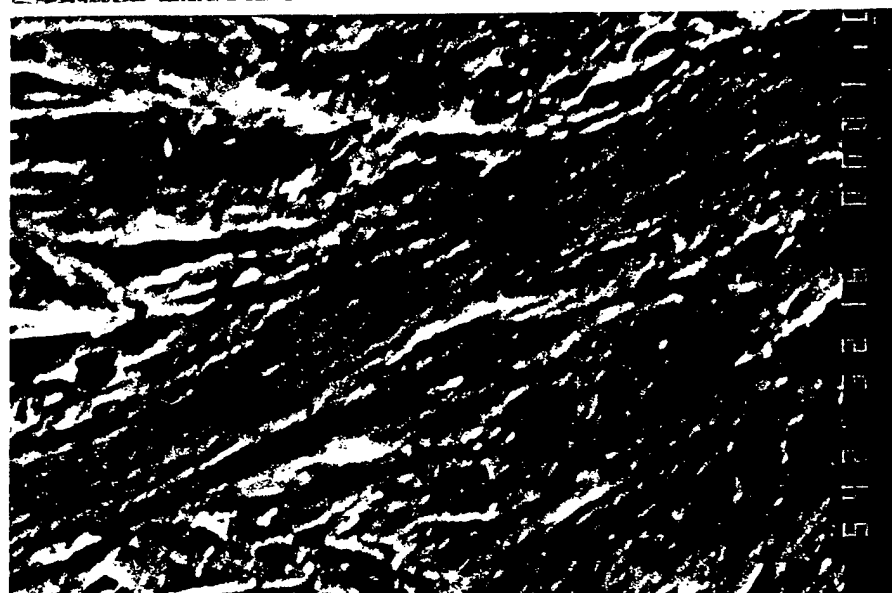
Fig.4.26. Parallel laths arranged along ASB length in specimen, loaded with energy 54,4
J. SEM, x940; b) SEM, x5400; c) TEM replica, x6000
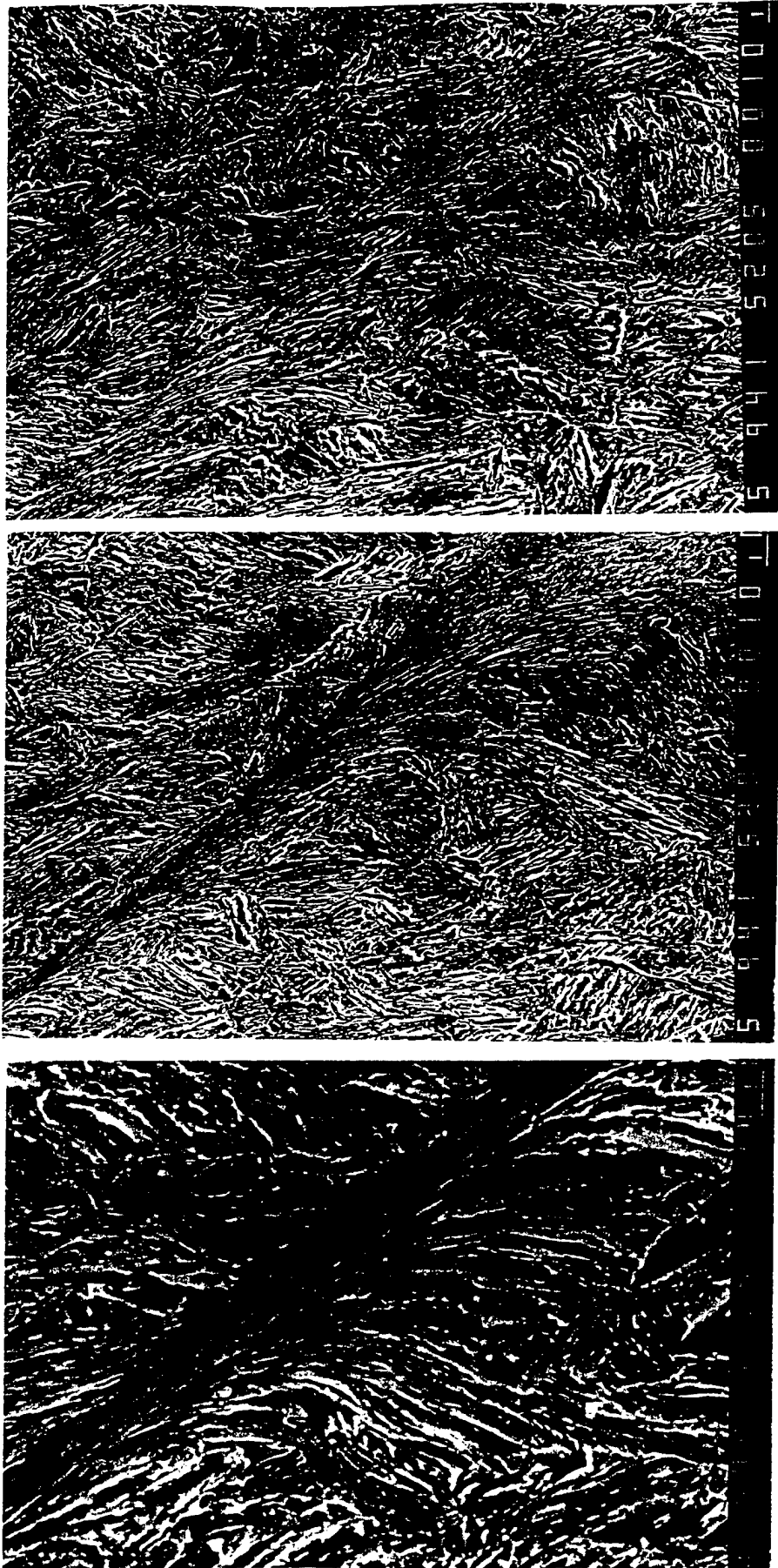
Fig.4.27. Final part of ASB in specimen, loaded with energy 54,4 J. SEM:
a) End part, x9400; b) Fan-like part, x940; c)Fan-like part, x4000
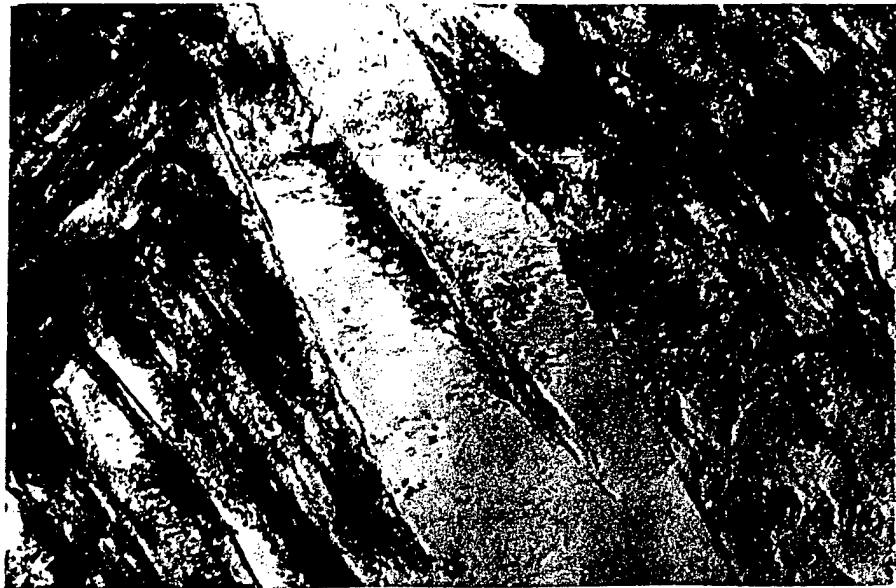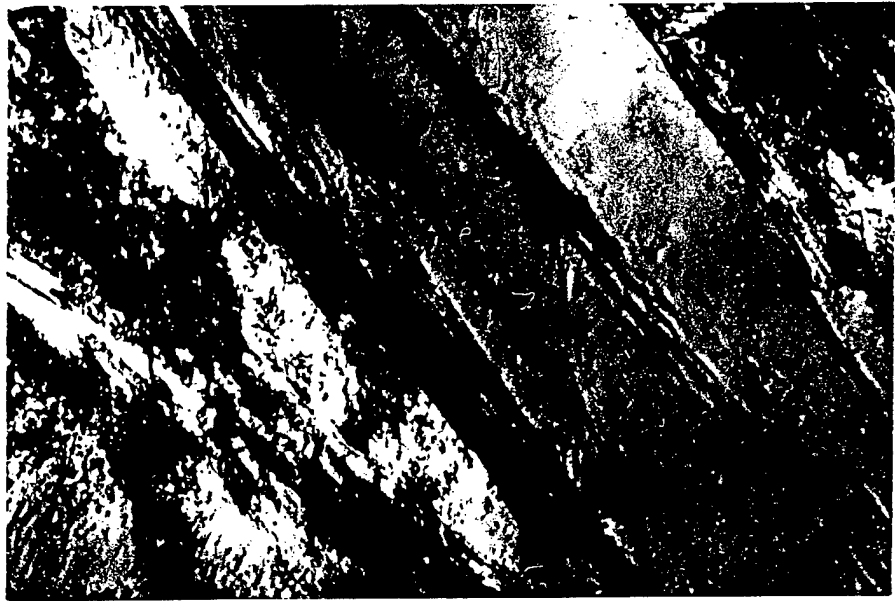
Fig.4.28. ASB in specimen, loaded with energy 54,4 J, containing transformed laths, TEM, x20000
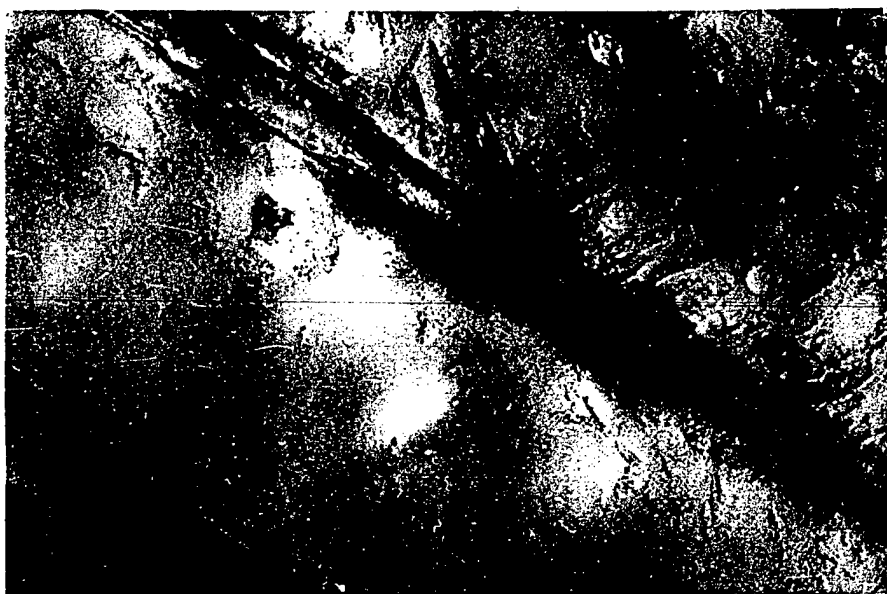
Fig.29. Microstructure of transformed laths. TEM: a) x40000, b) x60000

Fig.30. Dislocation structure of transformed laths. TEM: a) x60000, b) x100000

Fig.31. Band of ultrafine grains attached to the wall of microcrack in specimen, loaded
with energy 54,4 J. TEM:
a) x40000, b) x40000, c) x100000
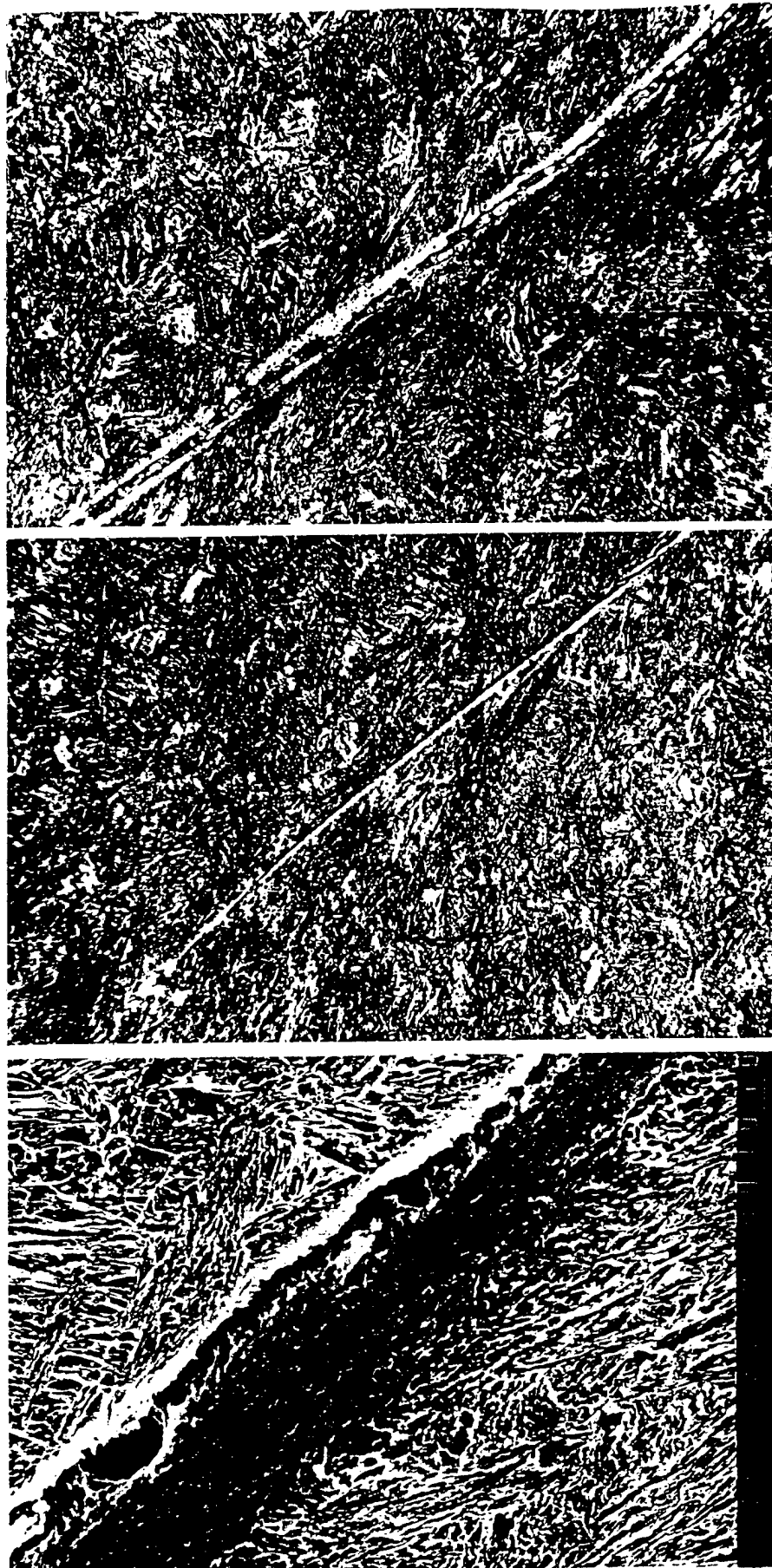
Fig.32. Crack in the specimen loaded with energy 64,2 J:
a) In the zone with large grains, LM, x100,
b) In the zone of transformed laths, LM, x200
c) One-side propagation of crack, SEM, x2000
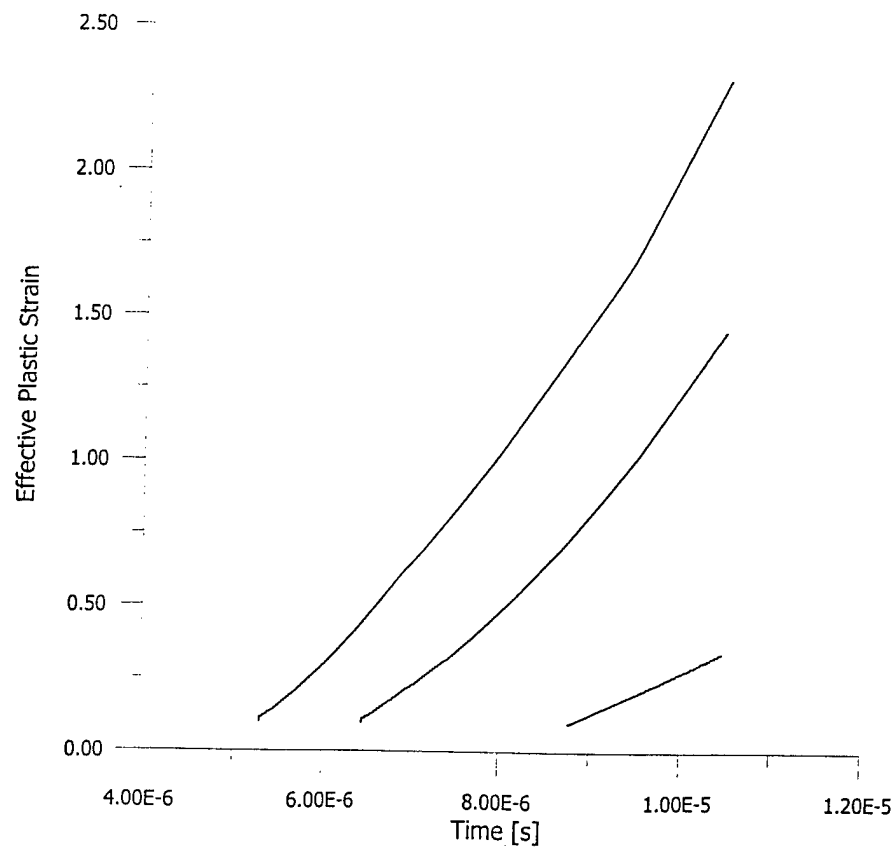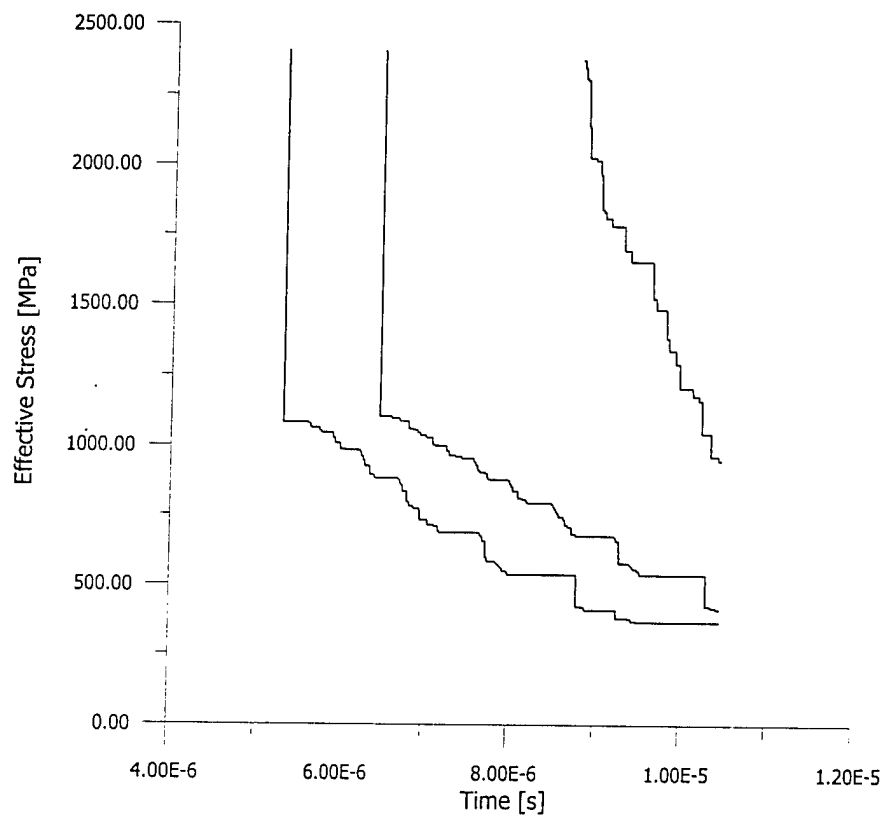
Fig. 5.1, 5.2
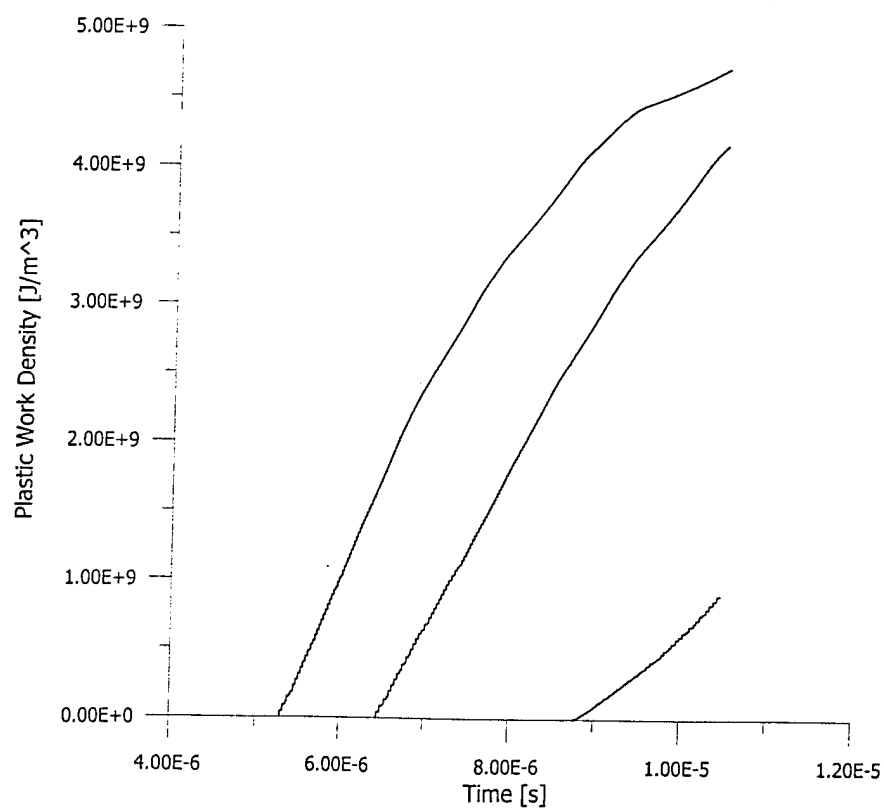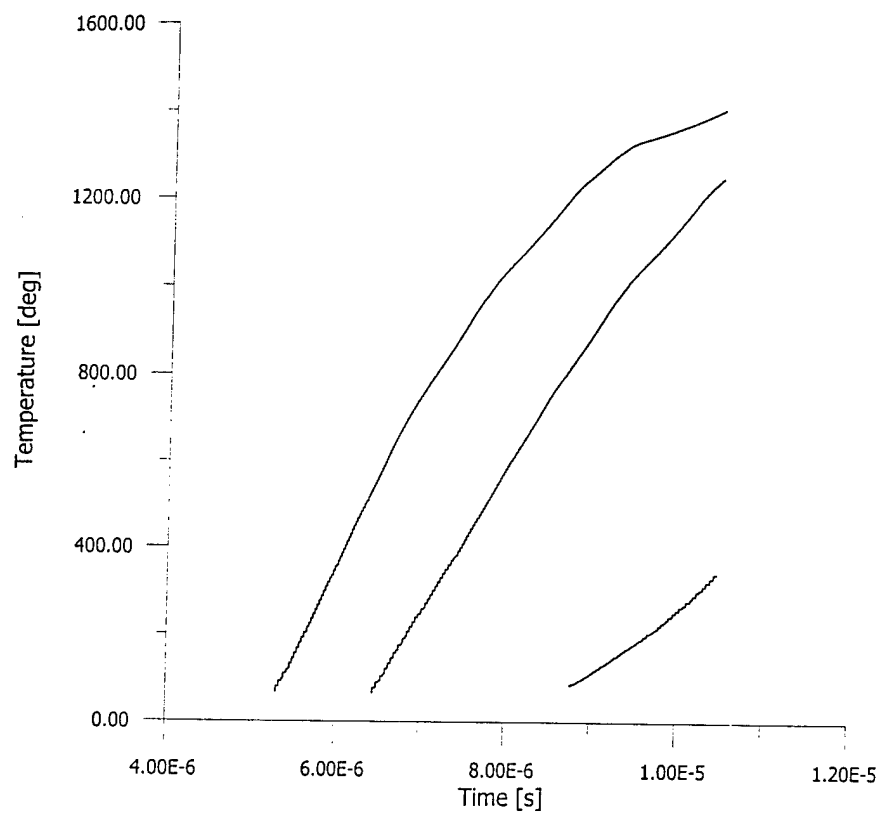
Fig. 5.3, 5.4

Fig. 5.5, 5.6

Fig. 5.7, 5.8

MPa

2000

1500

1000

500

Fig. 5.9

Fig. 5.10

T ^{0}C
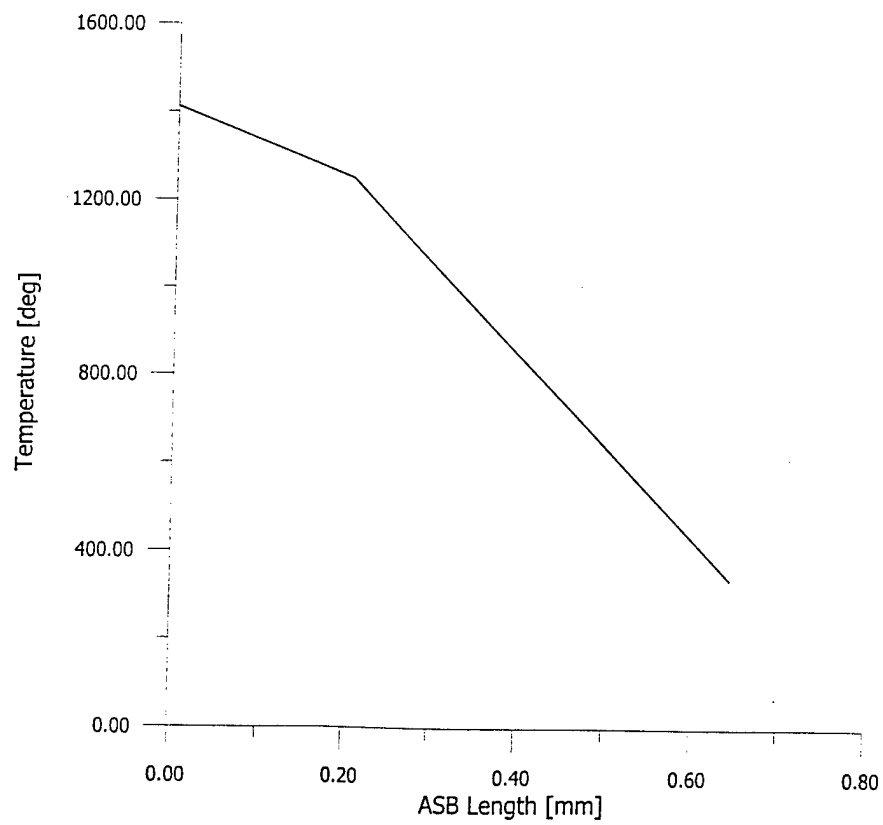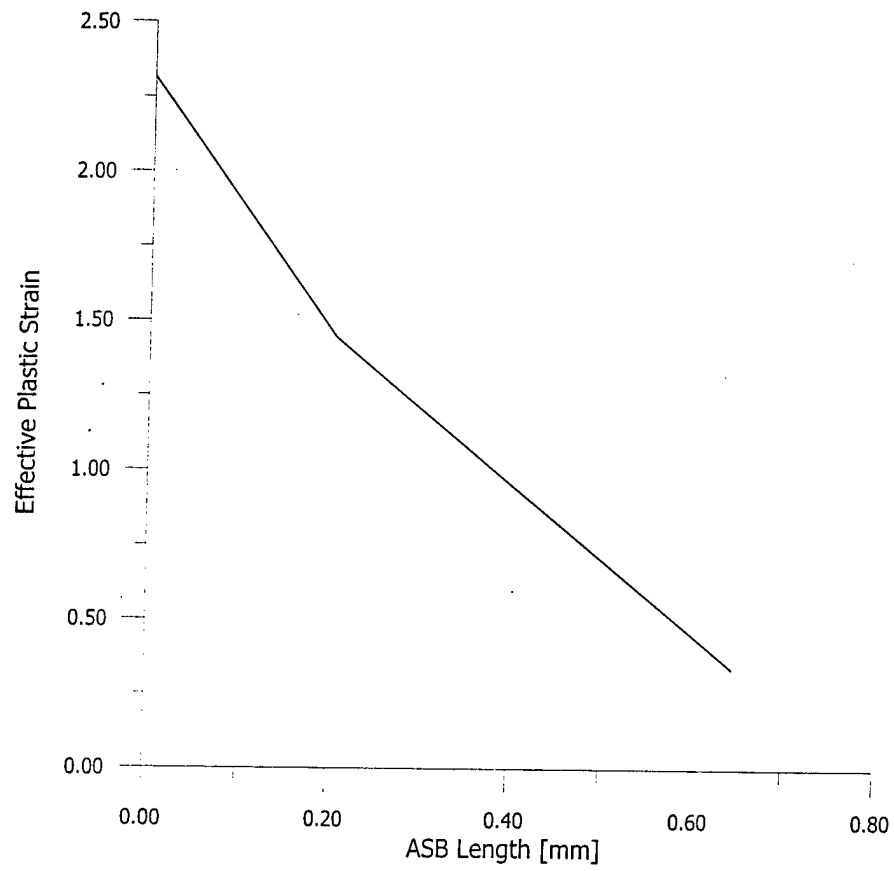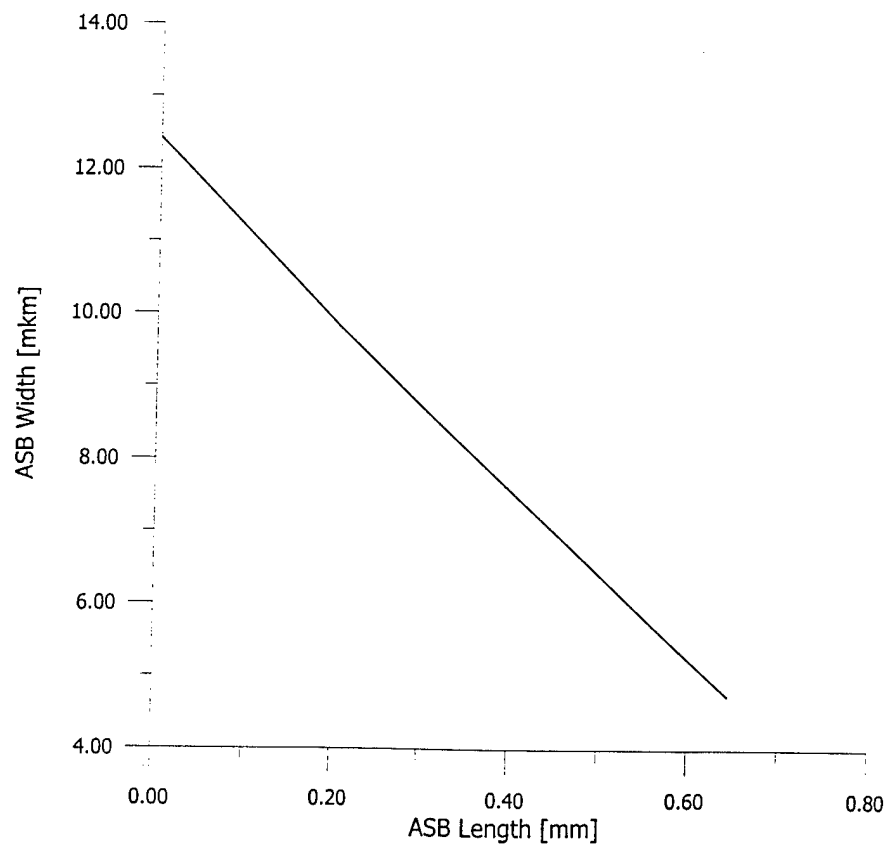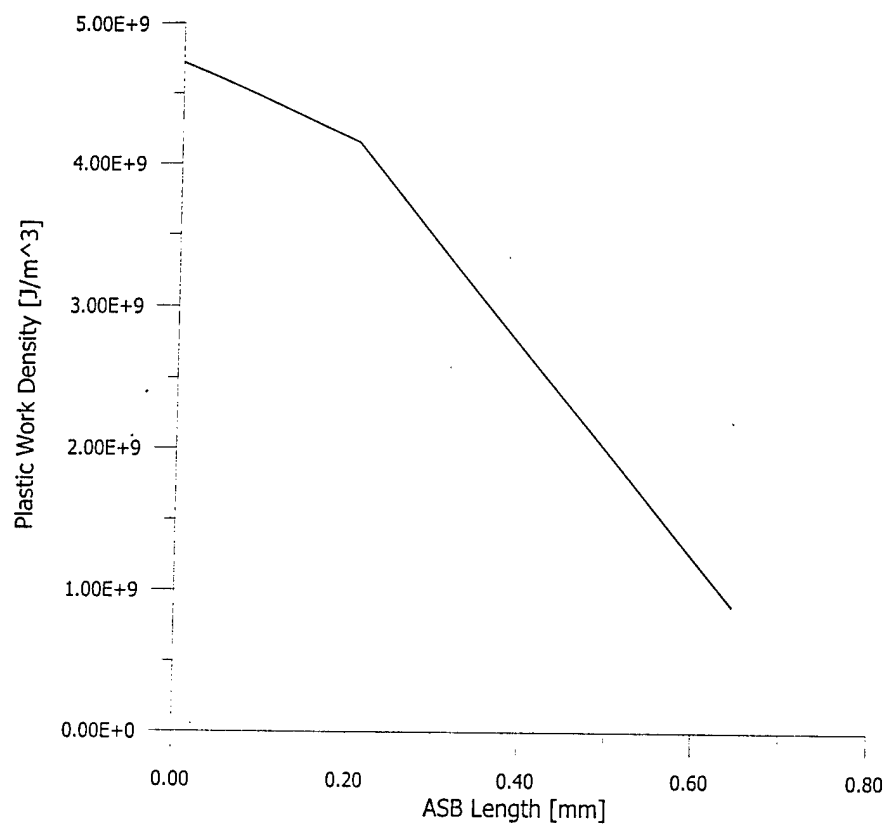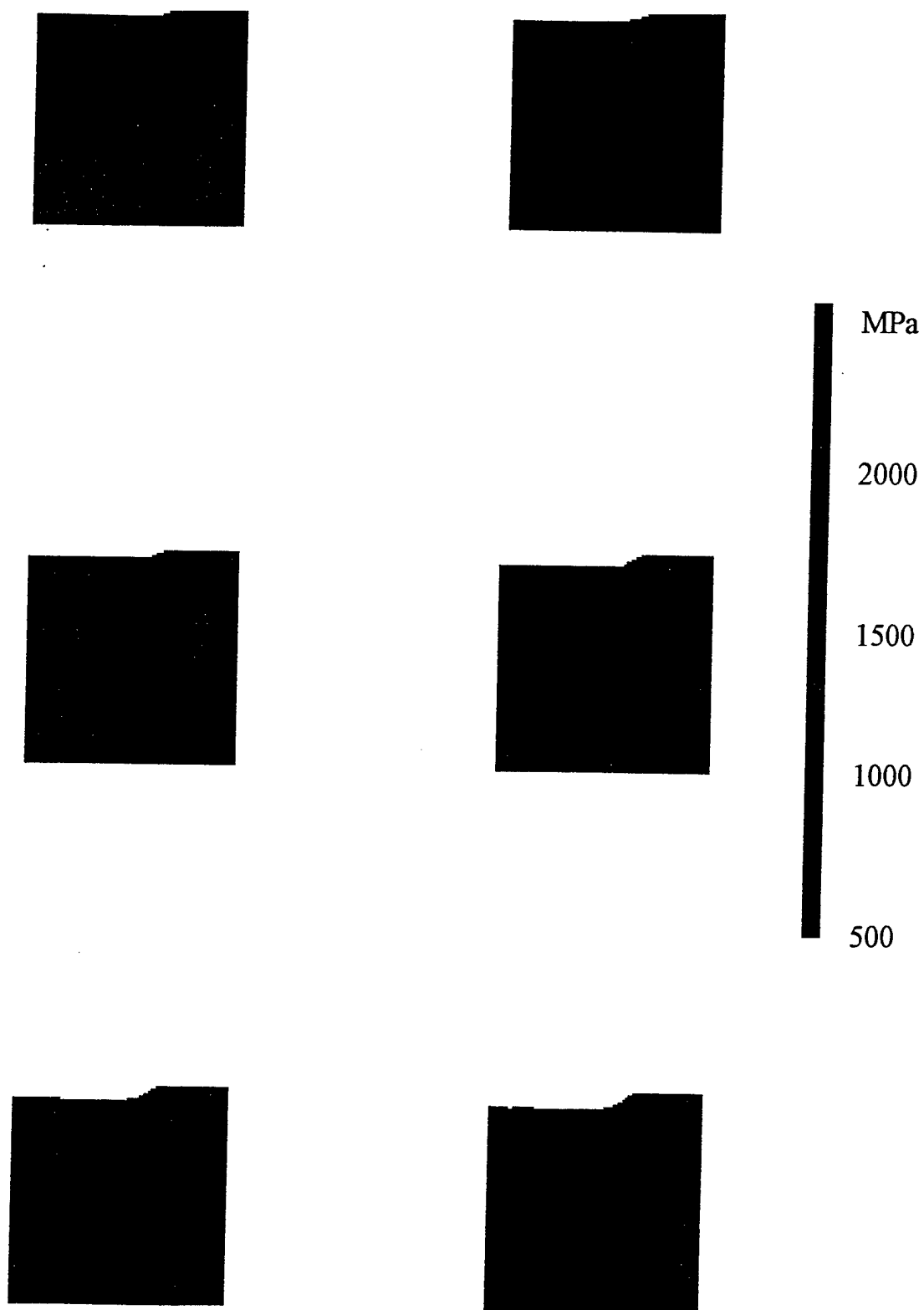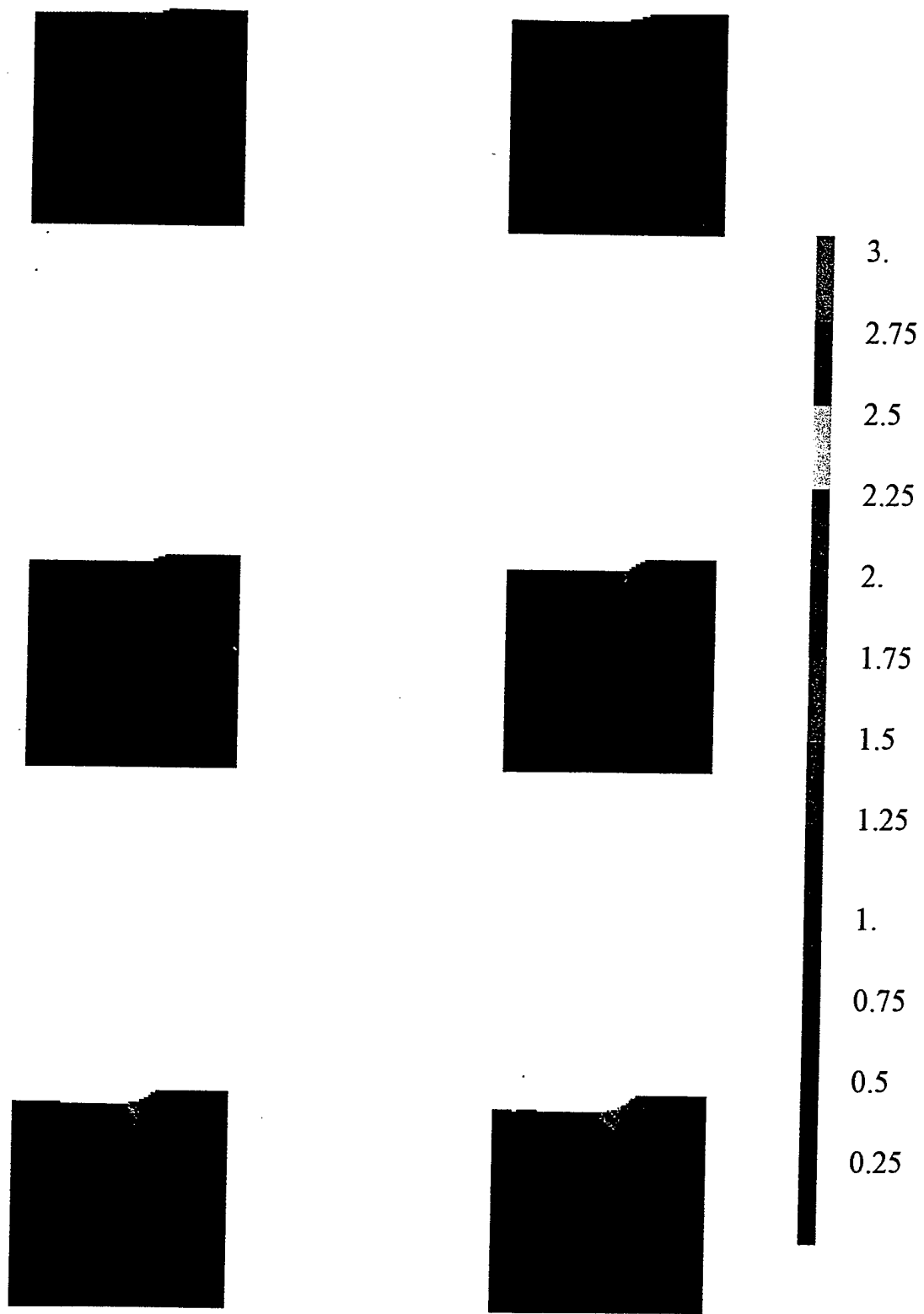
1500
1430
1300
1170
1040
920
790
660
530
400
275
150
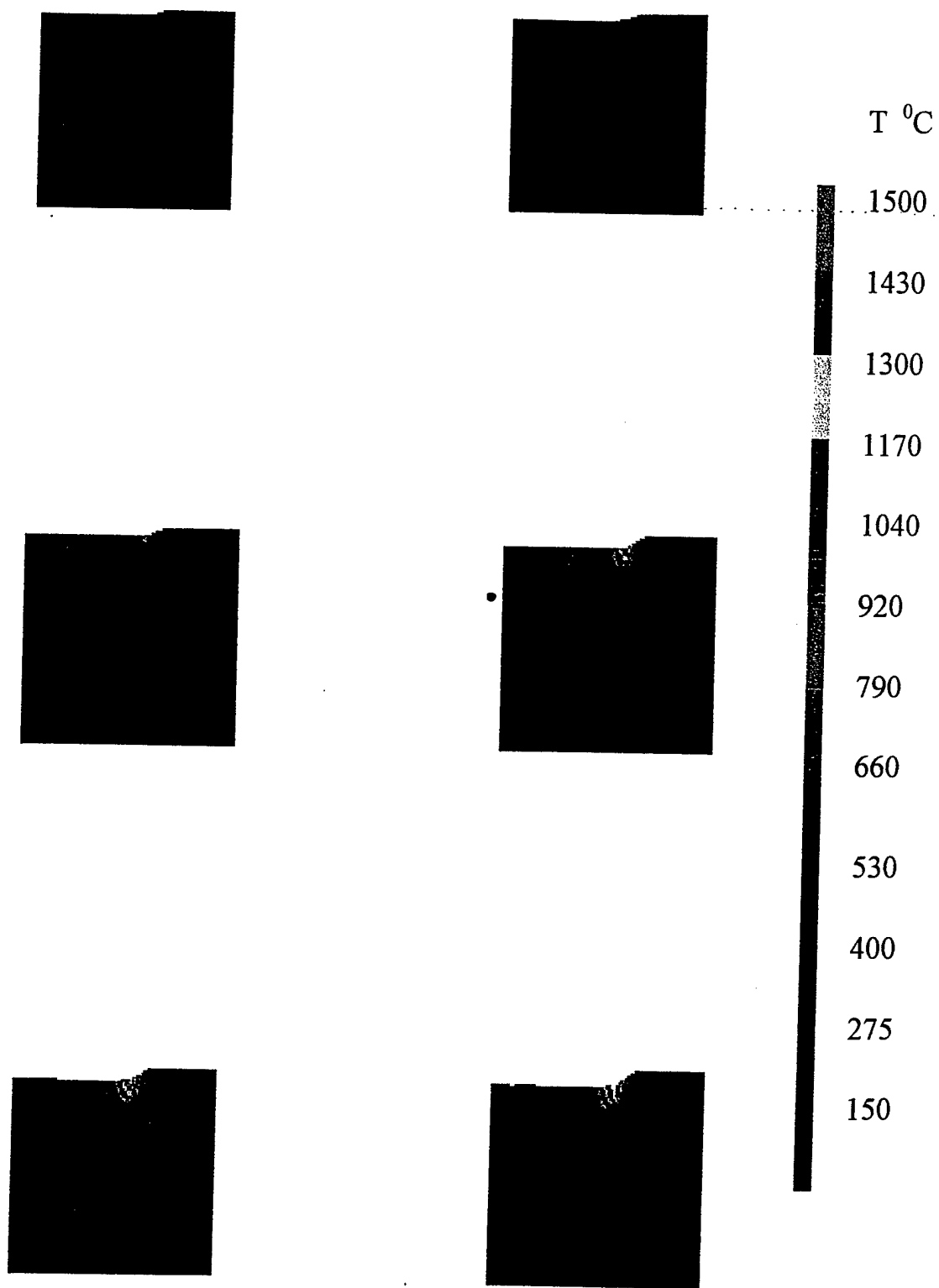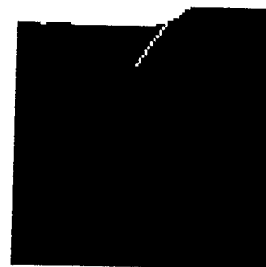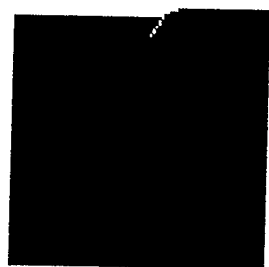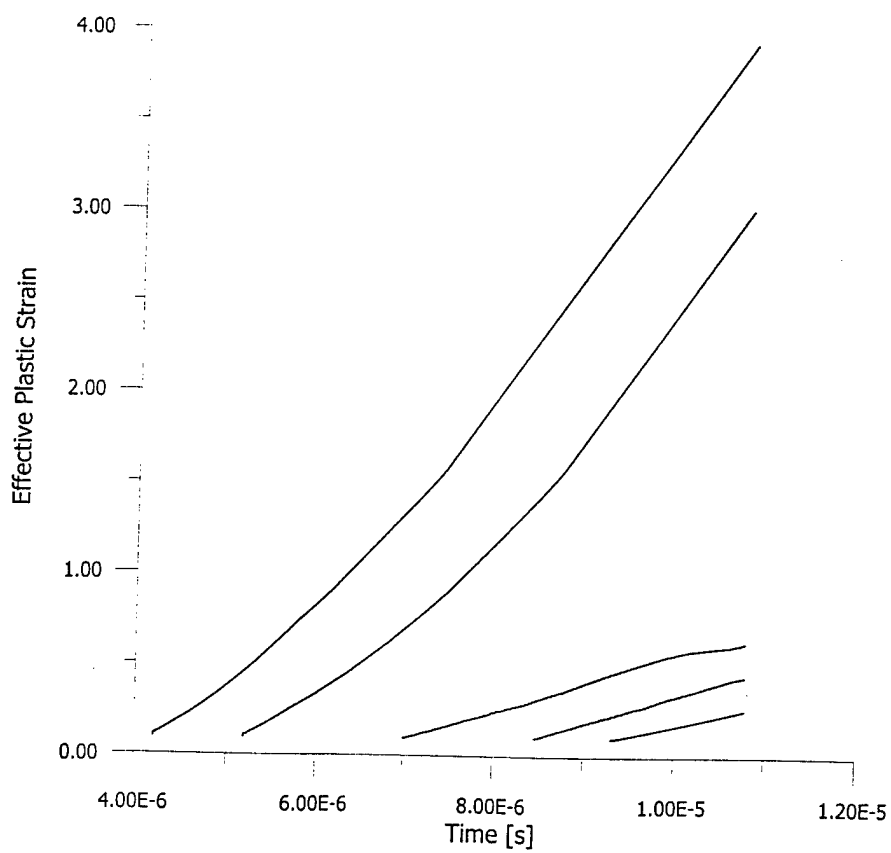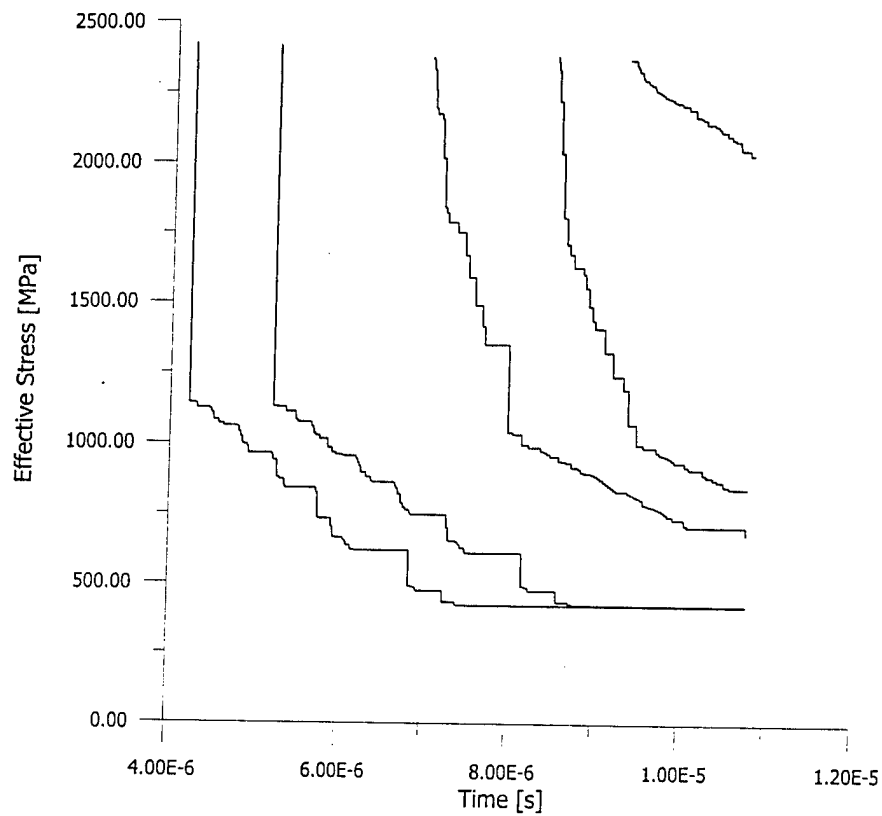
Fig. 5.11

Fig. 5.12

Fig. 5.13, 5.14
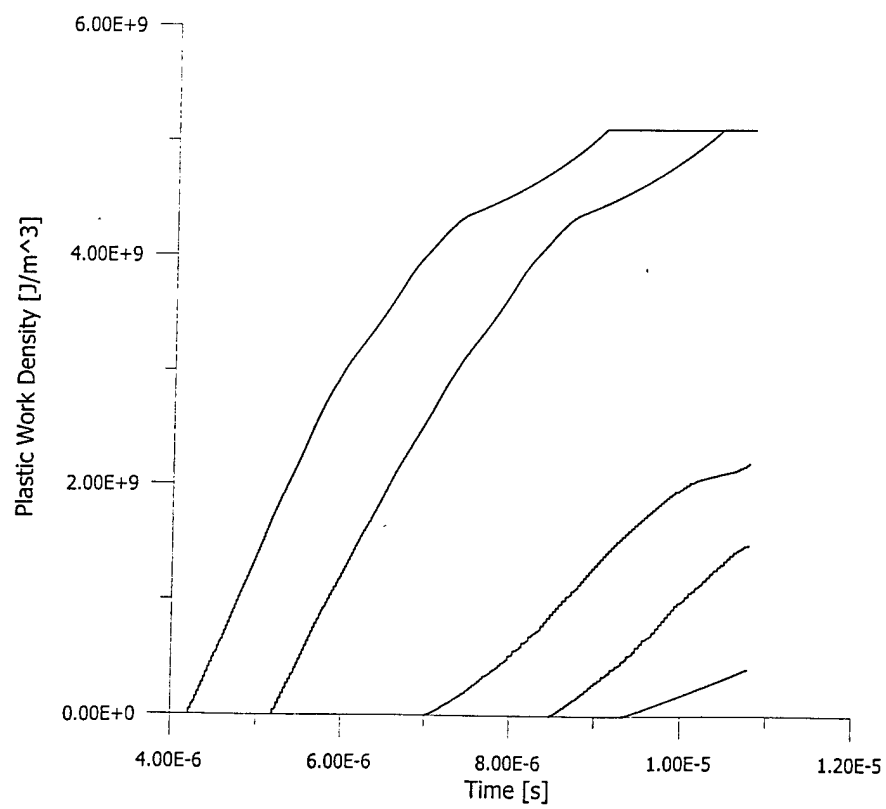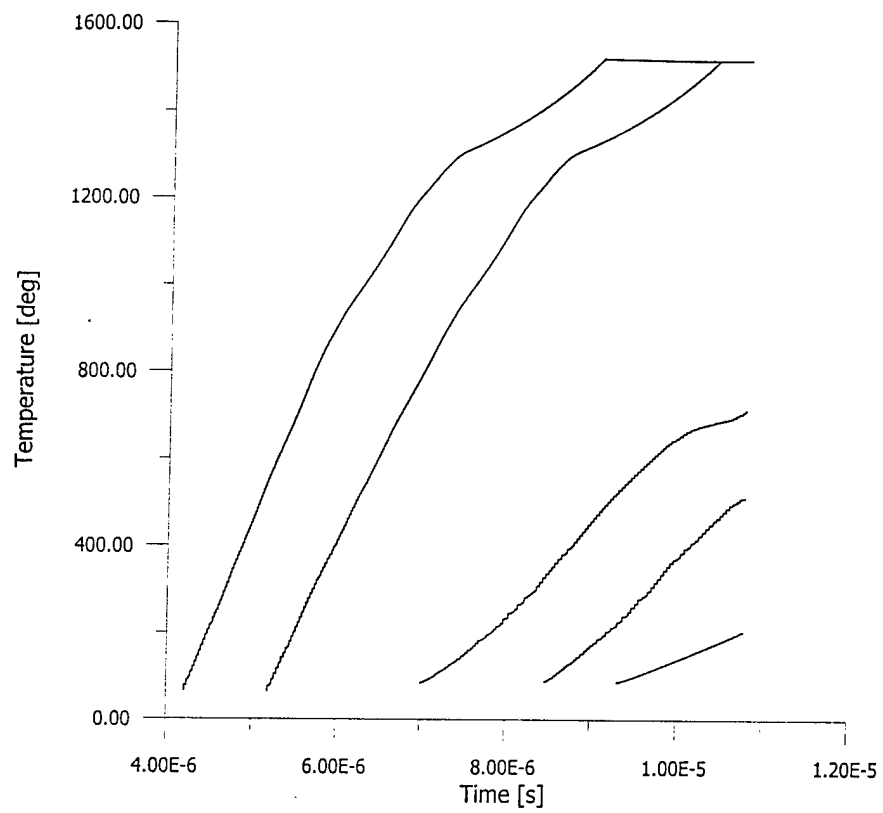
Fig. 5.15, 5.16
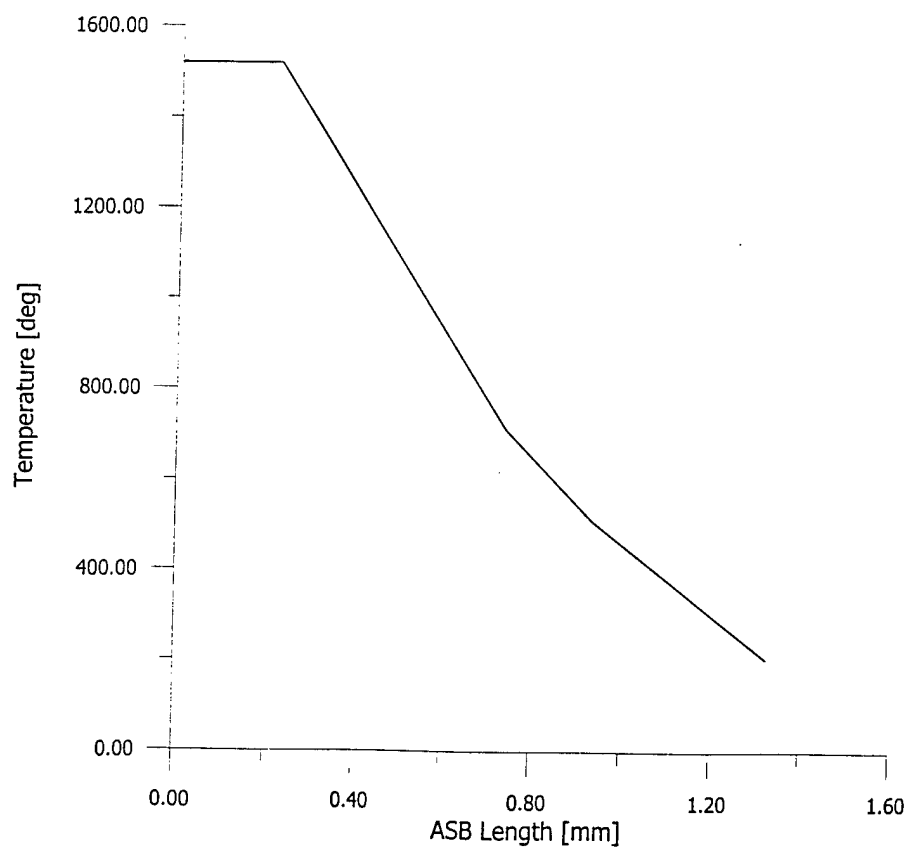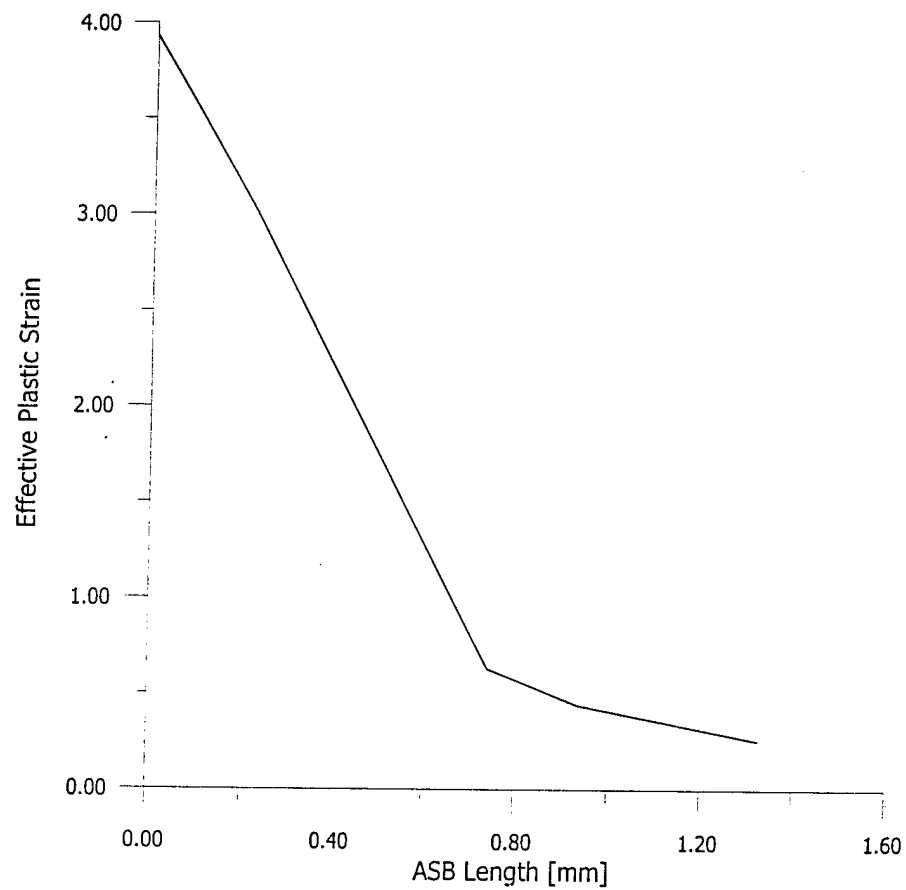
Fig. 5.17 5.18
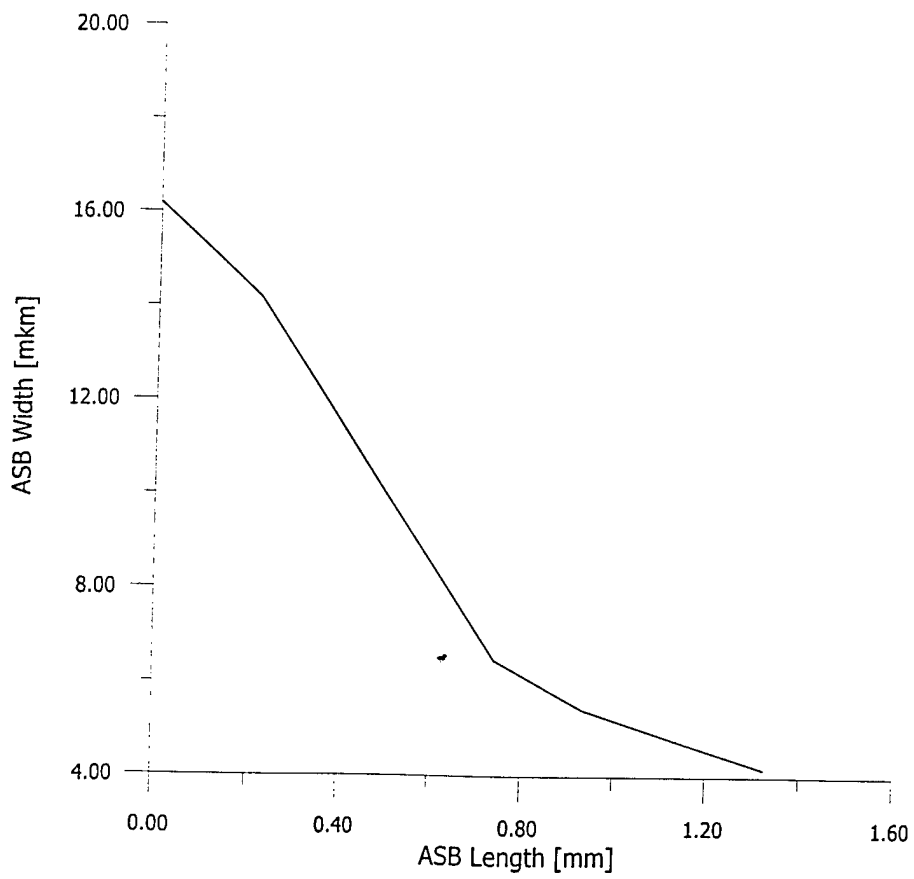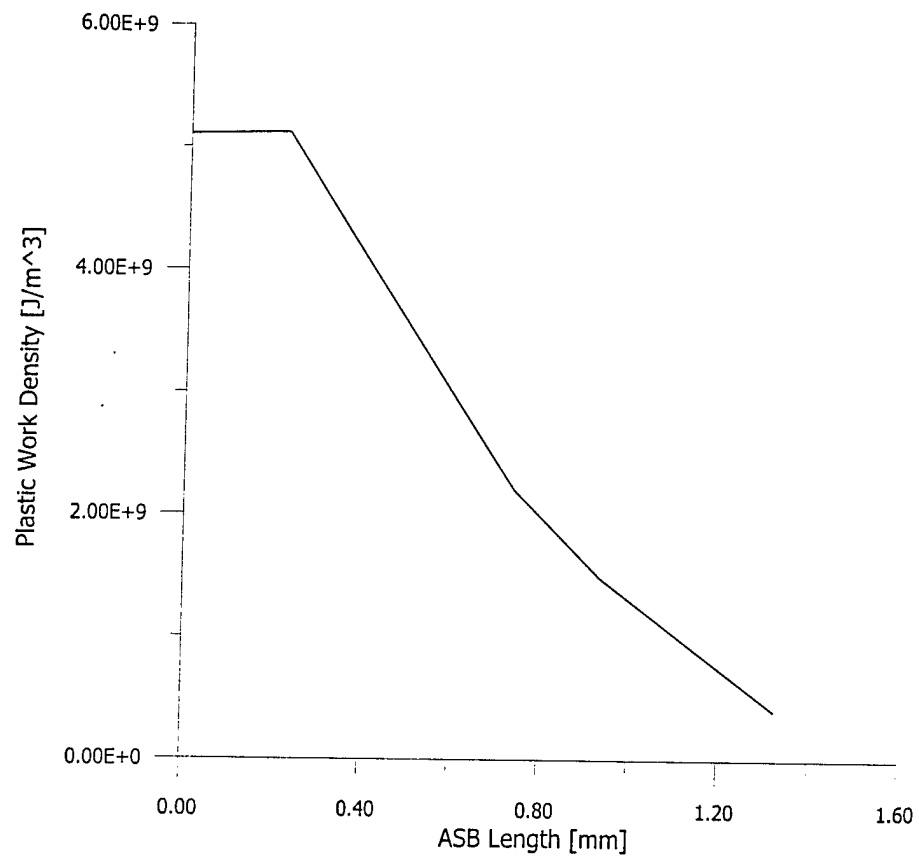
Fig. 5.19, 5.20

Fig. 5.21

Fig. 5.22

T ^{0}C

1500

1430

1300

1170

1040

920

790

660

530

400

275

150

Fig. 5.23

Fig. 5.24